UNIVERSIDADE FEDERAL DO RIO GRANDE DO SUL
PROGRAMA DE PÓS-GRADUAÇÃO EM FÍSICA
INSTITUTO DE FÍSICA

Modelling a group-scale lens at $z \sim 0.6$ *

Mônica Tergolina

Dissertação realizada sob orientação da Professora Dra. Cristina Furlanetto e da Professora Dra. Marina Trevisan e apresentada ao Instituto de Física da UFRGS em preenchimento parcial dos requisitos para a obtenção do título de Mestre em Física.

Porto Alegre, Março de 2020.

*Trabalho financiado pela Coordenação de Aperfeiçoamento de Pessoal de Nível Superior (CAPES).

Para meus amados pais, avó
e irmã, essenciais na minha vida.

Agradecimentos

Primeiramente, gostaria de agradecer a minha mãe e meu pai, Flávia e Claudio, por sempre me incentivarem a ir atrás dos meus sonhos e por terem me proporcionado a oportunidade de estudar na UFRGS. Sou muito grata por todo apoio e amor incondicional que recebi de vocês, da minha irmã Maria Alice e a minha avó Zilah.

Agradeço ao meu amor Henrique, por todo amor, paciência, compreensão, carinho e cuidado. Tua companhia foi essencial para que eu finalizasse esse trabalho. Queria agradecer aos meus cachorros, Mocki, Bacon, Costelinha e Minnie pelo amor e pelo constante suporte emocional. Vocês foram fudamentais para manter minha sanidade mental nesse período.

Sou muito grata à minha orientadora Profa. Dra. Cristina Furlanetto e à minha co-orientadora Prof. Dra. Marina Trevisan. Obrigada pela confiança depositada em mim, pelos ensinamentos, conselhos, risadas e por me ajudarem a não entrar em desespero na reta final, vocês foram incansáveis. Obrigada pelas reuniões com chocolate, figurinhas e gatos. Tenho muito orgulho de ter sido orientada por duas grandes mulheres cientistas. Agradeço também a minha colega de trabalho Daniela pela amizade e pelos conselhos. Sou muito grata a ti e ao Vitor pela ajuda com a redução de dados e, principalmente, pela paciência com o *IRAF*.

Aos meus amigos João Pedro, Eduardo, Cristiane, Otávio e Nicholas, os quais conheci graças ao Departamento de Astronomia, obrigada pela amizade sincera, por toda ajuda e por todos os rolês, principalmente no gringo. Vocês são demais.

Expresso meu agradecimento aos meus amigos da UFRGS, Gustavo, Gabriel Ramos, Gabriel Roier e Rodrigo, por toda ajuda e pelas discussões produtivas. Carlos e Pedro, agradeço os conselhos e todo o apoio de vocês na semana anterior à entrega dessa dissertação. Aos colegas da sala M208, obrigada por proporcionarem um ambiente de trabalho tão agradável.

Agradeço muito às minhas amigas Ohana, Aline e Gabriela pela amizade, companheirismo e por me proporcionarem muitos momentos felizes na vida fora da academia. Também agradeço às minhas amigas Amanda e Vitoria pelas conversas, fofocas e momentos incríveis que me ajudaram a distrair a cabeça conforme o final desse trabalho se aproximava. Nossa amizade começou graças ao amor pelos cães e tomou proporções enormes.

Tenho muito o que agradecer à minha psicóloga, Rélim, pelo auxílio nesses últimos anos e, principalmente nos últimos meses. Teus conselhos foram fundamentais para a finalização desse trabalho. Agradeço também à minha psiquiatra, Ana Paula, pela ajuda e por me medicar. Tu e o Zetron foram essenciais para que eu conseguisse me manter focada e acabar o mestrado.

Expresso minha gratidão à equipe do Gemini e do LNA, em especial Mateus Angelo por, além do suporte durante a Fase 2 das observações com o Gemini, ter deixado disponível um guia prático para redução dos dados GMOS do Gemini (http://drforum.gemini.edu/topic/gmos-mos-guidelines-part-1/).

Por fim, mas não menos importante, agradeço à CAPES por financiar esse trabalho.

Resumo

Como as galáxias se formam e evoluem ainda é uma questão em aberto na Astronomia moderna e caracterizar galáxias em altos desvios para o vermelho pode fornecer informações sobre esse processo. Galáxias submilimétricas são uma população importante em $z \sim 2-4$, já que elas possuem uma alta atividade de formação estelar com taxas de formação estelar indo de 100 a 1000 $M_\odot\,\mathrm{ano}^{-1}$ e luminosidades no infravermelho $> 10^{12} L_\odot$. Galáxias submilimétricas podem ser magnificadas devido ao efeito de lentes gravitacionais, aumentando a resolução espacial e a razão sinal-ruído da observação, assim possibilitando o estudo dessas galáxias com um grande nível de detalhe. A detecção de galáxias submilimétricas lenteadas também permite a investigação do objeto que atua como lente, o qual pode ser uma galáxia, um grupo ou um aglomerado de galáxias. Estudar a distribuição de massa desses sistemas pode fornecer vínculos em como a estrutura em grande escala do Universo se formou e evoluiu. A distribuição de massa de grupos de galáxias é particularmente interessante, já que eles fazem a ponte entre galáxias individuais e aglomerados de galáxias. Sabe-se que o lenteamento gravitacional é uma ferramenta útil para medir distribuição de massa para uma ampla variedade de sistemas. Nesse trabalho nós estudamos o sistema HELMS18, um grupo de galáxias com duas galáxias centrais, uma elíptica e um quasar, em $z = 0.6$ que está lenteando gravitacionalmente uma galáxia submilimétrica em $z = 2.39$, do Herschel HerMES Large Mode Survey (HELMS). Apresentamos o modelamento desse grupo de galáxias que atua como lente gravitacional e a reconstrução da emissão não lenteada da fonte. Usamos o método de inversão semilinear para modelar dados de alta resolução do HELMS18, obtidos com o Atacama Large Millimeter/submillimeter Array (ALMA). O modelo que recupera características observacionais é uma combinação de um perfil de densidade de Navarro-Frenk-White, para a componente do grupo, e dois elipsóides isotérmicos singulares, para as duas galáxias centrais. O modelamento recupera a distribuição de brilho superficial da fonte e a reconstrução revela que a emissão não lenteada da fonte possui duas componentes alongadas e distorcidas, separadas por 9.5 kpc, sugerindo uma possível fusão de galáxias. Como parte desse projeto, nós conduzimos observações de espectroscopia multi-objeto com o telescópio Gemini a fim de obter dados das duas galáxias centrais e dos possíveis membros do grupo. Com os dados do Gemini nós confirmamos que as duas galáxias centrais estão no mesmo desvio para o vermelho. Nós determinamos o desvio para vermelho da galáxia passiva e do quasar, respectivamente $z_{\mathrm{ETG}} = 0.60246 \pm 0.00004$ e $z_{\mathrm{QSO}} = 0.59945 \pm 0.00009$. Baseado nisso, determinamos que a velocidade relativa entre as duas galáxias centrais é $\Delta v = 903 \pm 30$ km s^{-1}.

Abstract

Understanding galaxy formation and evolution is still an open question in modern Astronomy and characterizing high-redshift galaxies can provide insights on these topics. Submillimeter galaxies (SMG) are an important population at high redshifts ($z \sim 2-4$), since they have extremely high star formation activity with star formation rates (SFR) ranging from 100 to 1000 $M_\odot\,\mathrm{year}^{-1}$ and infrared luminosities $> 10^{12} L_\odot$. SMGs can be magnified due to the gravitational lensing effect, increasing the spatial resolution and the signal-to-noise ratio of the observations, making the study of these galaxies with a great level of detail possible. The detection of lensed SMGs also allows for the investigation of the foreground object, which can be galaxies, galaxy groups or galaxy clusters. Studying the mass distribution of these systems can provide constrains on how large-scale structure in the Universe formed and evolved. Of particular interest is the mass distribution of galaxy groups, since they bridge the gap between individual galaxies and galaxy clusters. It is well known that gravitational lensing is a suitable tool for measuring the distribution of mass for a wide range of systems. In this work we study the HELMS18 system, a galaxy group with two central galaxies, an early-type galaxy (ETG) and one containing a quasar, at $z = 0.6$ that is gravitationally lensing a submillimeter galaxy at $z = 2.39$, from the Herschel's HerMES Large Mode Survey (HELMS). We present the modelling of this group-scale lens and the reconstruction of the unlensed emission of the source. We have used the semilinear inversion method to model the high-resolution data of HELMS18, obtained with the Atacama Large Millimeter/submillimeter Array (ALMA). The modelling that recovers observational features is a combination of Navarro-Frenk-White for the group component and two singular isothermal ellipsoids for the two central galaxies of the group. Our modelling recovers the source surface brightness distribution and the reconstruction reveals that the unlensed emission of HELMS18 has two elongated and disturbed components separated by 9.5 kpc, suggesting a possible merger. As part of this project we conducted Gemini GMOS multi-object spectroscopy, targeting the two central galaxies and the possible members of the group. With Gemini data we confirmed that the two central galaxies are at the same redshift. We determined that the early-type galaxy is at redshift $z_{\mathrm{ETG}} = 0.60246 \pm 0.00004$ and the quasar is at redshift $z_{\mathrm{QSO}} = 0.59945 \pm 0.00009$, and the relative velocity between the two central galaxies is $\Delta v = 903 \pm 30$ km s^{-1}.

Contents

List of Tables

List of Figures

List of abbreviations

AGN Active Galactic Nuclei

ALMA Atacama Large Millimeter/Submillimeter Array

CCD Charge-Coupled Device

DM Dark Matter

DSFG Dusty Star Forming Galaxy

ETG Early-Type Galaxy

GALEX Galaxy Evolution Explorer

GMOS Gemini Multi-Object Spectrograph

H-ATLAS Herschel Astrophysical Terahertz Large Area Survey

HELMS HerMES Large Mode Survey

IR Infrared

IRAF Image Reduction and Analysis Facility

MCMC Markov Chain Monte Carlo

MOS Multi-Object Spectroscopy

NFW Navarro Frenk White

PIEMD Pseudo Isothermal Elliptical Mass Distribution

PSF Point Spread Function

QSO Quasi-Stellar Object

SDSS Sloan Digital Sky Survey

SED Spectral Energy Distribution

SFR Star Formation Rate

SIE Singular Isothermal Ellipsoid

SIS Singular Isothermal Sphere

SL Strong Lensing

SLI Semilinear Inversion

SMG Submillimeter Galaxy

ULIRG Ultra-Luminous Infrared Galaxies

UV Ultraviolet

Chapter 1

Introduction

The way galaxies form and evolve remains one of the most challenging open questions in modern Cosmology and Astrophysics. In the past decades, very deep photometric and spectroscopic surveys unveiled the Universe when it was only a few hundred Myr old and enabled the astronomers to identify that distant galaxies are very different from those at $z = 0$. For instance, these systems have more irregular morphologies, higher gas fractions of a factor 3-10 (Daddi et al., 2010; Tacconi et al., 2010; Geach et al., 2011) and are more dusty compared to their local counterparts. Besides, galaxies were observed to have much higher star formation rates (SFRs) of $\gtrsim 100\,\mathrm{M_\odot\,year^{-1}}$ in the past (Barger et al., 1998; Daddi et al., 2005; Gruppioni et al., 2013; Lilly et al., 1996; Schiminovich et al., 2005; Le Floc'h et al., 2005), when compared to local spiral galaxies with $\sim 3\,\mathrm{M_\odot\,year^{-1}}$ (Bothwell et al., 2011; Elbaz et al., 2011; Chomiuk & Povich, 2011). As shown by Madau & Dickinson (2014), the peak of star formation occurred at redshift $z \sim 2$, when the Universe was approximately 3.5 Gyr. Figure 1.1 shows an increasing cosmic SFR from $z \sim 8$ to $z \sim 3$, peaking at $z \sim 2$ and declining until the present epoch.

The cosmic star formation history can be better constrained by studying submillimeter galaxies (SMGs) at high redshifts ($z \sim 2-4$), which are galaxies with submillimeter emission mainly due to dust thermal emission. These objects represent a population of galaxies with extremely high star formation activity and might represent a significant contribution to the comic SFR density in the early Universe. At high redshifts, a great fraction of the bolometric luminositiy densities are due to SMGs (Chapman et al., 2003). The star formation rate in SMGs ranges from hundreds to thousands of $\mathrm{M_\odot\,year^{-1}}$ and they have infrared luminosities $> 10^{12}\ \mathrm{L_\odot}$ (Casey et al., 2014). SMGs are objects that have rest-frame far-infrared emission primarily due to thermal emission from heated dust grains, with typical dust temperatures of $T_d \sim 40$ K (Symeonidis et al., 2013). One of the major questions in studying these galaxies is to understand the origin of the mechanism that is heating the dust grains, which means whether is an active galactic nuclei (AGN) or young stars.

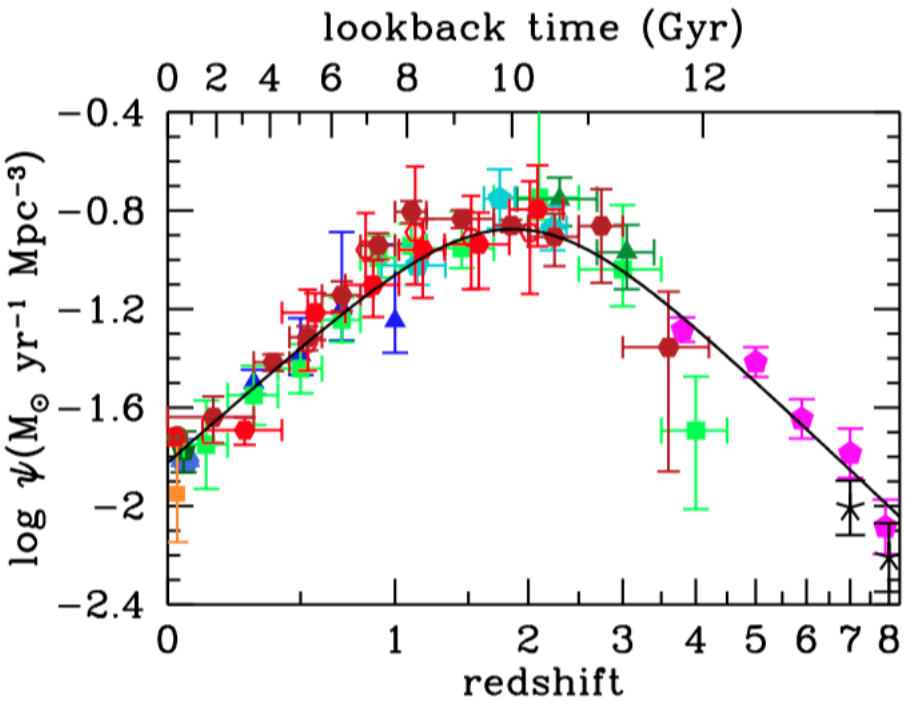

Figure 1.1: Cosmic star formation history from UV + IR restframe showing the increase of the SFR at $3 \leq z \leq 8$; a peak at $z \sim 2$, when the Universe had ~ 3.5 Gyr; and a decline until the present (Madau & Dickinson, 2014).

Different studies revealed that the SMGs are the high-redshift ($z \sim 2-4$) counterparts of the ultra-luminous infrared galaxies (ULIRGs) in the local Universe, since they have similar bolometric luminosities, $L_{Bol} \sim 10^{12}$ $L_{\odot}$(Engel et al., 2010; Swinbank et al., 2010; Alaghband-Zadeh et al., 2012; Rowlands et al., 2014). Being local analogs of the SMGs, it is also important to study these nearby galaxies in order to better understand the galaxy formation and evolution processes. Very luminous ULIRGs at low redshift enabled resolved studies of their central regions, indicating that most of the dust emission comes from the inner sub-kpc regions (Downes & Solomon, 1998; Sakamoto et al., 1999).

ULIRGs have infrared luminosities greater than 10^{12} $L_{\odot}$ and seem to be late-state merger-induced starbursts, so that SMGs seem to be linked with merger events (Engel et al., 2010; Ivison et al., 2012; Alaghband-Zadeh et al., 2012; Fu et al., 2013; Chen et al., 2015; Oteo et al., 2016). In fact, Conselice et al. (2003) showed consistent evidence that $40\% - 80\%$ of the SMGs are undergoing major mergers. They also excluded statistically with 5σ confidence the possibilty that SMGs are ordinary galaxies at high redshift. These results imply directly in the formation of local massive galaxies since SMGs compose most of the population of galaxies at high redshift and their majority undergoes major mergers. Thus, SMGs will likely evolve into massive nearby galaxies (Sanders & Mirabel, 1996; Conselice et al., 2003; Simpson et al., 2017).

The discovery of SMGs by Smail et al. (1997); Hughes et al. (1998) brought the low frequency region of the spectrum into observational Cosmology and Astrophysics, opening

a new window of possibilities in galaxy formation and evolution studies. There are two main sources of submillimeter radiation in galaxies: atomic and molecular transitions in the interstellar gas resulting in line emissions and thermal emission from dust grains.

The first large sample measuring stellar mass of high-redshift SMGs was studied by Borys et al. (2005). In this work, they showed that SMGs have stellar masses in the range $\log(M_*/\mathrm{M}_\odot) = [11.14, 12.15]$ with median $\langle M_* \rangle = 2.5 \times 10^{11}$ $\mathrm{M}_\odot$. Hainline (2008) derived the stellar mass of a large sample of SMGs observed with Spitzer and found a median stellar mass of $6.3-6.9 \times 10^{10}$ $\mathrm{M}_\odot$. Michałowski et al. (2010) obtained a median value of 3.5×10^{11} $\mathrm{M}_\odot$ for the stellar mass of SMGs, despite of using the same observational data set as Hainline (2008). Tacconi et al. (2006) measured the size of SMGs based on CO emission using interferometric data and mm-continuum data and found that they are relatively compact galaxies with median diameter 4 kpc.

To better understand the nature and determine the properties of SMGs, large submillimeter surveys, such as the Herschel Astrophysical Terahertz Large Area Survey (H-ATLAS, Eales et al., 2010a), the Herschel Multi-tiered Extragalactic Survey (HerMES, Oliver et al., 2012), and the South Pole Telescope surveys (Carlstrom et al., 2011; Vieira et al., 2013) were conducted to provide data for these systems. With the Atacama Large Millimeter/submillimeter Array (ALMA) and other interferometers, it is possible to have high-resolution data of SMGs at high redshift. Ma et al. (2015) presented rest-frame optical SEDs and inferred stelar masses ranging from 8×10^{10} $\mathrm{M}_\odot$ to 4×10^{11} $\mathrm{M}_\odot$. They also found SFRs around 100 $\mathrm{M}_\odot\,\mathrm{year}^{-1}$ which is consistent with the scenario of major mergers triggering star formation. Brisbin et al. (2017) carried out ALMA observations and detected 152 galaxies and estimated photometric and spectroscopic redshifts for the sources. The median redshift of their sample is $z = 2.48 \pm 0.05$, which is consistent with previous works (Simpson et al., 2014; Chapman et al., 2005). They also found that a significant percentage of the sample are multi-component systems. Simpson et al. (2017) presented a multi-wavelength study of 52 SMGs identified by ALMA. They modelled the FIR emission from the sources and found a median value of FIR luminosity $L_{FIR} = 3.2 \times 10^{12}$ $\mathrm{L}_\odot$. Moreover, analysing the SMGs' possible evolutionary pathways they show that SMGs are progenitors of local elliptical galaxies and they probably do not evolve into spiral and lenticular galaxies.

By using ALMA interferometry, it is also possible to target strongly lensed SMGs that are at higher redshift, enabling high-resolution studies of these distant sources. Gravitational lensing is predicted by Albert Einstein's theory of General Relativity. The light from a distant source is bent by the presence of a massive body, such as a galaxy or a galaxy cluster, which distorts spacetime. When this effect is strong enough, it produces multiple and distorted images, like arcs or even complete rings. The latter occurs when there is exact alignment of the source, lens and observer. This is useful since strongly lensed systems are magnified, increasing the spatial resolution and signal-to-noise ratio of the observation.

Blain (1996) and Negrello et al. (2007) were the pioneers in proposing that strongly lensed systems could be found in the submillimeter, however, it was only a few years later that Negrello (2010), Vieira et al. (2010), Hezaveh & Holder (2011), and Wardlow et al. (2013) confirmed the existence of lensed SMGs in the submillimetric with the surveys mentioned previously. Several authors proposed that instead of using wide-area surveys to detect multiple images, a cut in the flux density could be used to detect lensed sources (Blain, 1996; Perrotta et al., 2002, 2003; Negrello et al., 2007). Negrello et al. (2010) showed an efficient technique to detect strongly lensed SMGs using the number of galaxies at a given flux density. The explanation is that even a small number of magnified SMGs could change the shape of the bright tail of the submilllimeter source counts. Apart from the SMGs, other objects such as high-redshift radio-loud AGNs (de Zotti et al., 2005) and starbursts and spiral galaxies (Serjeant & Harrison, 2005) can affect the bright end of the submillimeter source counts. However, these contaminants can be easily removed by using optical/near-IR/radio imaging analysis, so that flux-limited submillimeter surveys could be used to detect lensed SMGs with almost 100% accuracy. Based on a subset of bright galaxies detected in the Herschel-Astrophysical TeraHertz Large Area Survey (Eales et al., 2010b), they proposed a flux density cut at 100 mJy at 500 μm (1.2). Since then, several lensed SMGs have been confirmed in Herschel surveys (Conley et al., 2011; Fu et al., 2012; Bussmann et al., 2012; Wardlow et al., 2013; George et al., 2013; Calanog et al., 2014; Negrello et al., 2017). After that, many follow-ups were conducted in order to study these sources with a great level of detail.

One example of follow-up using the flux density cut method to find lensed SMGs from Negrello et al. (2010) was the work from Messias et al. (2014). They studied a candidate lensed galaxy selected by the Herschel-ATLAS field. Using multi-wavelength and high-resolution imaging they confirmed the lensing scenario, which revealed that the foreground galaxy is surrounded by an almost complete Einstein radius $\theta_E = 2.18$ kpc, which is half the angular separation of the distorted images. The system was modelled using the semilinear inversion method (Warren & Dye, 2003), allowing the estimation of the total and stellar masses within the Einstein radius, which are respectively, $M_T = 8.13 \times 10^{10}$ M$_\odot$ and $M_* = 1.60 \times 10^{10}$ M$_\odot$. The source reconstruction indicates a possible merger event with tens-of-kpc-long tidal tail. The dynamical mass of one of the components is 5.8×10^{10} M$_\odot$ and the dynamical analysis shows that this component is morphologically disturbed. Another example of follow-up is the work from Dye et al. (2015), where they modelled the strong lens system SDP.81, one of the first five systems discovered by H-ATLAS, that was selected as a target for ALMA Science Verification. Using CO emission line, they reconstructed the kinematics of the source which indicated the presence of a rotating disk. They also found a dynamical mass of $3.5 \pm 0.5 \times 10^{10}$ M$_\odot$ within 1.5 kpc. The total dust mass $1.8 \pm 0.3 \times 10^{10}$ M$_\odot$ was estimated by SED fitting by combining ALMA data with photometry of the source. Also,

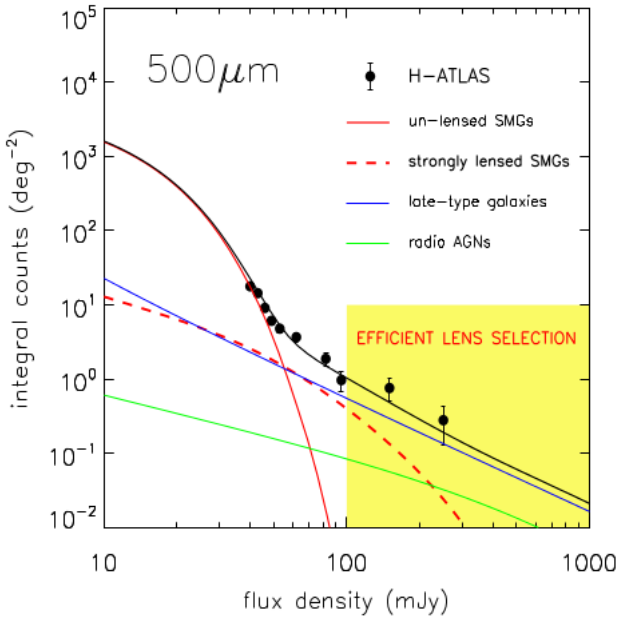

Figure 1.2: Number counts of dust-obscured star-forming galaxies. Three populations can be distinguished at 500 μm source counts: low-redshift starbursts or spiral galaxies, radio loud AGNs and high-redshift SMGs. Flux densities above 100 mJy are dominated by lensed SMGs and the contaminants can be removed using imaging analysis. The data points are from H-ATLAS (Clements et al., 2010). Figure was taken from Negrello et al. (2010).

they estimated a total gas mass of $2.7 \pm 0.5 \times 10^{10}$ $M_\odot$ and a SFR of $\sim 470 \pm 80$ $M_\odot$ year^{-1} and found evidence of a possible merger.

By detecting lensed SMGs it is also possible to study the foreground object, which can be individual galaxies, groups of galaxies or even galaxy clusters. Characterizing the mass distribution of these systems can provide critical constrain on theories of formation and evolution of large-scale structures in the Universe (Bartelmann et al., 2013). Of particular interest is the radial density profile of dark matter (DM) haloes, which can be sensitive to many baryonic processes, such as feedback from active galactic nuclei (AGNs) and supernovae explosions. Since the effects of each of these processes on the density profile might vary with the stellar mass, halo mass, and star formation history of the structure, it is important to examine the baryonic and DM content in structures across the full range of masses, i.e., from individual galaxies to massive clusters.

Galaxy clusters are the most massive virialized objects, have the highest density contrast and are rare, whereas individual galaxies are less massive and more abundant. In this framework, groups of galaxies bridge the gap between isolated galaxies and clusters. They can contain dozens of galaxies and are the most common structures in the Universe, harboring at least 50% of all galaxies at low redshift (Eke et al., 2004). Moreover, they trace large scale structure and offer a new window of investigation in the mass spectrum.

Several N-body simulations for a cold DM Universe have shown that the mass distribution within DM halos follow a Navarro-Frenk-White (NFW) density profile (Navarro, 1996; Navarro et al., 1997). For the inner part of the DM halo, the profile scales with r^{-1}, whereas for the outer part of the halo it scales with r^{-3}, for any halo mass. In the Universe, the density profile depends on both dark and baryonic matter. In order to form galaxies, baryons cool and condense in the central regions of DM halos. Since dissipative gas-cooling processes (Blumenthal et al., 1986; Gnedin et al., 2004), feedback from AGN (Martizzi et al., 2013) and supernovae (Navarro et al., 1996; Pontzen & Governato, 2012) and dynamical heating in mergers (El-Zant et al., 2001; Nipoti et al., 2004; Tonini et al., 2006; Laporte & White, 2015) can create a much more concentrated mass distribution at the center of the DM halo, baryonic processes can change drastically the inner density profile, making it steeper than the NFW (Hammer & Rigaut, 1989). Thus, accurate measurements of the mass distribution across a wide range of systems can be used to test and constrain galaxy formation models.

It is widely recognised that gravitational lensing is the most suitable tool for measuring the distribution of mass (dark + baryonic) across galaxies, groups and clusters. Modelling the strong lensing effect allow us to measure the total mass within the system of multiple images, defined as the Einstein radius (θ_E). This technique is robust in the sense that is insensitive to the dynamical properties of the mass that causes the deflection of passing light rays from a background source. This is in contrast to methods using dynamics to probe the gravitational potential of the mass since these must make several uncertain assumptions.

Combining strong lensing technique with other observations allows us to measure the density profile at different radii. For instance, the combination of strong lensing and stellar kinematics is used to probe the mass profile of galaxy-scale lenses ($\theta_E < 2$" and halo masses $M_{\rm vir} < 10^{13}$ M$_\odot$) (Treu & Koopmans, 2002; Auger et al., 2010; Barnabè et al., 2013) and the combination of strong lensing, weak lensing and stellar kinematics of the centrally-located galaxies is now established as one of the most reliable techniques for analyzing the mass distribution in clusters ($\theta_E > 8$" and halo masses $M_{\rm vir} > 10^{14}$ M$_\odot$; see Bartelmann (2010) for a review). While some studies suggest that baryons and DM follow a nearly isothermal density profile (with logarithmic slope $\gamma = 2$) in early-type galaxies (ETGs), other studies found that the inner DM density slope in galaxy clusters is shallower than the NFW slope, suggesting a connection between the inner halo and the assembly of stars in the central galaxies (Sand et al., 2008; Newman et al., 2013; Schaller et al., 2015).

Such techniques have been mainly applied to galaxy-scale and cluster-scale lenses, so the main goal of this project is to bridge the gap in the trends observed in the density profiles of small and large scale structures (see Figure 1.3) by studying the intermediate mass range of group-scale lenses ($2'' < \theta_{\rm E} < 8''$). So far, very few studies focused on the measurement of the density profile of group-scale lenses (Newman et al., 2015; Verdugo et al., 2007).

In the past few years, Newman et al. (2015) presented new observations and analysis combining SL and stellar kinematics of 10 group-scale lenses at $z = 0.36$ characterized by

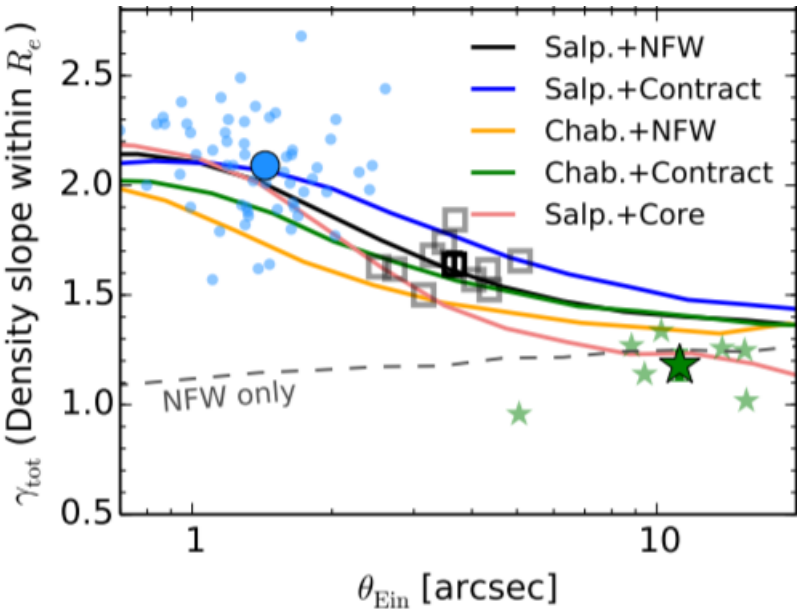

Figure 1.3: Trends in the total density slope γ_{tot} within the effective radius as a function of Einstein radius θ_E. The galaxy-scale lenses are represented by blue dots, the group-scale lenses by black squares and BCGs of massive clusters by green stars. Darker symbols show the mean of each data. The dashed line represents an unmodified NFW profile halo without stars. The solid lines represent the mean trends for the 5 halo occupation with different IMFs and inner density profiles. Figure taken from Newman et al. (2015).

Einstein radii $\theta_E = 2.5" - 5.1"$. All group-scale lenses are ETGs in intermediate mass halos of $M_{200} = 10^{14}$ $M_\odot$. Figure 1.3 shows the trends in the slope of the total density profile. They found that the average slope of the total density profile within effective radius, which is the radius containing half of the light of the galaxy, is $\langle\gamma_{tot}\rangle = 1.64 \pm 0.05$ for the group-scale lenses.

Another result within the past decade is that Verdugo et al. (2011) combined SL modelling with dynamical constraints to study SL2S J02140-0535, a galaxy group at $z = 0.44$. The best fit model that recovered observational features was a single halo for the group component, described by a NFW profile, plus three galaxy scale components associated with the central galaxies, described as Pseudo Isothermal Mass Distribution (PIEMD) density profile (Elíasdóttir et al., 2007).

In this work, we focus on the strong lensing regime and, more specifically, on the study of the HELMS18 system, a group of galaxies at $z = 0.6$ that is lensing a SMG at $z = 2.39$ from the Herschel's HELMS survey. The main goal of this project is to model the group-scale lens, and with the modelling, reconstruct the unlensed emission of HELMS18, thus enabling the study of the submillimeter source. This project also involved obtaining multi-object spectroscopic data from Gemini. These observations targeted the two central galaxies and also the possible members of this galaxy group. With Gemini data we were able to confirm that the two central galaxies are at the same redshift.

The layout of this dissertation is as follows: Chapter 2 describes the gravitational lensing effect, and in Chapter 3 we describe the HELMS18 lens system and the data available for this object. Chapter 4 presents results of the lens modelling and the source reconstruction of HELMS18 lens system. Chapter 5 summarises our results and describes the perspectives. Throughout this dissertation, the cosmological parameters assumed are: $H_0 = 67$ km $s^{-1}Mpc^{-1}$, $\Omega_m = 0.32$, $\Omega_\Lambda = 0.68$ (Planck Collaboration et al., 2014).

Chapter 2

Gravitational Lensing

Gravitational lens effect occurs when the light from a distant source is bent by the presence of a massive body. This phenomenon happens due to the distortion of space-time by a massive body and was predicted by Albert Einstein's General Theory of Relativity.

The properties of the original image can be modified in different ways by gravitational lensing. Some visible effects are the magnification of the source, resulting in an increased measured flux and the appearance of multiple and distorted images from the same source. These effects depend on the alignment and distances of the observer, lens and source and also on the gravitational potential. The lens is the mass distribution causing the deflection of light and it can be galaxies, galaxy groups or clusters of galaxies.

The phenomenon can be divided into two regimes: strong and weak lensing. The strong regime causes visible deformations on the sources and sometimes produces multiple images, like gravitational arcs. The weak regime also causes distortions, however it is only detected statistically using a large number of sources. Figure 2.1 is an example of the strong lens regime, showing multiple and distorted images, while Figure 2.2 is an example of the weak lens regime. In the weak regime it is not possible to observe directly the lensing, but it is detected in statistical analysis of the images of background galaxies.

The first cosmological lensing configuration was discovered by Walsh et al. (1979a). A few years later, Soucail et al. (1987) found a blue giant ring-like structure in Abell 370, which was the first detection of gravitational lensing in galaxy clusters. After that, the lensing effect became a suitable tool to study different topics in Astrophysics and Cosmology. One of the main uses of gravitational lensing is to measure the mass distribution of the lenses. The main advantage of this technique is that the internal physical processes and the dynamical state of the lens do not impact the lensing phenomenon. Owing to this fact, the study of density profiles can provide information about the distribution of dark matter and the baryonic processes in the inner parts of the lenses. For instance, using such technique it was possible to discover that the mass distribution in galaxy clusters is smoother than in individual galaxies (Bergmann et al., 1990; Hammer et al., 1989). Another result is that the density profile in

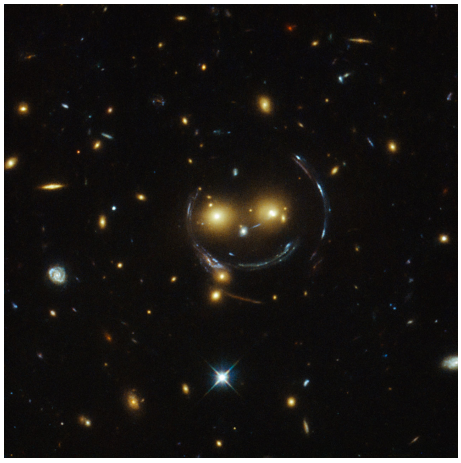

Figure 2.1: Cosmic Smile (NASA): example of a strong lens system. The group of galaxies acts as a lens, distorting the images of background galaxies into gravitational arcs.

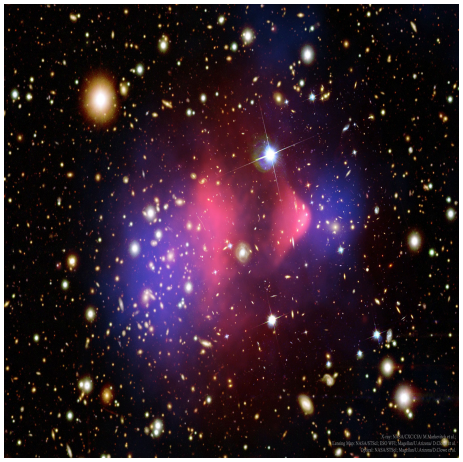

Figure 2.2: Bullet Cluster (NASA): example of weak lensing regime. The small distortions of background galaxies were used to measure the distribution of dark matter (in blue) in this merging cluster system.

clusters is steeper in their central regions compared to their outskirts (Hammer & Rigaut, 1989). Moreover, the magnification provided by the gravitational lensing effect allows for the study of distant sources that otherwise would be too faint to be detected (Zwicky, 1937; Kneib et al., 1993). Through gravitational lensing it is also possible to measure the Hubble constant (Wucknitz et al., 2004; Suyu et al., 2010).

In this work we focused on the strong lensing regime, more specifically, on the study of a group of galaxies at $z = 0.6$ that is strongly lensing the submillimeter galaxy, at $z = 2.39$. This system is called HELMS18. In the following, we introduce the main concepts and the basic equations of the gravitational lens theory, that describes the deflection of light by a gravitational field. More detailed descriptions can be found at Meneghetti (2016); Furlanetto (2012); Lima Neto (2020). We also introduce the semilinear inversion method (Warren & Dye, 2003) that was adapted and used to perform the lens modelling and source reconstruction.

2.1 Lens Theory

2.1.1 Historical Context

The idea that a massive body should deflect light had been speculated even by Newton in his works, however he had never presented any mathematical description about it. In 1804, von Soldner was the first to publish the deflection of light using Newtonian mechanics and estimated that the light from a background source which propagates in a gravitational field of a point mass M at a distance ξ is deflected by an angle

$$\hat{\alpha} = \frac{2GM}{c^2\xi}, \tag{2.1}$$

where G and c are, respectively, the gravitational constant and the speed of light. Based on that, he inferred that the light beam of a distant star would be deflected by an angle $\hat{\alpha} = 0.84''$ when propagating through the Sun's gravitational potential.

In 1911, Einstein proposed that the deflection angle could be measured during a Solar eclipse Einstein (1911). He suggested that during the eclipse it would be possible to observe the shifts in the positions of the stars due to the deflection of light. However, it was only with the General Theory of Relativity that Einstein correctly predicted the path of photons in the presence of a massive object (Einstein, 1916). With the General Relativity Theory, Einstein proposed that the deflection angle would be

$$\hat{\alpha} = \frac{4GM}{c^2\xi}. \tag{2.2}$$

This equation is valid only for the case of weak gravitational fields. Considering $M = M_\odot$ and $\xi = R_\odot$, the equation 2.2 leads to a deflection angle of 1.74", which is the light deflection near the Solar disk. This prediction was confirmed during the the Solar eclipse observed in May 1919 (Dyson et al., 1920).

In 1924, Chwolson suggested that the alignment of two stars in the line-of-sight could generate multiple images and, if the lens and the source were perfectly aligned, a circular image in the form of a ring would appear (Chwolson, 1924). In 1936, Einstein obtained the same result as Chwolson. Considering the lensing of a star by another star, he estimated the magnification, the position and the separation of the images (Einstein, 1936). In that same work, the configuration of the perfect alignment between source, lens and observer was calculated. The resulting image was later called Einstein ring.

The hypothesis that galaxies (called extragalactic nebulae at the time) could act as lenses was first considered by Fritz Zwicky in 1937 (Zwicky, 1937). Given that these objects were distant and more massive, the separation between the lensed images could reach the order of few arcseconds, making the galaxies interesting candidates to observe the gravitational lensing effect.

The first observational evidence of lensing in galaxies was obtained in 1979. Walsh et al. (1979b) observed multiple images of a quasi-stellar object (QSO) in the optical, and spectroscopic measurements indicated that both sources were at redshift $z = 1.41$. In 1987, gravitational arcs in galaxy clusters were first detected by Soucail et al. (1987) in Abell 370. More recently, the first exoplanet was detected using the gravitational lensing technique Bond et al. (2004).

2.1.2 Lens Equation

The mass distribution between the source and the observer has an effect on the propagation of light beams. However, with the exception of large scale mass distribution, it is possible to assume that the deflecting mass is projected in a specific location between source and observer. Thus, light deflection occurs only at this specific location, called the lens plane. This assumption is called thin lens approximation and it is only possible because the deflecting object has a small extent along the line-of-sight if compared to the distances between observer and lens (D_{OL}) and between lens and source (D_{LS}). The thin lens approximation is valid for most of physical situations of interest, since the typical extent of a galaxy is approximately 50 kpc and the typical extent of a galaxy cluster is 1 Mpc, while the distances between observer and lens, and lens and source are typically of the order of Gpcs.

The geometric configuration of a gravitational lens system is depicted in Figure 2.3. The light from a source located at redshift z_s, which corresponds to a distance D_S, is deflected by a mass distribution, also called lens, at a redshift z_l, which corresponds to a distance D_{OL}. The distance between the lens and the source is D_{LS}. Note that for cosmological distances, $D_{LS} \neq D_S - D_{OL}$. In Figure 2.3, the dashed line represents the optical axis that connects the observer and the source in the perpendicular source plane. This optical axis passes through the mass distribution at the lens plane, which is perpendicular to the line-of-sight.

Considering that the true, two dimensional position of the source in the source plane is $\boldsymbol{\eta}$ and that the true angular position of the source is $\boldsymbol{\beta}$, it is possible to see that $\boldsymbol{\eta} = \boldsymbol{\beta} D_S$. The impact parameter $\boldsymbol{\xi}$ is the position of the deflected light in the lens plane and can be expressed in terms of $\boldsymbol{\theta}$, the corresponding angular position, as $\boldsymbol{\xi} = \boldsymbol{\theta} D_{OL}$. For small $\boldsymbol{\theta}$, $\boldsymbol{\beta}$ and $\hat{\boldsymbol{\alpha}}$, the following geometric relation is valid:

$$\boldsymbol{\eta} = \frac{D_S}{D_{OL}} \boldsymbol{\xi} - D_{LS} \hat{\boldsymbol{\alpha}}(\boldsymbol{\xi}). \tag{2.3}$$

Dividing 2.3 by D_S and replacing $\boldsymbol{\eta}$ and $\boldsymbol{\xi}$, we obtain

$$\boldsymbol{\beta} = \boldsymbol{\theta} - \frac{D_{LS}}{D_S} \hat{\boldsymbol{\alpha}}(D_{OL} \boldsymbol{\theta}). \tag{2.4}$$

Defining the reduced deflection angle as

$$\boldsymbol{\alpha}(\boldsymbol{\theta}) := \frac{D_{LS}}{D_S} \hat{\boldsymbol{\alpha}}(D_{OL} \boldsymbol{\theta}), \tag{2.5}$$

it is possible to rewrite 2.4 so that the lens equation attains the simple form

$$\boldsymbol{\beta} = \boldsymbol{\theta} - \boldsymbol{\alpha}(\boldsymbol{\theta}). \tag{2.6}$$

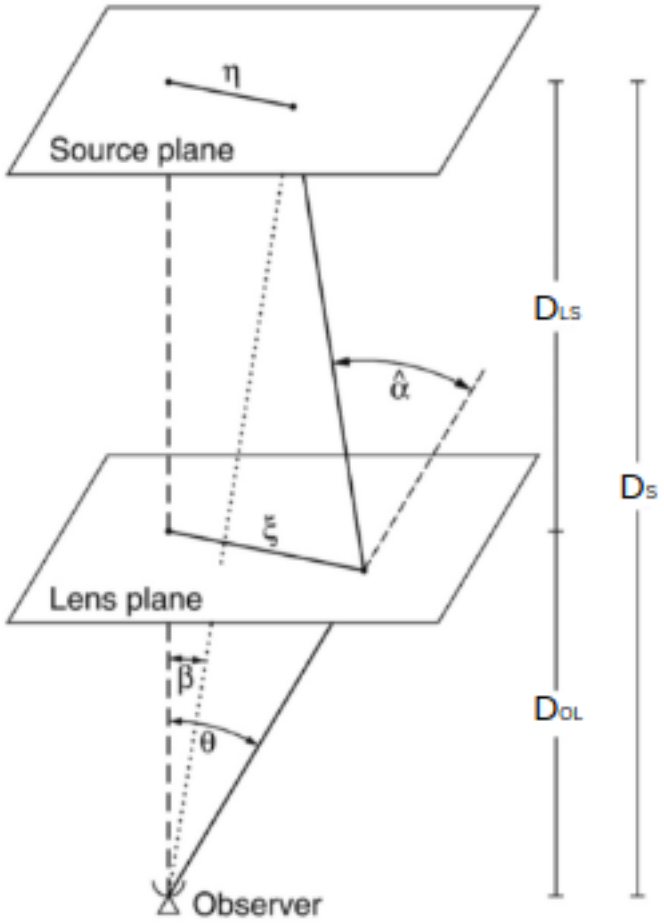

Figure 2.3: Illustration of lens configuration. Image adapted from Bartelmann & Schneider (2001)

This lens equation states that the light from a source at the true position $\boldsymbol{\beta}$ can be seen at the observed position $\boldsymbol{\theta}$. If there is more than one solution for the lens equation, the source at $\boldsymbol{\beta}$ will be observed in different positions, that is, multiple images will be detected.

2.1.3 Lens Potential

The thin lens approximation considers that the mass distribution along the line-of-sight is projected in the lens plane, so that the gravitational field of the deflector acts over light in a single point. Therefore, instead of using the three dimensional mass density, it is used the surface mass density Σ, which is obtained by integrating the mass density ρ along the line-of-sight:

$$\Sigma(\boldsymbol{\xi}) = \int_0^\infty \rho(\boldsymbol{\xi}, z) dz, \tag{2.7}$$

where $\boldsymbol{\xi}$ is a two-dimensional vector in the lens plane. Since we are considering weak gravitational fields, it is possible to describe an extended mass distribution as a linear superposition of mass elements, each one acting as a point mass. The deflection angle for a point mass is given by equation 2.2, consequently, for an extended lens, the contribution of each mass element of size $d^2\xi'$ can be expressed as

$$d\hat{\boldsymbol{\alpha}} = \frac{4G}{c^2}\Sigma(\boldsymbol{\xi'})\frac{\boldsymbol{\xi}-\boldsymbol{\xi'}}{|\boldsymbol{\xi}-\boldsymbol{\xi'}|^2}d^2\xi', \tag{2.8}$$

where ξ' is the distance of the mass element $\Sigma(\boldsymbol{\xi'})d^2\xi'$ from the origin. The total deflection angle is obtained by summing the contribution of all mass elements,

$$\hat{\boldsymbol{\alpha}}(\boldsymbol{\xi'}) = \frac{4G}{c^2}\int d^2\xi'\Sigma(\boldsymbol{\xi'})\frac{\boldsymbol{\xi}-\boldsymbol{\xi'}}{|\boldsymbol{\xi}-\boldsymbol{\xi'}|^2}. \tag{2.9}$$

This equation is valid for any mass distribution. Using the equation 2.5 and the relation $\boldsymbol{\xi} = D_{OL}\boldsymbol{\theta}$ it is possible to rewrite equation 2.9 as

$$\boldsymbol{\alpha}(\boldsymbol{\theta}) = \frac{1}{\pi\Sigma_{crit}}\int d^2\theta'\Sigma(D_{OL}\boldsymbol{\theta'})\frac{\boldsymbol{\theta}-\boldsymbol{\theta'}}{|\boldsymbol{\theta}-\boldsymbol{\theta'}|^2}, \tag{2.10}$$

where

$$\Sigma_{crit} = \frac{c^2}{4\pi G}\frac{D_S}{D_{OL}D_{LS}} \tag{2.11}$$

is the critical surface density, a quantity that characterizes the lens system and which is a function of the angular diameter distances of lens and source.

It is possible to compress equation 2.10 by defining a new quantity, the dimensionless surface mass density, or convergence, as

$$\kappa(\boldsymbol{\theta}) := \frac{\Sigma(D_{OL}\boldsymbol{\theta})}{\Sigma_{crit}}. \tag{2.12}$$

The convergence is used to distinguish the gravitational lensing regimes. A mass distribution with $\kappa \geq 1$ (or $\Sigma \geq \Sigma_{crit}$) acts as a strong lens and produces multiple and distorted images for some positions of the source. On the other hand, a mass distribution with $\kappa \ll 1$ (or $\Sigma \ll \Sigma_{crit}$) acts as a weak lens. Hence, Σ_{crit} is a specific amount for the surface mass density that represents the transition from the strong lens regime to the weak lens regime.

The identity

$$\boldsymbol{\nabla}_\theta \ln|\boldsymbol{\theta}-\boldsymbol{\theta'}| = \frac{\boldsymbol{\theta}-\boldsymbol{\theta'}}{|\boldsymbol{\theta}-\boldsymbol{\theta'}|^2}, \tag{2.13}$$

is true for any two-dimensional vector $\boldsymbol{\theta}$, thus it is possible to write $\boldsymbol{\alpha}$ as the gradient of a function

$$\boldsymbol{\alpha}(\boldsymbol{\theta}) = \boldsymbol{\nabla}_\theta \left[\frac{1}{\pi} \int \kappa(\boldsymbol{\theta'}) \ln |\boldsymbol{\theta} - \boldsymbol{\theta'}| \, d^2\theta' \right]. \tag{2.14}$$

Defining the lens potential $\psi(\boldsymbol{\theta})$ as the expression inside the brackets,

$$\psi(\boldsymbol{\theta}) = \frac{1}{\pi} \int \kappa(\boldsymbol{\theta'}) \ln |\boldsymbol{\theta} - \boldsymbol{\theta'}| \, d^2\theta', \tag{2.15}$$

it is possible to obtain that

$$\boldsymbol{\alpha}(\boldsymbol{\theta}) = \boldsymbol{\nabla}_\theta \psi(\boldsymbol{\theta}), \tag{2.16}$$

which means that the lens mapping given by equation 2.6 is a gradient mapping.

2.1.4 Distortion and Magnification

Given that the gravitational field of the lens deflects the light from a background source, multiple and distorted images are formed. These distorted images are one of the main features of the gravitational lensing effect. The shape and position of these images can be determined by solving the lens equation. If the angular scale which the properties of the lens vary is greater than the source, the lens mapping can be linearized locally, and the distortion of the images can be described by a Jacobian matrix

$$\mathcal{A}(\boldsymbol{\theta}) \equiv \frac{\partial \boldsymbol{\beta}}{\partial \boldsymbol{\theta}} = \left(\delta_{i,j} - \frac{\partial \boldsymbol{\alpha}_i(\boldsymbol{\theta})}{\partial \theta_j} \right) = \left(\delta_{i,j} - \frac{\partial^2 \psi(\boldsymbol{\theta})}{\partial \theta_i \partial \theta_j} \right), \tag{2.17}$$

which used the equations 2.6 and 2.16.

Another main feature of the gravitational lensing effect is the magnification, which is a consequence of the distortion. The deflection changes the path of the light beam without altering the number of photons emitted by the source or its wavelength (in other words, it is an achromatic effect), ensuring that the surface brightness of the lensed image is conserved. Since the surface brightness is preserved, the change of the solid angle in which the source is observed implies that the flux measured from this object is magnified (or demagnified).

Magnification is defined as the ratio between the solid angles of the image and of the source and is quantified by the inverse of the determinant of the Jacobian matrix

$$\mu \equiv \det M = \frac{1}{\det \mathcal{A}}. \tag{2.18}$$

The inverse of the Jacobian matrix, $M = \mathcal{A}^{-1}$ is called the magnification tensor and its eigenvalues, μ_r and μ_t, measure the amplification in the radial and tangential directions, respectively.

There are some particular positions for the source in the source plane where the determinant of the Jacobian is zero, hence the magnification diverge and is formally infinite.

This divergence is not a physical phenomenon, since infinite magnifications do not occur in nature. These positions define a curve in the source plane called caustics, which are not necessarily smooth and can present cusps. The critical curves, which are closed smooth curves, are obtained by mapping the caustics to the lens plane through the lens equation.

2.1.5 Lens Models

In this section we present some simple lens models. We begin with the simplest case of a point mass. We also present the models that are used in the lens modelling described in Chapter 4.

Point Mass

Gravitational lensing by point masses is the simplest case, given the simplicity of the lens and the fact that it can be solved analytically. Considering a punctual mass M at the origin of the lens plane and using equation 2.9 with $\Sigma(\boldsymbol{\xi}) = M\delta_D(\boldsymbol{\xi})$, it is possible to write the deflection angle as

$$\hat{\boldsymbol{\alpha}} = \frac{4GM}{c^2}\frac{\boldsymbol{\xi}}{|\boldsymbol{\xi}|^2}. \tag{2.19}$$

Replacing this expression in equation 2.5, the lens equation becomes

$$\boldsymbol{\beta} = \boldsymbol{\theta} - \frac{4GMD_{LS}}{c^2 D_{OL} D_S}\frac{\boldsymbol{\theta}}{|\boldsymbol{\theta}|^2} = \boldsymbol{\theta} - \theta_E^2\frac{\boldsymbol{\theta}}{|\boldsymbol{\theta}|^2}, \tag{2.20}$$

where $\theta_E = \sqrt{\frac{4GM}{c^2}\frac{D_{LS}}{D_{OL}D_S}}$ is the Einstein radius. The two possible solutions for this equation are:

$$\boldsymbol{\theta} = \frac{|\boldsymbol{\beta}| \pm \sqrt{4\theta_E^2 + |\boldsymbol{\beta}|^2}}{2}\frac{\boldsymbol{\beta}}{|\boldsymbol{\beta}|} \tag{2.21}$$

Having two possible solutions means that for each source position $\boldsymbol{\beta}$ two images are formed. For the specific case where the source is positioned exactly behind the lens ($\boldsymbol{\beta} = 0$), the solution to the lens equation is the circle $|\boldsymbol{\theta}| = \theta_E$, which is known as the Einstein ring.

The magnification follows from the Jacobian matrix

$$\det\mathcal{A} = 1 - \frac{1}{(\theta/\theta_E)^4}. \tag{2.22}$$

Thus, the magnification is

$$\mu = \left(1 - \frac{1}{(\theta/\theta_E)^4}\right)^{-1}. \tag{2.23}$$

The eigenvalues of the magnification tensor are

$$\mu_r = \left(1 + \frac{1}{(\theta/\theta_E)}\right)^{-1}, \tag{2.24}$$

$$\mu_t = \left(1 - \frac{1}{(\theta/\theta_E)}\right)^{-1}. \tag{2.25}$$

Considering the case in which $\theta \to \theta_E$, the radial magnification (μ_r) is finite while the tangential magnification (μ_t) diverges, thus forming the Einstein ring.

Singular Isothermal Sphere

Gravitational lensing by axially symmetric lenses is advantageous because their surface density is independent on the position angle with respect to the lens center. The singular isothermal sphere (SIS) profile can be used to model lenses, at least as a first approach, in order to describe properties of the galaxies or galaxy clusters that are acting as gravitational lenses. Assuming that the lens is an ideal gas in hydrostatic and thermal equilibrium confined by a spherical potential it is possible to obtain the density profile

$$\rho(r) = \frac{\sigma_v^2}{2\pi G r^2}, \tag{2.26}$$

where r is the distance to center of the sphere and σ_v^2 is the velocity dispersion of the gas particles.

Since the model is symmetric, it is possible to write $\Sigma(\boldsymbol{\xi}) = \Sigma(\xi)$, where ξ is the distance from any point to the center of the sphere. Therefore the deflection angle is

$$\hat{\boldsymbol{\alpha}} = \frac{4GM(\xi)}{c^2\xi}, \tag{2.27}$$

and M is the projected mass within radius ξ.

The surface mass density is obtained by projecting the three-dimensional density given by 2.26 along the line-of-sight. Thus, the surface mass density is

$$\Sigma_{SIS} = \frac{\sigma_v^2}{2\pi G}\int_{-\infty}^{\infty}\frac{dz}{\sqrt{\xi^2+z^2}} = \frac{\sigma_v^2}{2G\xi}. \tag{2.28}$$

The projected mass inside the radius ξ is

$$M(\xi) = 2\pi\int_0^{\xi}\Sigma(\xi')\xi' d\xi' = \frac{\pi\sigma_v^2}{G}\xi, \tag{2.29}$$

hence, the deflection angle is

$$\hat{\boldsymbol{\alpha}}_{SIS} = \frac{4\pi\sigma_v^2}{c^2}. \tag{2.30}$$

Thus, the reduced deflection angle is

$$\alpha_{SIS} = 4\pi \left(\frac{\sigma_v}{c}\right)^2 \left(\frac{D_{LS}}{D_{OS}}\right) = \theta_E. \tag{2.31}$$

It is important to mention that circularly symmetric lenses are too idealized to describe astronomical objects, like galaxies, groups of galaxies or even galaxy clusters. More realistic models can be constructed by adding more parameters, like ellipticity and a position angle to describe the lens orientation. Replacing the coordinate ξ by

$$\zeta = \sqrt{\xi_1^2 + f^2\xi_2^2}, \tag{2.32}$$

where f is the axis ratio which is taken from the interval $0 < f \leq 1$, it is possible to get the equations for the corresponding elliptical case. Hence, the surface mass density for the singular isothermal ellipsoid (SIE) is given by

$$\Sigma_{SIE} = \frac{\sqrt{f}\sigma_v^2}{2G} \frac{1}{\sqrt{\xi_1^2 + f^2\xi_2^2}} = \frac{\sqrt{f}\sigma_v^2}{2G\zeta}, \tag{2.33}$$

where $f' = \sqrt{1 - f^2}$, and the deflection angle of the SIE is given by

$$\hat{\boldsymbol{\alpha}}_{SIE} = \frac{\sqrt{f}}{f'} \left[\arcsin\left(\frac{f'}{f}\cos\phi\right)\boldsymbol{e}_1 + \arcsin(f'\sin\phi)\boldsymbol{e}_2\right], \tag{2.34}$$

where ϕ is the angle of the polar coordinates and $\boldsymbol{e}_i$ is the unit vector in the x_i direction (Kormann et al., 1994).

Navarro-Frenk-White Density Profile

In order to model groups of galaxies and clusters it is necessary to take into account the dark matter contribution. A very well known model is the Navarro-Frenk-White (NFW) density profile (Navarro et al., 1997), which was obtained from dark matter N-body simulations. This profile is described by

$$\rho(r) = \frac{\rho_s}{\left(\frac{r}{r_s}\right)\left(1 + \frac{r}{r_s}\right)^2}, \tag{2.35}$$

where ρ_s is a characteristic density, given by

$$\rho_s = \frac{\Delta\rho_c}{3} \frac{c^3}{\left[\ln(1 + c_\Delta) - \frac{c_\Delta}{1+c_\Delta}\right]}, \tag{2.36}$$

and r_s is a scale radius, given by

$$r_s = \frac{r_\Delta}{c_\Delta} = \frac{1}{c_\Delta}\left(\frac{3M_\Delta}{4\pi\Delta\rho_c}\right)^{1/3}, \tag{2.37}$$

and the halo concentration, c_Δ is defined as

$$c_\Delta \equiv \frac{r_\Delta}{r_s} \ . \tag{2.38}$$

The mass enclosed within radius r is given by

$$M(r) = \int_0^r 4\pi r'^2 \rho(r)' dr' = \frac{4\pi\rho_s r^3}{c_\Delta^3}\left[\ln(1+c_\Delta) - \frac{c_\Delta}{1+c_\Delta}\right]. \tag{2.39}$$

When, $r \to \infty$ the mass of the cluster diverges, however, it is possible to define a "cluster radius", $r = r_\Delta$, which encircles a region with density Δ times greater than a reference density. The reference density is usually adopted to be the critical density of the Universe, ρ_c. The virial mass and radius of the cluster is usually defined for $\Delta = 200$, but the exact value of the virial Δ depends on the Cosmology. For the Einstein – de Sitter model ($\Omega_m = 1$ and $\Omega_\Lambda = 0$), $\Delta \sim 178$, and for $\Omega_m = 0.3$ and $\Omega_\Lambda = 0.7$, $\Delta \sim 100$ (Bryan & Norman, 1998).

It is important to notice that the profile has slopes that depend on the range fitted, steepening from -1 near the center to -3 at large r/r_s. The scale radius r_s corresponds to the region where the logarithmic slope of the density profiles equals the isothermal value. Therefore, the NFW profile is shallower than a SIE profile in the central region of the cluster, and steeper than SIE in the outskirts of the cluster.

Taking equation 2.35 and choosing $r_s = \xi_0$ it is possible to obtain the surface density

$$\Sigma = \frac{2\rho_s r_s}{x^2-1} f(x), \tag{2.40}$$

where $f(x)$ is

$$f(x) = \begin{cases} 1 - \frac{2}{\sqrt{x^2-1}}\arctan\sqrt{\frac{x-1}{x+1}} & (x>1) \\ 1 - \frac{2}{\sqrt{1-x^2}}\operatorname{arctanh}\sqrt{\frac{1-x}{1+x}} & (x<1) \\ 0 & (x=1) \end{cases} \ . \tag{2.41}$$

and x is the position of the lensed image normalized by r_s.

The lens potential is given by

$$\psi = 4\kappa_s g(x), \tag{2.42}$$

with

$$\kappa_s = \rho_s \Sigma_{cr}^{-1}, \tag{2.43}$$

and

$$g(x) = \frac{1}{2}\ln^2\frac{x}{2} + \begin{cases} 2\arctan^2\sqrt{\frac{x-1}{x+1}} & (x>1) \\ 2\operatorname{arctanh}^2\sqrt{\frac{1-x}{1+x}} & (x<1) \\ 0 & (x=1) \end{cases} \ . \tag{2.44}$$

Therefore, the deflection angle is given by

$$\alpha(x) = \frac{4\kappa_s}{x} h(x) \tag{2.45}$$

where

$$h(x) = \ln\frac{x}{2} + \begin{cases} \frac{2}{\sqrt{x^2-1}}\arctan\sqrt{\frac{x-1}{x+1}} & (x > 1) \\ \frac{2}{\sqrt{1-x^2}}\operatorname{arctanh}\sqrt{\frac{1-x}{1+x}} & (x < 1) \\ 1 & (x = 1) \end{cases} . \tag{2.46}$$

2.2 Lens modelling

In this work, we use the semilinear inversion (SLI) method (Warren & Dye, 2003) to model the mass distribution of the lens and to reconstruct the unlensed emission of the source.

This methods assumes a pixelized source plane and a parametric model for the lens mass distribution. For a given lens model, the method computes the linear superposition of lensed images of each source plane pixel that best fit the observed lensed image. The SLI method simplifies the parameter space by separating the lens parameters from the source parameters. The step of inverting the image to obtain the pixelized source light distribution that minimize the merit function is a linear one, for a given lens mass distribution. Thus, by searching the mass parameter space for the lens model, it is possible to find the minimum of these minimum of the merit function. Searching the parameter space is a nonlinear step, being the reason why the method is called semilinear. This process simplifies the search for best-fit parameters, speeding up the inversion and producing an unbiased solution.

The SLI method was successfully applied in many science cases, such as the measurement of the density profile of the lens galaxy in the Einstein ring system 0047-2808 (Dye & Warren, 2005). It was also used on the modelling of the first strong lenses systems from the Herschel-ATLAS survey (Dye et al., 2014). The method is suitable to model high-resolution data, being used to reveal the complex nature of SDP.81 lens system (Dye et al., 2015). Moreover, the SLI method was adapted to deal with interferometric data and it was used to analyze highly star-forming lensed galaxies that were detected with Herschel and observed with ALMA (Dye et al., 2018).

In the following, we briefly describe the theory of the SLI method. We begin with the case in which the parameters of the lens model are fixed and then we expand for the general case, in which the minimization is also on the lens mass parameters.

2.2.1 Semilinear Inversion method

For a fixed lens model, in order to find the counts in the source pixels, it is required to minimize the merit function G, which is simply

$$G = \chi^2. \tag{2.47}$$

Pixels in the source plane can change in size and shape, and are labeled $i = 1, ..., I$. Pixels in the image plane should include only counts from the lensed source and are labeled $j = 1, ..., J$. This method assumes that the data in each pixel are characterized by the counts d_j and uncertainty σ_j. It is also assumed that the image pixels are independent, i.e., that there is no covariance between pixels, which is appropriate for CCD data.

Using a given lens model, an image of each pixel i is formed by suitable ray tracing using the lens equation 2.6 and convolving with the point spread function (PSF). Thus, the problem is to minimize G combining these I images and the scalings s_i, which are the source counts.

Rewriting the merit function

$$G = \chi^2 = \sum_{j=1}^{J} \left(\frac{\sum_{i=1}^{I} s_i f_{ij} - d_j}{\sigma_j} \right)^2, \tag{2.48}$$

where f_{ij} is the mapping from the source to the image plane, which uses the lens equation, including the appropriate deflection angle for that given lens model.

Minimizing the merit function with respect to the source terms s_i, we obtain

$$\frac{1}{2}\frac{\partial G}{\partial s_i} = 0 = \sum_{j=1}^{J} \left(\frac{f_{ij} \sum_{k=1}^{I} s_k f_{kj} - f_{ij} d_j}{\sigma_j^2} \right), \tag{2.49}$$

where the factor 1/2 will be explained later. Rewriting these equations in the matrix form

$$\mathbf{FS} = \mathbf{D}, \tag{2.50}$$

where $\boldsymbol{F}$ is a symmetric $I \times I$ matrix containing the elements $F_{ik} = \sum_{j=1}^{J} f_{ij} f_{kj} / \sigma_j^2$, $\boldsymbol{S}$ is a column matrix of length I with elements s_i and $\boldsymbol{D}$ is a column matrix of length I with elements $D_i = \sum_{j=1}^{J} f_{ij} d_j / \sigma_j^2$.

It is possible to find the counts in the source pixels by calculating the matrix inversion

$$\boldsymbol{S} = \boldsymbol{F}^{-1} \boldsymbol{D}. \tag{2.51}$$

Searching for the covariance matrix in the source pixels provide a simple solution for the errors. The matrix $\boldsymbol{F}$

$$F_{ik} = \frac{1}{2}\frac{\partial^2 G}{\partial s_i \partial s_k}, \tag{2.52}$$

is 1/2 of the Hessian matrix of the χ^2, explaining the factor 1/2 in equation 2.49.

In order to find the solution for the errors, it is required to obtain the covariance matrix of $\boldsymbol{S}$, which is $\boldsymbol{C} = \boldsymbol{F}^{-1}$. The covariance between source pixels i and k is given by

$$\sigma_{ik}^2 = \sum_{j=1}^{J} \sigma_j^2 \frac{\partial s_i}{\partial d_j}\frac{\partial s_k}{\partial d_j}, \tag{2.53}$$

for independent pixels. Using equation 2.51,

$$\sigma_{ik}^2 = \sum_{j=1}^{J} \sigma_j^2 \sum_{l=1}^{I} C_{il}\frac{f_{ij}}{\sigma_j^2} \sum_{m=1}^{I} C_{km}\frac{f_{mj}}{\sigma_j^2}, \tag{2.54}$$

resulting in

$$\sigma_{ik}^2 = C_{ik}. \tag{2.55}$$

This linear approach is for a given lens model. For the purpose of finding the full solution, it is necessary to search through the mass distribution parameter space, which is a nonlinear procedure. During the search in the parameter space, the χ^2 is minimized at each point by linear inversion, therefore, finding the global minimum.

2.2.2 Semilinear Inversion with Regularization

In order to penalize noisy solutions, it is possible to form a different merit function by adding to the χ^2 a term G_L that is a linear combination of terms $s_i s_k$,

$$G_L = \sum_{i,k} a_{ik} s_i s_k, \tag{2.56}$$

since the partial differentials of these terms are linear. Thus, the merit function can be written as

$$G = \chi_{im}^2 + \lambda G_L, \tag{2.57}$$

where λ is a constant that "weights" the regularization term.

Minimizing the merit function with respect to the source terms, it is possible to write the solution for the counts in the source pixels in the matrix form

$$\boldsymbol{S} = [\boldsymbol{F} + \lambda \boldsymbol{H}]^{-1} \boldsymbol{D}, \tag{2.58}$$

where $\boldsymbol{H}$ is the regularization matrix with elements

$$H_{ik} = \frac{1}{2}\frac{\partial^2 G_L}{\partial s_i \partial s_k}. \tag{2.59}$$

One example of linear regularization term is

$$G_L = \sum_{i=1}^{I} s_i^2, \tag{2.60}$$

which was termed "zeroth-order" regularization in the literature.

The source covariance matrix can be obtained by writing $\boldsymbol{R} = [\boldsymbol{F} + \lambda \boldsymbol{H}]^{-1}$ and following through the same analysis as § 2.2.1. Therefore,

$$\sigma_{ik}^2 = \sum_{j=1}^{J} \sigma_j^2 \sum_{i=1}^{I} R_{il} \frac{f_{lj}}{\sigma_j^2} \sum_{m=1}^{I} R_{km} \frac{f_{mj}}{\sigma_j^2}, \tag{2.61}$$

resulting in

$$\sigma_{ik}^2 = R_{ik} - \lambda \sum_{l=1}^{I} R_{il} \left[\boldsymbol{RH}\right]_{kl}. \tag{2.62}$$

Again, this linear approach is for a given lens model. The procedure to find the full solution is the same as for the unregularized case.

2.2.3 Markov Chain Monte Carlo

The search for the global minimum in the mass distribution parameter space is performed by using Markov Chain Monte Carlo (MCMC) method. The MCMC begins at any location $\overrightarrow{p}$ in the parameter space and this should result in convergence. The initial location is given by

$$\overrightarrow{p} = (p_{1,i}, p_{2,i}, ..., p_{n,i}), \tag{2.63}$$

where $p_{1,i}, p_{2,i}, ..., p_{n,i}$ are the initial n parameters.

After that, the likelihood at this point is computed $\mathcal{L}_{\overrightarrow{p}}$. The jump function proposes a jump to a different location given by

$$\overrightarrow{n} = (p_{1,j}, p_{2,j}, ..., p_{n,j}), \tag{2.64}$$

and the likelihood is also computed at this point. Calculating the ratio of the likelihood

$$a = \frac{\mathcal{L}_{\overrightarrow{p}}}{\mathcal{L}_{\overrightarrow{n}}}, \tag{2.65}$$

the algorithm determines whether to accept or reject the jump. The acceptance criteria is, if $a \geq 1$ then always accepts the jump, however, if $a < 1$ accepts the jump with a probability of a. Thus, iteratively it converges towards the global minimum.

Chapter 3

HELMS18 lens system

Negrello (2010) proposed a method to select a sample of strongly lensed sources from Herschel Space Observatory surveys that achieves almost 100 per cent of efficiency. Several Herschel teams, such as the Herschel Astrophysical Terahertz Large Area Survey (H-ATLAS; Eales et al., 2010a) and Herschel's Hermes Large Mode Survey (HELMS; Oliver et al., 2012), have used this method to select samples of lensed sources candidates. Then, they used molecular line spectroscopy to measure the redshifts and confirm the lensing nature of the sources and interferometric observation in submillimeter wavelengths to obtain high-resolution data for an accurate lensing model.

The H-ATLAS and HELMS teams submitted a joint proposal to obtain Atacama Large Millimeter/Submillimeter Array (ALMA) observations of a sample of 42 sources selected from both surveys with the highest $500-\mu$m flux densities, with $z > 1$ and without any radio-loud AGN signature. Of the 42 sources, only 16 were observed by ALMA in its Cycle 2 (Amvrosiadis et al., 2018). Among the observed sources is HELMS18, which is the subject of this work. The lens modelling of ALMA imaging of six galaxy-galaxy strong lens systems from this sample was presented in Dye et al. (2018). For the remaining nine sources in the sample, the modelling of the submillimeter emission is ongoing.

HELMS18 is a submillimeter source at redshift $z = 2.39$. This object is also called HeLMS J005159.4+062240. The first detection was in the HELMS survey as a candidate of gravitationally lensed dusty-star forming galaxies by Nayyeri et al. (2016), using the method described in Negrello et al. (2010). The spectroscopic redshift of HELMS18 was obtained using CO emission lines. HELMS18 is part of the sample that was followed-up with ALMA in order to confirm the lensing nature of this source and to obtain some of its intrinsic properties (Amvrosiadis et al., 2018).

In Table 3.1, we present the coordinates and the submillimeter photometry obtained by the Herschel Space Observatory using the Spectral and Photometric Imaging Receiver (SPIRE; Griffin et al., 2010) at the wavelengths 250, 350, and 500 μm. In Figure 3.1, we present the postage stamp images of HELMS18 in the Herschel far-infrared bands.

Object name	RA	Dec	$S_{250} \sim$ (mJy)	$S_{350} \sim$ (mJy)	$S_{500} sim$(mJy)
HELMS18	$00^h51^m59^s.5$	$+06°\ 22'41''$	166 ± 6	195 ± 6	135 ± 7

Table 3.1: Coordinates and flux densities of HELMS18 in Herschel/SPIRE bands.

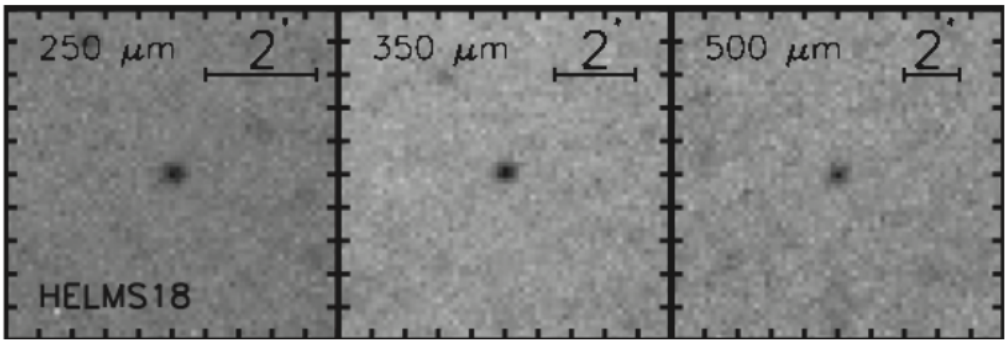

Figure 3.1: Postage stamp images of HELMS18 obtained with Herschel/SPIRE. Image taken from Nayyeri et al. (2016).

According to Amvrosiadis et al. (2018), HELMS18 system has an Einstein radius of $\theta_E = 6.54'' \pm 0.05$, which was measured from the observed image and compared with a preliminary lensing model. Nayyeri et al. (2016) fitted the far-infrared spectral energy distribution (SED) of HELMS18 with modified black-body, which provided the best-fit total infrared luminosity (integrated over $8-1000$ μm) $\log(L_{IR}/\mathrm{L}_\odot) = 13.46$ and dust temperature $T_d = 30.5$ K. In both works, no redshift for the foreground lens was assigned.

In this chapter we describe all the multi-wavelength data we gathered of the HELMS18 system, which includes the public ALMA Band 7 data, photometric and spectroscopic optical data from the 14th data release of Sloan Digital Sky Survey and new multi-object spectroscopic data we obtained with the Gemini Telescope. These data are used to obtain a complete description of HELMS18 lens system.

3.1 ALMA data

In this section we briefly describe the technique used to obtain high-resolution images of astronomical objects using interferometry and the follow-up observations of HELMS18 obtained with the interferometer ALMA.

3.1.1 Interferometry

ALMA is an interferometer located in northern Chile and consists of an array of 66 antennas that can be positioned in many configurations (Figure 3.2).

Figure 3.2: ALMA antennas on the Chajnantor Plateau of the Chilean Andes. Photograph taken by Norikazu Mizuno (NAOJ, https://alma-telescope.jp/en/news/mt-post_31-2).

Interferometers like ALMA measure the interference pattern of the signal from two antennas separated by a baseline B. This interference pattern is directly related to the source brightness. More especifically, an interferometer measures discrete components of the spatial frequency spectrum of the observed object's brightness distribution on the sky. This spatial spectrum is often called the "visibility function", a complex function in the general case. In particular, for small fields of view, the complex visibility function, $V(u, v)$, is the two-dimensional Fourier transform of the brightness distribution on the sky, $I(x, y)$:

$$V(v, v) = \int \int I(l, m) e^{-2\pi i[ux+vy]} dxdy. \tag{3.1}$$

The spatial frequencies sampled are a function of the locations of the interferometer's apertures (coordinates u and v on the uv plane), the location of the source in the sky (coordinates x and y on the image plane), and the wavelength of observation (see Figure 3.3). The locus of a baseline in the visibility plane is the projected length as seen from a source at the interferometer pointing center.

The interferometer measures $V(u, v)$ only where the baselines are, which means that this function is sampled on a discrete number of points. A good image quality requires a good coverage of the uv plane. The Earth rotation, which slowly turns the antennas with respect to the source, can be used to increase the number of different baselines included in an observation.

The Fourier transform of the sampling function results in the dirty beam (point spread function). Taking the Fourier transform of the sampled visibilities results on the dirty image, which is the true sky brightness distribution convolved with the dirty beam. This image usually presents several artifacts, that reflect the incompleteness of the uv sampling. In order to correct for the incomplete sampling of the uv plane a deconvolution process called "CLEAN" is performed. The resulting cleaned image corresponds to the true image

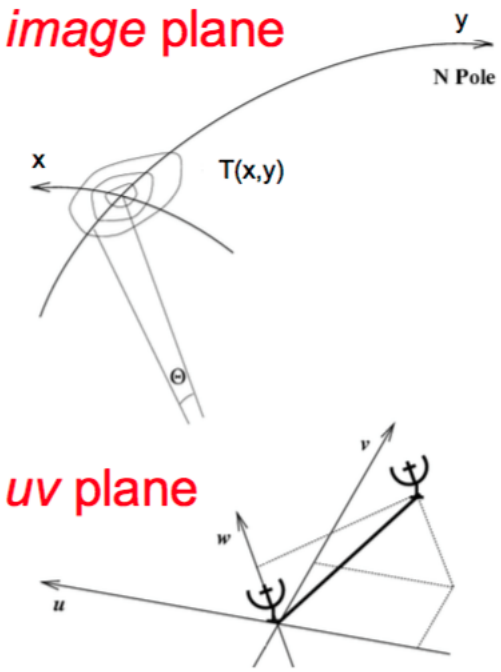

Figure 3.3: Illustration of the image and uv planes used in interferometry. Image taken from https://science.nrao.edu.

convolved with the clean beam, which is described by the two-dimensional Gaussian fitting of the dirty beam. The cleaned image is the final image used for scientific purposes.

3.1.2 ALMA observations of HELMS18

ALMA observations of HELMS18 were taken from the ALMA Science Portal* (data set ADS/JAO.ALMA#2013.1.00358.S; PI: S. Eales) The spectral setup comprises Band 7 continuum observations in four spectral windows, each of width 1875 MHz centerd on the frequencies 336.5, 338.5, 348.5 and 350.5 GHz. In each spectral window, there are 128 frequency channels giving a resolution of 15.6 MHz. Forty two 12 m antennas were used with an on-source integration time of 151.2 s. This results in an angular resolution of approximately 0.12″. The calibration and imaging of the data were performed using the scripts provided on the ALMA Science Portal and the Common Astronomy Software Application package (CASA†).

Figure 3.4 shows the cleaned ALMA image of the system, where two gravitational arcs (distorted images of the background HELMS18 submillimeter source), with Einstein radius $\theta_E = 6.54''$ (Amvrosiadis et al., 2018), are observed. It is worth noticing that both arcs are not pointed to the same geometrical center.

*http://www.almasicence.org
†http://casa.nrao.edu

The image from Figure 3.4 will be used for the lens modelling performed in Chapter 4.

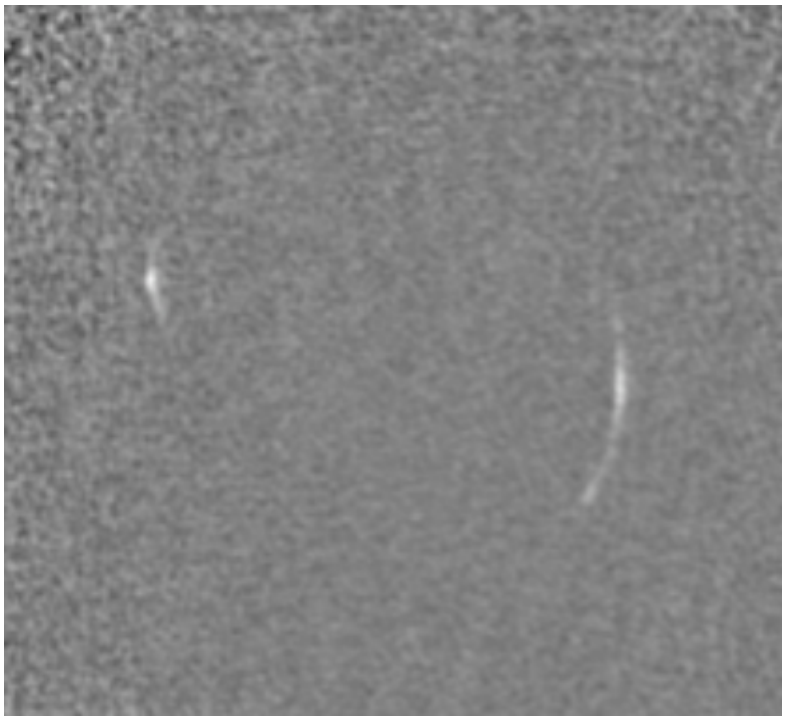

Figure 3.4: ALMA Band 7 observation of the lensed emission of HELMS18 submillimeter galaxy, showing the two gravitational arcs. North is up and East is left.

3.2 Sloan Digital Sky Survey data

We obtained the optical information of this lens system from the Sloan Digital Sky Survey - Data Release 14 (SDSS-DR14) database. When superposing the ALMA data and the SDSS image of the system, we found that there are two objects within the gravitational arcs, which indicates that this is a group-scale lens with two central galaxies. In Figure 3.5, we show the colour-composite SDSS image of the group of galaxies and the superposition of the SDSS and ALMA data. One of these central objects is a red and passive early-type galaxy (ETG) that has SDSS spectroscopic data and is at $z = 0.6$. The SDSS spectrum of this galaxy is shown in Figure 3.6.

The other object is very blue and has no SDSS spectrum available and it is classified as a star in the photometric catalogue. However, bright and compact extragalactic systems, such compact starburst galaxies and distant quasars, can be wrongly classified as stars when only photometry is used for the classification (e.g. Bai et al., 2019; Logan & Fotopoulou, 2020). Therefore, to investigate the true nature of this blue object, we compared its colour and magnitude with those of quasars at redshifts close to that of the passive central galaxy ($z \sim 0.6$). To obtain the SDSS-DR14 colours and magnitudes of the quasars, we used the following query:

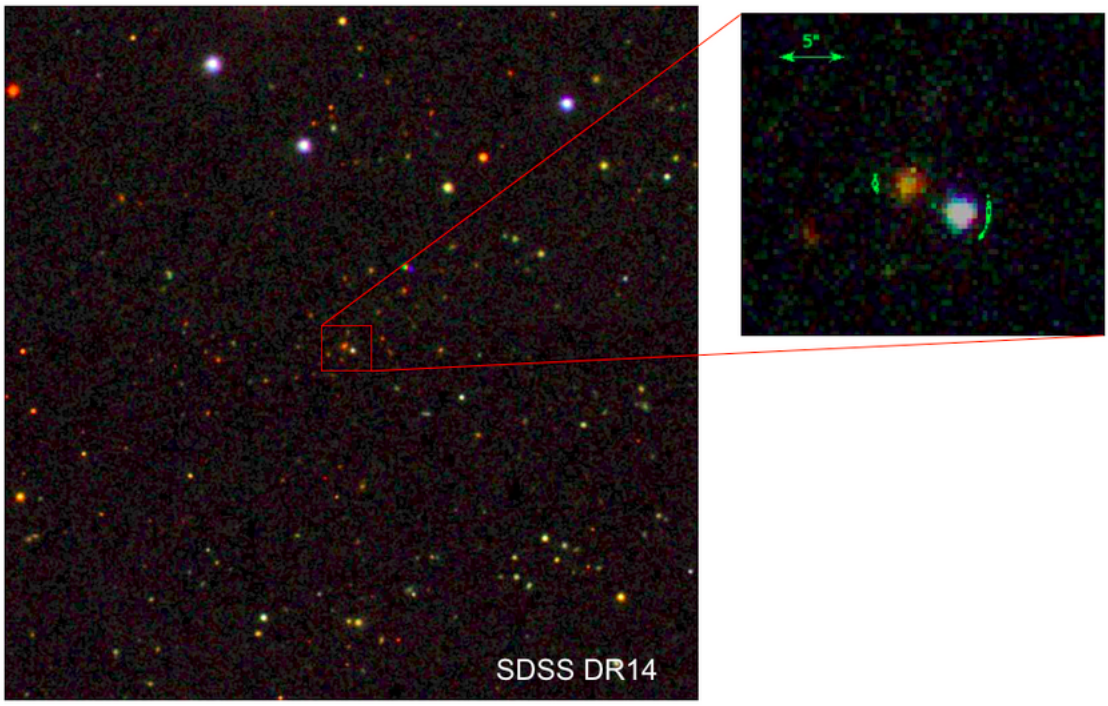

Figure 3.5: SDSS colour-composite image of the group of galaxies (5.6 x 5.6 arcmin, *left*). The *right* panel shows the superposition of the optical (*colored*) and ALMA data (*green*) of the central region of the group. North is up and East is left.

```
SELECT  p.objID, s.ra, s.dec, s.z,
        p.petromag_g - p.extinction_g as g_Petro,
        p.petromag_r - p.extinction_r as r_Petro,
        p.petromag_i - p.extinction_i as i_Petro
FROM    SpecObj as s, PhotoObj as p
WHERE   p.petromag_r <= 22 AND p.petromag_r >= 18 AND
        s.class = 'QSO' AND
        s.z > 0.55 AND s.z < 0.65 AND
        p.objID = s.bestobjID
```

We found 16 106 objects that satisfy the query criteria, i.e., spectroscopic objects with r-band Petrosian magnitudes `petromag_r` between 18 and 22 that are spectroscopically classified as QSOs and are at $0.55 < z < 0.65$. In Figure 3.7 we show the $(g-i)_{\rm Petro}$ colours versus $r_{\rm Petro}$ of the quasars, where $g_{\rm Petro}$, $r_{\rm Petro}$, and $i_{\rm Petro}$ are the extinction-corrected Petrosian magnitudes in the g, r, and i bands. The position of the blue central object in the colour-magnitude diagram shown in Figure 3.7 suggests that this system is likely to be a quasar at the same redshift of the passive central galaxy (what we later confirmed with data obtained at Gemini Observatory, see Section 3.3).

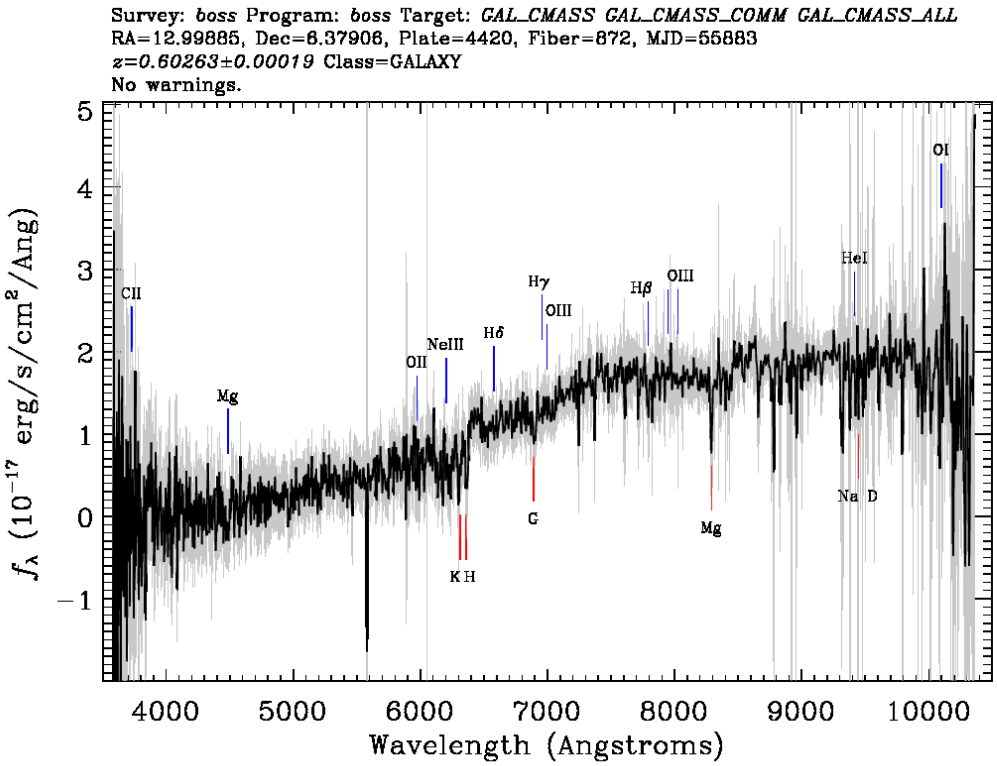

Figure 3.6: SDSS spectrum of the passive galaxy within the gravitational arcs of the HELMS18 lens system. This galaxy is at $z = 0.6$ and it is likely to be one of the central galaxy of a group that is lensing the background galaxy HELMS18. This figure was extracted from the Skyserver SDSS webtool (http://skyserver.sdss.org/).

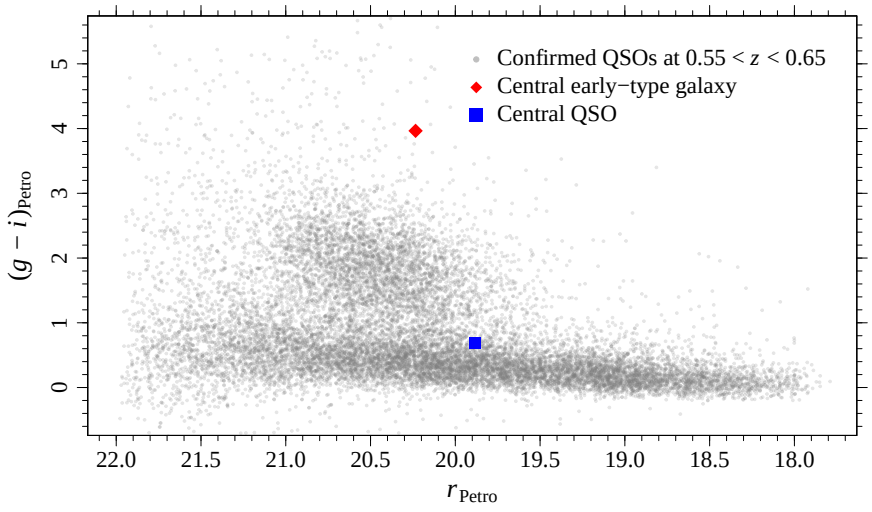

Figure 3.7: Colour-magnitude diagram of spectroscopically confirmed quasars at $0.55 < z < 0.65$ (*grey circles*) and with $18 \leq r_{\rm Petro} \leq 22$, where $r_{\rm Petro}$ is the extinction-corrected Petrosian magnitude in the r band. The quasars were selected from the SDSS-DR14 database by retrieving objects classified as "QSO" in the spectroscopic catalogue. The position of the blue central galaxy (*blue square*) in the colour-magnitude diagram is compatible with the position of the confirmed quasars at the redshift of the central ETG galaxy ($z = 0.6$, *red diamond*).

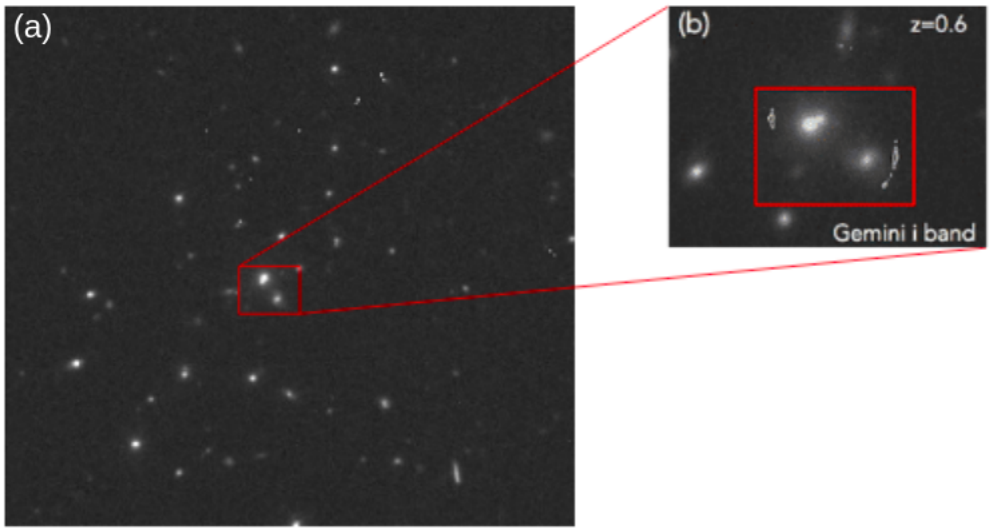

Figure 3.8: (a) Gemini i band image of the group of galaxies. (b) Zoom in the inner region of the group showing the two brightest central galaxies superposed with ALMA observations (*white*) of the lensed emission of HELMS18. North is up and East is left.

3.3 Gemini multi-object spectroscopic data

As part of the project, we conducted multi-object spectroscopic observations using the Gemini Multi-Object Spectrograph (GMOS[‡]) installed in the Gemini South Observatory to target both the group members and the two brightest central galaxies of the group that is strongly lensing the background galaxy in HELMS18 system. In Figure 3.8, we show Gemini i band image of the group of galaxies and a zoom in the inner region of showing the two brightest central galaxies superposed with ALMA data. The observation setup, data description and reductions are described below.

3.3.1 Observations

The observations were carried out from September to November 2019 (Gemini program ID GS-2018B-Q-113). We used GMOS-MOS with the R400-G5325 grating combined with G455 high-order blocking filter to observe the group-scale lens. The grating's resolution of R $\sim$ 1000 (for slitlet width of 1″) was suitable for our purposes, and the grating covers the rest-frame spectral interval from $\sim$ 3500 Å to $\sim$ 6000 Å, allowing the observation of the 4000 Å break, the CaII HK, Hγ, Hβ, Mgb, and NaD absorption features, and the Hγ, Hβ, [OIII]λ4959, 5007 Å emission lines of the QSO candidate.

To maximize the number of observed group-member candidates, we created observation masks for two different position angles. The criteria used to select the target galaxies for

[‡]https://www.gemini.edu/sciops/instruments/gmos/

each mask were based on the optical information retrieved from the SDSS-DR14 database. We selected the targets in the following order of priority: *i*) galaxies that are likely to be in the red sequence of the group; *ii*) galaxies with photometric redshifts close the redshift of the central ETG; *iii*) other bright galaxies in the field, regardless of their colour.

The galaxy color magnitude diagram shows two distinct populations, the red sequence, which are elliptical galaxies that are no longer forming stars and can be found on galaxy clusters, and the blue cloud, which usually are spiral galaxies that still have ongoing star formation(Strateva et al., 2001). To identify the red sequence of the group, we selected all photometric objects within 3′ from the central ETG and obtained their magnitudes and photometric redshits from the SDSS database using the query below.

```
SELECT  p.objID, p.ra, p.dec, z.z as photoZ, z.zErr as photoZerr,
        p.petromag_g - p.extinction_g as g_Petro,
        p.petromag_r - p.extinction_r as r_Petro,
        p.petromag_i - p.extinction_i as i_Petro
FROM    PhotoObj as p, fGetNearbyObjEq(12.99894, 6.37902, 3) as n,
        PhotoZ as z
WHERE   n.objID = p.objID AND z.objID = m.objID AND z.z > 0
```

In Figure 3.9, we illustrate how we used the colours and photometric redshifts to identify the red sequence of the group. We selected the galaxies indicated as red symbols in the colour-magnitude diagram (left panel in Figure 3.9) and found that the distribution of their photometric redshifts peaks around $z \sim 0.6$. The median photometric redshifts of galaxies with colours between $0.9 \leq (r-i)_{\rm Petro} \leq 1.5$ is $z_{\rm photo} = 0.59$ with scatter $\sigma_{z\rm photo} = 0.12$. We also identified other possible structure at $z \sim 0.4$ containing red-sequence member galaxies with colours $0.1 \leq (r-i)_{\rm Petro} \leq 0.7$, as indicated in the colour-magnitude diagram in the left panel of Figure 3.9.

3.3.2 Data Reduction and Analysis

The data reduction was performed using the Gemini `IRAF` package v1.14[§], following the standard reduction procedure. This process included: subtraction of the overscan level, bias subtraction, flat field correction, wavelength calibration, quantum efficiency correction, cosmic rays removal, sky subtraction, spectra extraction and flux calibration. Here we present the results for the two central galaxies; the data reduction of the remaining galaxies is still ongoing. For the purposes of the lens modelling, only the redshifts of the two central targets that are within the lens arcs are required.

[§] https://www.gemini.edu/node/11823

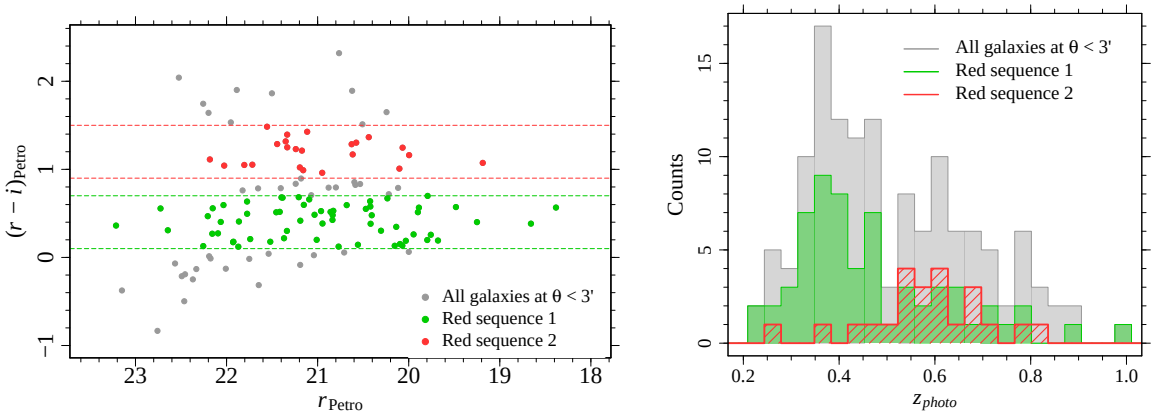

Figure 3.9: Possible structures identified along the line of sight of the HELMS18 system. **Left:** Colour-magnitude diagram of SDSS galaxies at angular distances $\theta < 3'$ from the central ETG. The galaxies with $(r-i)_{\rm Petro}$ colours ranging from 0.1 to 0.7 and from 0.9 to 1.5 are indicated by the *green* and *red* symbols, respectively. **Right:** Ditribution of the photometric redshifts of the galaxies shown in the left panel, indicating two structures at $z \sim 0.4$ and $z \sim 0.6$. The latter corresponds to the group that is lensing the background galaxy of the HELMS18 system.

To determine the spectroscopic redshift of the two central galaxies we used the tasks `EMSAO` and `XCSAO` of the `IRAF` Radial Velocity Package `RVSAO`[¶] (Kurtz & Mink, 1998). The task `EMSAO` uses emission line shifts to measure the radial velocities, while the `XCSAO` relies on cross-correlation methods. We used the rest-frame spectra of 10 nearby passive galaxies as templates for the `XCSAO` cross-correlation procedure. Using the task `XCSAO`, we find that the redshift of the central ETG is $z_{\rm ETG,XC} = 0.60246 \pm 0.00004$, and the agreement with the value from the SDSS-DR14 is within the errors ($z_{\rm ETG,SDSS} = 0.6026 \pm 0.0002$).

The redshift of the quasar was determined using both the emission-line ($z_{\rm QSO,EM}$) and the cross-correlation ($z_{\rm QSO,XC}$) methods, and we obtain $z_{\rm QSO,EM} = 0.59852 \pm 0.00007$ and $z_{\rm QSO,XC} = 0.59945 \pm 0.00009$. The difference between these two measurements suggests an outflow of gas with velocity $v_{\rm gas} = 278 \pm 34\,{\rm km\,s^{-1}}$ relative to the quasar, and the relative velocity between the two central galaxies is $\Delta v = c\,(z_{\rm ETG,XC} - z_{\rm QSO,XC}) = 903 \pm 30\,{\rm km\,s^{-1}}$.

In Figures 3.10 and 3.11, we show the spectra of these two objects. We compare the Gemini spectrum of the central ETG with that from the SDSS database, and the differences between them due to slit size, resolution and difference between instruments is within 10%, as shown in Figure 3.10. The spectrum of the second object is shown in Figure 3.11. We were able to identify the [OII]λ3727, [NeIII]λ3869, Hγ, Hβ, [OIII]λ4959, and [OIII]λ5007 emission lines, as indicated in Figure 3.11. We computed the bolometric luminosity, $L_{\rm bol}$, by applying the $L_{\rm bol} - L_{\rm [OIII]}$ relation by Pennell et al. (2017), where $L_{\rm [OIII]}$ is the [OIII]λ5007 emission-line luminosity:

$$\log(L_{\rm bol}) = (0.5617 \pm 0.0978)\ \log(L_{\rm [OIII]}) + (22.186 \pm 4.164). \quad (3.2)$$

[¶] http://tdc-www.harvard.edu/iraf/rvsao/

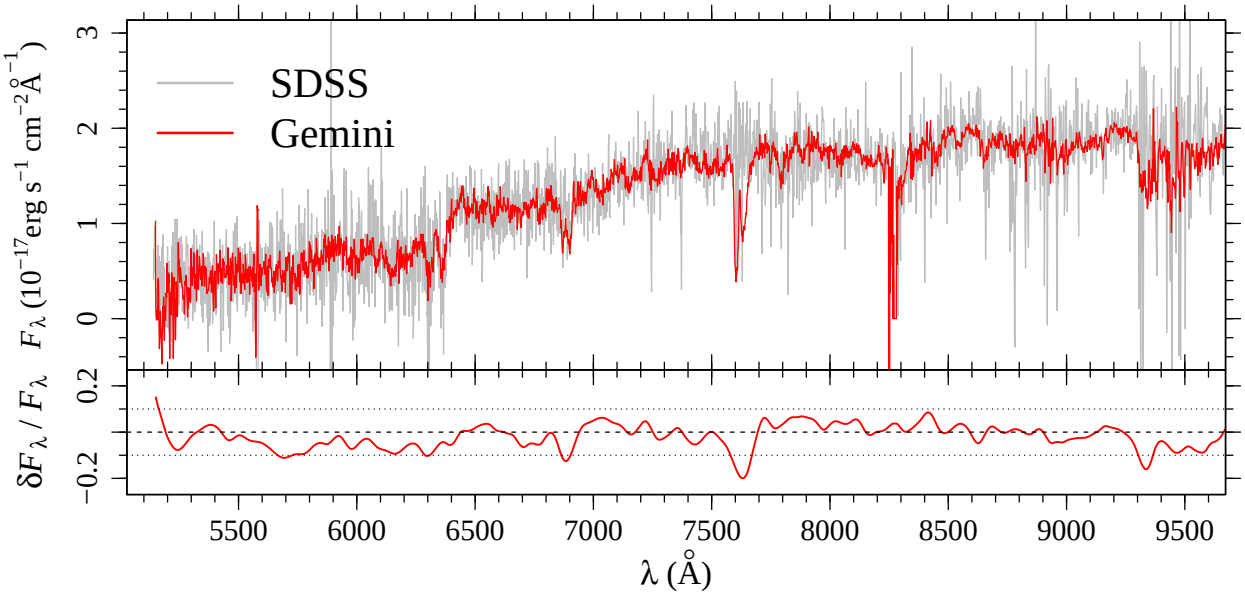

Figure 3.10: The SDSS (*grey line*) and Gemini (*red line*) spectra of the central passive group galaxy. The lower panel shows the residuals of the comparison between the SDSS and Gemini spectra. The *dashed* and *dotted* lines indicate $\delta F_\lambda/F_\lambda = 0 \pm 10\%$, which is due to the slit size, the resolution and the difference between instruments.

We used the `IRAF` task `SPLOT` to measure the [OIII]λ5007 flux within the slitlet aperture of $1''$. To compute the total flux, $F_{[\mathrm{OIII}]}$, we applied a correction factor that takes into account the fraction of the flux outside the aperture of the slitlet. Using the SDSS Petrosian radius of this galaxy, $\theta_{\mathrm{Petro}} = 1.63''$, we estimate that the flux within the slitlet aperture is 38.4% of the total flux, $F_{[\mathrm{OIII}]}$. Following this procedure, we obtain $F_{[\mathrm{OIII}]} = 5.94 \times 10^{-16}\,\mathrm{erg\,s^{-1}}$. Therefore,

$$L_{[\mathrm{OIII}]} = F_{[\mathrm{OIII}]}\, 4\,\pi\, D_{\mathrm{L}}(z_{\mathrm{QSO,XC}}) = 9.5 \times 10^{41}\mathrm{erg\,s^{-1}}, \tag{3.3}$$

where $D_{\mathrm{L}}(z_{\mathrm{QSO,XC}})$ is the luminosity distance at $z = z_{\mathrm{QSO,XC}}$, computed by assuming the cosmological parameters $H_0 = 67\,\mathrm{km\,s^{-1}\,Mpc^{-1}}$, $\Omega_{\mathrm{M}} = 0.32$ and $\Omega_\Lambda = 0.68$. Finally, using Equation 3.2, we find that the bolometric luminosity of this galaxy is $L_{\mathrm{bol}} = 5.8 \times 10^{45}\,\mathrm{erg\,s^{-1}}$. This value is very close to the median value of SDSS objects spectrocopically classified as QSO at $z \sim 0.6$, $\langle L_{\mathrm{bol}}(z \sim 0.6)\rangle = 6.5 \times 10^{45}\,\mathrm{erg\,s^{-1}}$. To compute the bolometric luminosities of the QSO objects at $0.59 \leq z \leq 0.61$, we adopted the same approach and used the [OIII]λ5007 emission-line flux measurements from the MPA-JHU catalogue (table `galSpecLine` in SDSS-DR14, Brinchmann et al., 2004; Tremonti et al., 2004).

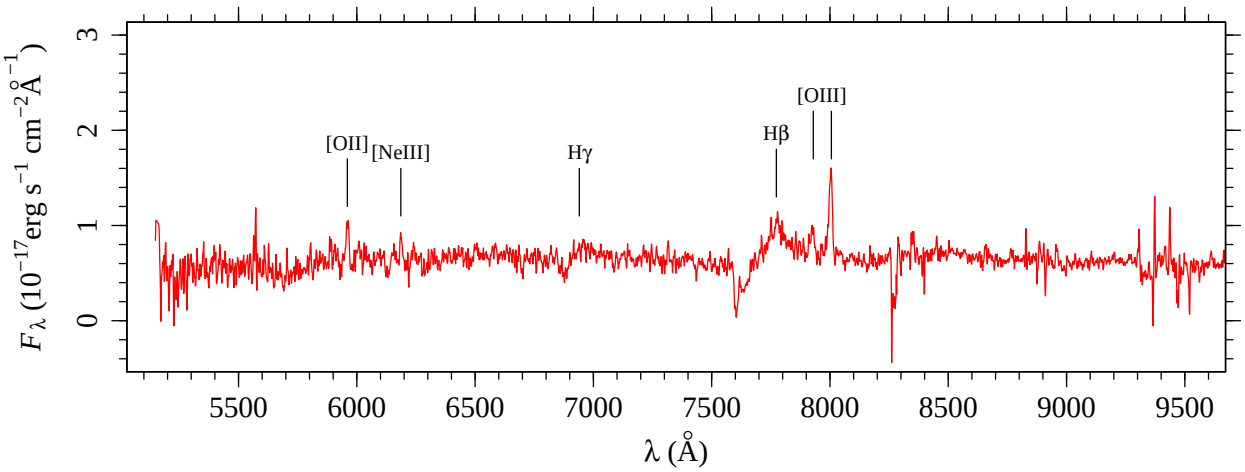

Figure 3.11: Gemini spectrum of the blue central galaxy, which was confirmed to be a quasar at $z = 0.6$.

Chapter 4

Lens modelling and source reconstruction of HELMS18 lens system

In this chapter we present the results on the lens modelling and source reconstruction of HELMS18 system. The semilinear inversion (SLI) method presented in Chapter 2 was adapted to deal with the more complex mass distribution of a group-scale lens. The ALMA Band 7 continuum emission of the background source, presented in Chapter 3, was used in the modelling. The HELMS18 lens system was the first group-scale lens modelled with ALMA observations. The redshifts of the two central galaxies of the group-scale lens, obtained in Chapter 3, were used to obtain accurate measurements of the parameters that describe the lens mass distribution.

4.1 Semilinear inversion method implementation

The semilinear inversion method Warren & Dye (2003) described in 2.2.2 was implemented in Fortran by Simon Dye. The code was primarily developed to model galaxy-scale lenses, so that it has different profiles that can be chosen in the configuration file to describe the lens mass distribution. However, such implementation did not allow to construct a more complex mass distribution for the lens, e.g., by combining different models to describe different mass components.

As described in Chapter 3, the HELMS18 system consists of a submillimeter source at $z = 2.39$ (Nayyeri et al., 2016) that is lensed by a group of galaxies at $z = 0.6$. The group-scale lens has two central galaxies, an early-type galaxy and a quasar, as shown in Figure 3.8. Given such complicated lens configuration, a more sophisticated lens mass model,

taking into account the different mass components of this group-scale lens, should be used. Therefore, the code needed to be adapted to include the possibility of combining two or more density profiles. The deflection angle at a given position of the lens plane due to a mass distribution that consists of more than one component is the sum of the deflection angles of each component calculated for that same position in the lens plane. This is a linear problem, since the step of inverting the image to obtain the source light distribution is also a linear one, as said previously.

As a first approach for the lens modelling, we adapted the code to include the possibility of using N components with the same surface density profile. We then used two SIEs, one for each of the central galaxies. The parameters used to describe the model were: c, which is a normalization parameter associated to the mass that is being modelled, x_c and y_c, which are the position of the center of the lens in the Cartesian coordinate system, θ which is the position angle, and e which is the elongation of each mass distribution, defined as

$$e = \frac{a}{b} \tag{4.1}$$

where a and b are the major and minor axis, respectively. Therefore, the lens model had ten parameters. More details on the SIE profile can be found in Chapter 2.

This first approach using two SIEs was able to reproduce the position of the arcs, however the arcs were too thick and the minimum reduced χ^2 was $\chi^2 \sim 2$. Moreover, this model produced two counter-images that were not observed in the ALMA imaging.

Since the first approach using two SIE components to describe the mass distribution of the lens did not reproduce well the observed lensed image, we decided to add a NFW density profile to describe the dark matter halo of the group. We also included external shear to take into account other galaxies in the lens vicinity. Similar model was used in Verdugo et al. (2011), where they modelled the mass distribution of a galaxy group with three central galaxies. Their model is a combination of a NFW profile for the group component and 3 pseudo-isothermal mass distributions (PIEMD) for each of the galaxies.

In order to model the group with a NFW and two SIE components, we adapted the code to include the possibility of combining different profiles. The combination of these profiles created a more complex model that was able to reproduce the observed data.

This model has eighteen parameters, including five parameters for each SIE, as described above. The NFW density profile is described by six parameters: c, a normalization associated to the total mass of the component, x_c and y_c, the position of the center of the component in the Cartesian coordinate system, θ and e which are, respectively, the position angle and the elongation of the profile, r_s, the scale radius of the NFW profile. The remaining two parameters are θ_γ and γ, which are the position angle and the strength of the shear component, respectively.

We carried out the lens modelling in the image plane rather than the uv-plane. There are two main advantages of modelling ALMA data in the image plane. First, the image can be masked in the region of interest, that means, regions where there are detected emission from the background source. This gives a much more sensitive figure of merit for the fitting, since the modelling in the uv plane fits visibilities and the visibilities describe large areas of the background sky. Another main advantage is the efficiency. Modelling in the image plane is much more efficient, because the visibility data sets are particularly large and usually they have to be trimmed anyway in Fourier space to make the modelling process feasible, as in Rybak et al. (2015).

The disadvantage of performing the lens modelling in the image plane is that the Fourier transform of the visibilities are modelled, instead of modelling the visibilities directly. The main side effect of this approach is that the image pixels are correlated by the beam, leading to a biased image-plane modelling. This can be avoided by taking into account the covariance between pixels in the uncertainties. However, measuring this covariance between pixels is not a simple task.

Moreover, according to Dye et al. (2018), minor differences are found in the reconstructed source and lens parameters when comparing the results produced by the SLI method by modelling the cleaned image data and the visibility data directly. In that work, the authors modelled six strong galaxy-galaxy gravitational lens systems from the same sample as HELMS18 using both methods. The expectation is that such differences will be more notable when the coverage of the uv plane becomes more sparse, resulting in a poorer angular resolution.

In the following we presents the results of the lens modelling and source reconstruction.

4.2 Lens modelling and source reconstruction

We modelled the group-scale lens at $z = 0.6$ that is gravitationally lensing the submillimeter galaxy at $z = 2.39$ using the semilinear inversion method outlined in Section 2.2.2. The model that recovered observational features was a NFW density profile for the group component and two SIEs, one for each of the central galaxies.

Figure 4.1 shows the lensed image of the reconstructed source obtained using the best-fit lens modelling parameters. The best-fit parameters are listed in Table 4.1 and the minimum reduced χ^2 was $\chi^2 = 1.59$.

The semilinear inversion method recovers the source surface brightness when modelling the lens mass distribution. The reconstructed unlensed emission of HELMS18 shown in 4.2 presents a two-component source separated by 9.5 kpc assuming that the two components are in the same plane. Both components present elongated and disturbed morphology, suggesting that they are undergoing a merger.

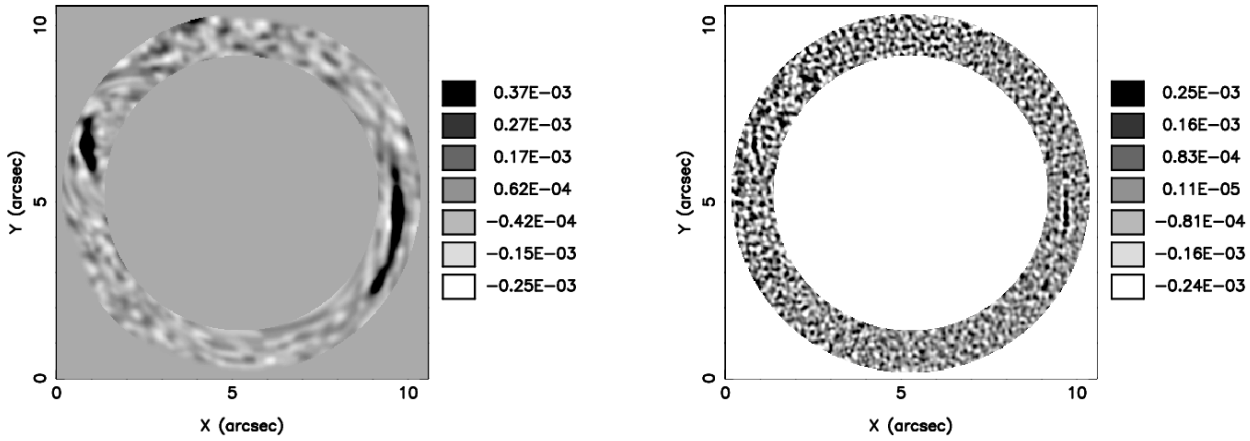

Figure 4.1: Left: lensed image from the reconstructed source. Right: residuals between the original image and the lensed image from the reconstructed source

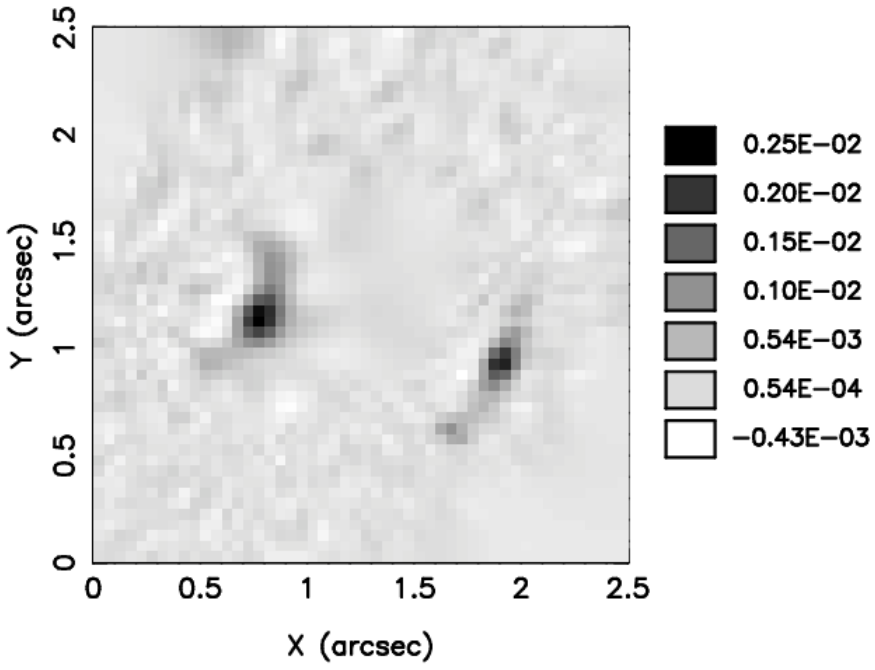

Figure 4.2: Reconstructed unlensed emission of the source.

Table 4.1: Parameters of the best-fit lens model. The positions of the center of the component are relative to the center of the image. θ is the angle of semi-major axis of ellipsoid to y axis (counter clockwise). e is the elongation of the ellipsoid.

Component	x_c (")	y_c (")	θ (°)	e	r_s (kpc)	θ_γ (°)	γ
SIE_1(ETG)	-3.413	1.306	-21.278	1.220	-	-	-
SIE_2(quasar)	0.895	-1.377	78.857	1.442	-	-	-
NFW	0.996	-0.5428	-32.467	1.623	129.230	41.071	0.0011

The spectroscopic redshift from the lensed submillimeter galaxy was obtained by Nayyeri et al. (2016) using CO emission line. Given the poor resolution of this measurement, the detection of the emission was not resolved, that is, not being able to separate the arcs and measure the redshift of each one individually. To confirm the hypothesis that the two components of the source are a result of a merger, spectroscopic observations of each of the arcs are needed, so that it is possible to check precisely the redshift of the two components. It is important to mention that we did not consider in the modelling the possibility of the two components of the source being in different redshifts. This is a valid hypothesis and, if confirmed with spectroscopic data, it could be used to better constrain the model.

An advantage of modelling the mass distribution of a lens using the semilinear inversion method is that it reconstructs the surface brightness of each pixel of the source. Most codes, like `LENSTOOL`, which was used by Verdugo et al. (2011), reconstruct the source positions but not the surface brightness of individual pixels. Recovering the unlensed emission of each pixel in the source plane is far more difficult and more computer power is needed, since the mapping is done for each pixel of the image.

The mass distribution of the galaxy group that is lensing HELMS18 could be complex enough, so that it cannot be described by a sum of only three density profiles. Combining more models means an increase in the total number of parameters, leading to a larger lens parameter space, which makes the search more complicated and more expensive computationally. For instance, galaxy clusters, which have very complex mass distributions, cannot be modelled using the semilinear inversion method since the combination of their density profiles would lead to an immense number of parameters, making the modelling computationally prohibitive. A possible next step, to confirm the results of our modelling, would be modelling the mass distribution of the galaxy group that is gravitationally lensing HELMS18 using another code. One alternative to model the group-scale lens is `LENSTOOL`* (Jullo et al., 2007), which is an open source code and is commonly used to model galaxy clusters.

*The `LENSTOOL` software is publicly available at https://projets.lam.fr/projects/lenstool/wiki.

Chapter 5

Summary & Perspectives

In this work we modelled the group-scale lens at $z = 0.6$ that is gravitational lensing HELMS18, a submillimeter galaxy at $z = 2.39$ using the semilinear inversion method. This system was first detected in the Herschel's Large Mode Survey (HELMS) and later it was followed up with ALMA. The modelling that recovered observational features was a NFW density profile for the group component and two SIEs as sub-halos for the two central galaxies. The lens modelling recovers the unlensed emission of the source. The reconstructed source presents two disturbed and elongated components, separated by 9.5 kpc, suggesting that they are undergoing a merger.

In chapter 2 we review the gravitational lensing effect, beginning with a brief description of the phenomena, explaining the lensing regimes and the reason why strong lensing is a suitable technique for studying different astronomical objects. After that, we described the historical context, followed by the lens equation and potential, explaining the visible effects, such as magnification and distortion.

We also explain the semilinear inversion method, which was used to model the HELMS18 system. This method separates the lens parameters from the source parameters. It uses a pixelised source plane and a parametric function for the lens mass distribution. Given a lens model, the method computes the linear superposition of the lensed images for each source plane pixel that best fit the data. The step to obtain the source distribution is a linear one, sine it is inverting the image. The nonlinear step is the search in the lens parameter space, which is used to find the best model.

In chapter 3 we present the HELMS18 lens system, beginning on its first detection by Herschel's Hermes Large Mode Survey. After that, HELMS18 was followed-up with ALMA and had the spectroscopic redshift $z = 2.39$ measured by molecular line spectroscopy. We also give a brief description of interferometry, which is the technique used to observe with ALMA.

We found out that the HELMS18 lens system has two central galaxies by looking at the optical counterpart in the SDSS. One of the galaxies was catalogued as an ETG and the

other one as a star. We analysed SDSS data and the object catalogued as star seemed to be a quasar. In order to confirm if the object was indeed a quasar we conducted multi-object spectroscopic observations, using GMOS in Gemini South Observatory.

We performed the data reduction of the GMOS data and confirmed that the quasar candidate was indeed a quasar. Another result using Gemini data is that we measured the spectroscopic redshifts for both ETG and the quasar. We confirmed that these two objects are similar redshifts, with separation of $\Delta z \sim 0.003$ ($\Delta v = 903 \pm 30\,\mathrm{km\,s^{-1}}$).

In chapter 4 we describe the implementation of the semilinear inversion method, explaining that we needed to adapt the code to include the possibility of combining two or more models. The first approach for the modelling was using two SIEs, however it did not provide a good fit to the data. The model that best reproduced the observed data was a NFW density profile for the group component and two SIEs for the two central galaxies.

By modelling the group-scale lens, we were able to reconstruct the source. The unlensed emission of HELMS18 presents two sources separated by 9.5 kpc. The morphology of the source is disturbed and elongated, suggesting strong interaction between two merging galaxies. However, to confirm this hypothesis, individual spectroscopic data of the arcs are needed.

The next steps of this work include refining our model by testing different lens configurations and to model the group-scale lens in the *uv* plane. We also need to determine the mass within the Einstein radius and the magnification, which will allow us to measure physical properties of the source. One possibility to validate the lens modelling is to use another code, such as `LENSTOOL`, an open source code to model galaxy clusters, which was used by Verdugo et al. (2011).

Another step is obtaining spectra of the arcs individually in order to measure their redshifts. If the arcs are confirmed to be at different redshifts, the code would need to be adapted to include the possibility of reconstructing the surface brightness of the sources at different redshifts. Also, this would exclude the scenario which the two components of the source resulted from a possible merger.

Finishing the data reduction of Gemini observations is also within the perspectives. With the spectra of all observed galaxies in the group field, we will be able to measure their redshifts and determine the group members. With the spectra we can perform stellar population synthesis, which will provide the stellar mass of the galaxies. Therefore, we can combine the strong lensing technique with stellar kinematics of the central galaxies and kinematics of the group members. This complementary techniques will allow us to investigate the mass distribution (both dark and luminous) at several widely separated radii. Moreover, we will be able to investigate a possible interaction between the two central galaxies, which might have triggered the nuclear activity in one of them.

Bibliography

ALAGHBAND-ZADEH, S.; CHAPMAN, S. C.; SWINBANK, A. M.; SMAIL, IAN; HARRISON, C. M.; ALEXANDER, D. M.; CASEY, C. M.; DAVÉ, R.; NARAYANAN, D.; TAMURA, Y.; UMEHATA, H. Integral field spectroscopy of 2.0< z<2.7 submillimetre galaxies: gas morphologies and kinematics. **Monthly Notices of the Royal Astronomical Society**, v. 424, n. 3, p. 2232–2248, August 2012.

AMVROSIADIS, A; EALES, S A; NEGRELLO, M; MARCHETTI, L; SMITH, M W L; BOURNE, N; CLEMENTS, D L; DE ZOTTI, G; DUNNE, L; DYE, S; FURLANETTO, C; IVISON, R J; MADDOX, S J; VALIANTE, E; BAES, M; BAKER, A J; COORAY, A; CRAWFORD, S M; FRAYER, D; HARRIS, A; MICHAÅOWSKI, M J; NAYYERI, H; OLIVER, S; RIECHERS, D A; SERJEANT, S; VACCARI, M. ALMA observations of lensed Herschel sources: testing the dark matter halo paradigm. **Monthly Notices of the Royal Astronomical Society**, v. 475, n. 4, p. 4939–4952, April 2018.

AUGER, M. W.; TREU, T.; BOLTON, A. S.; GAVAZZI, R.; KOOPMANS, L. V. E.; MARSHALL, P. J.; MOUSTAKAS, L. A.; BURLES, S. THE SLOAN LENS ACS SURVEY. X. Sâ¡LAR, DYNAMICAL, AND TOTAL MASS CORRELATIONS OF MASSIVE EARLY-TYPE GALAXIES. **The Astrophysical Journal**, v. 724, n. 1, p. 511–525, November 2010.

BAI, YU; LIU, JIFENG; WANG, SONG; YANG, FAN. Machine Learning Applied to Star-Galaxy-QSO Classification and Stellar Effective Temperature Regression. **Astronomical Journal**, v. 157, n. 1, p. 9, January 2019.

BARGER, A. J.; COWIE, L. L.; SANDERS, D. B.; FULTON, E.; TANIGUCHI, Y.; SATO, Y.; KAWARA, K.; OKUDA, H. Submillimetre-wavelength detection of dusty star-forming galaxies at high redshift. **Nature**, v. 394, n. 6690, p. 248–251, July 1998.

BARNABÈ, MATTEO; SPINIELLO, CHIARA; KOOPMANS, LÉON V. E.; TRAGER, SCOTT C.; CZOSKE, OLIVER; TREU, TOMMASO. A low-mass cut-off near the hydrogen burning limit for Salpeter-like initial mass functions in early-type galaxies. **Monthly Notices of the Royal Astronomical Society**, v. 436, n. 1, p. 253–258, November 2013.

BARTELMANN, M.; SCHNEIDER, P. Weak gravitational lensing. **Physics Reports**, v. 340, n. 4-5, p. 291–472, January 2001.

BARTELMANN, MATTHIAS. Gravitational lensing. **Classical and Quantum Gravity**, v. 27, n. 23, p. 233001, November 2010.

BARTELMANN, MATTHIAS; LIMOUSIN, MARCEAU; MENEGHETTI, MASSIMO; SCHMIDT, ROBERT. Internal Cluster Structure. **Space Science Reviews**, v. 177, n. 1, p. 3–29, August 2013.

BERGMANN, ANTON G.; PETROSIAN, VAHE; LYNDS, ROGER. Gravitational lens models of arcs in clusters. **The Astrophysical Journal**, v. 350, p. 23–35, February 1990.

BLAIN, A. W. Galaxy-galaxy gravitational lensing in the millimetre/submillimetre waveband. **Monthly Notices of the Royal Astronomical Society**, v. 283, n. 4, p. 1340–1348, December 1996.

BLUMENTHAL, G. R.; FABER, S. M.; FLORES, R.; PRIMACK, J. R. Contraction of dark matter galactic halos due to baryonic infall. **The Astrophysical Journal**, v. 301, p. 27, February 1986.

BOND, I. A.; UDALSKI, A.; JAROSZYÅSKI, M.; RATTENBURY, N. J.; PACZYÅSKI, B.; SOSZYÅSKI, I.; WYRZYKOWSKI, L.; SZYMAÅSKI, M. K.; KUBIAK, M.; SZEWCZYK, O.; ÅEBRUÅ, K.; PIETRZYÅSKI, G.; ABE, F.; BENNETT, D. P.; EGUCHI, S.; FURUTA, Y.; HEARNSHAW, J. B.; KAMIYA, K.; KILMARTIN, P. M.; KURATA, Y.; MASUDA, K.; MATSUBARA, Y.; MURAKI, Y.; NODA, S.; OKAJIMA, K.; SAKO, T.; SEKIGUCHI, T.; SULLIVAN, D. J.; SUMI, T.; TRISTRAM, P. J.; YANAGISAWA, T.; YOCK, P. C. M.; OGLE COLLABORATION, . OGLE 2003-BLG-235/MOA 2003-BLG-53: A Planetary Microlensing Event. **The Astrophysical Journal Letters**, v. 606, p. L155–L158, May 2004.

BORYS, C.; SMAIL, IAN; CHAPMAN, S. C.; BLAIN, A. W.; ALEXANDER, D. M.; IVISON, R. J. The Relationship between Stellar and Black Hole Mass in Submillimeter Galaxies. **Astrophysical Journal**, v. 635, n. 2, p. 853–863, December 2005.

BOTHWELL, M. S.; KENNICUTT, R. C.; JOHNSON, B. D.; WU, Y.; LEE, J. C.; DALE, D.; ENGELBRACHT, C.; CALZETTI, D.; SKILLMAN, E. The star formation rate distribution function of the local Universe. , v. 415, n. 2, p. 1815–1826, August 2011.

BRINCHMANN, J.; CHARLOT, S.; WHITE, S. D. M.; TREMONTI, C.; KAUFFMANN, G.; HECKMAN, T.; BRINKMANN, J. The physical properties of star-forming galaxies in the low-redshift universe. **Monthly Notices of the Royal Astronomical Society**, v. 351, p. 1151–1179, July 2004.

BRISBIN, DREW; MIETTINEN, OSKARI; ARAVENA, MANUEL; SMOLČIĆ, VERNESA; DELVECCHIO, IVAN; JIANG, CHUNYAN; MAGNELLI, BENJAMIN; ALBRECHT, MARCUS; ARANCIBIA, ALEJANDRA MUÑOZ; AUSSEL, HERVÉ; BARAN, NIKOLA; BERTOLDI, FRANK; BÉTHERMIN, MATTHIEU; CAPAK, PETER; CASEY, CAITLIN M.; CIVANO, FRANCESCA; HAYWARD, CHRISTOPHER C.; ILBERT, OLIVIER; KARIM, ALEXANDER; LE FEVRE, OLIVIER; MARCHESI, STEFANO; MCCRACKEN, HENRY JOY; NAVARRETE, FELIPE; NOVAK, MLADEN; RIECHERS, DOMINIK; PADILLA, NELSON; SALVATO, MARA; SCOTT, KIMBERLY; SCHINNERER, EVA; SHETH, KARTIK; TASCA, LIDIA. An ALMA survey of submillimeter galaxies in the COSMOS field: Multiwavelength counterparts and redshift distribution. **Astronomy and Astrophysics**, v. 608, p. A15, November 2017.

BRYAN, GREG L.; NORMAN, MICHAEL L. Statistical properties of x-ray clusters: Analytic and numerical comparisons. **The Astrophysical Journal**, v. 495, n. 1, p. 80–99, mar 1998.

BUSSMANN, R. S.; GURWELL, M. A.; FU, HAI; SMITH, D. J. B.; DYE, S.; AULD, R.; BAES, M.; BAKER, A. J.; BONFIELD, D.; CAVA, A.; CLEMENTS, D. L.; COORAY, A.; COPPIN, K.; DANNERBAUER, H.; DARIUSH, A.; DE ZOTTI, G.; DUNNE, L.; EALES, S.; FRITZ, J.; HOPWOOD, R.; IBAR, E.; IVISON, R. J.; JARVIS, M. J.; KIM, S.; LEEUW, L. L.; MADDOX, S.; MICHAŁOWSKI, M. J.; NEGRELLO, M.; PASCALE, E.; POHLEN, M.; RIECHERS, D. A.; RIGBY, E.; SCOTT, DOUGLAS; TEMI, P.; VAN DER WERF, P. P.; WARDLOW, J.; WILNER, D.; VERMA, A. A Detailed Gravitational Lens Model Based on Submillimeter Array and Keck Adaptive Optics Imaging of a Herschel-ATLAS Submillimeter Galaxy at z = 4.243. **Astrophysical Journal**, v. 756, n. 2, p. 134, September 2012.

CALANOG, J. A.; FU, HAI; COORAY, A.; WARDLOW, J.; MA, B.; AMBER, S.; BAKER, A. J.; BAES, M.; BOCK, J.; BOURNE, N.; BUSSMANN, R. S.; CASEY, C. M.; CHAPMAN, S. C.; CLEMENTS, D. L.; CONLEY, A.; DANNERBAUER, H.; DE ZOTTI, G.; DUNNE, L.; DYE, S.; EALES, S.; FARRAH, D.; FURLANETTO, C.; HARRIS, A. I.; IVISON, R. J.; KIM, S.; MADDOX, S. J.; MAGDIS, G.; MESSIAS, H.; MICHAŁOWSKI, M. J.; NEGRELLO, M.; NIGHTINGALE, J.; O'BRYAN, J. M.; OLIVER, S. J.; RIECHERS, D.; SCOTT, D.; SERJEANT, S.; SIMPSON, J.; SMITH, M.; TIMMONS, N.; THACKER, C.; VALIANTE, E.; VIEIRA, J. D. Lens Models of Herschel-selected Galaxies from High-resolution Near-IR Observations. **Astrophysical Journal**, v. 797, n. 2, p. 138, December 2014.

CARLSTROM, J. E.; ADE, P. A. R.; AIRD, K. A.; BENSON, B. A.; BLEEM, L. E.; BUSETTI, S.; CHANG, C. L.; CHAUVIN, E.; CHO, H. M.; CRAWFORD, T. M.; CRITES, A. T.; DOBBS, M. A.; HALVERSON, N. W.; HEIMSATH, S.; HOLZAPFEL,

W. L.; HRUBES, J. D.; JOY, M.; KEISLER, R.; LANTING, T. M.; LEE, A. T.; LEITCH, E. M.; LEONG, J.; LU, W.; LUEKER, M.; LUONG-VAN, D.; MCMAHON, J. J.; MEHL, J.; MEYER, S. S.; MOHR, J. J.; MONTROY, T. E.; PADIN, S.; PLAGGE, T.; PRYKE, C.; RUHL, J. E.; SCHAFFER, K. K.; SCHWAN, D.; SHIROKOFF, E.; SPIELER, H. G.; STANISZEWSKI, Z.; STARK, A. A.; TUCKER, C.; VAND ERLINDE, K.; VIEIRA, J. D.; WILLIAMSON, R. The 10 Meter South Pole Telescope. **Publications of the Astronomical Society of the Pacific**, v. 123, n. 903, p. 568, May 2011.

CASEY, CAITLIN M.; NARAYANAN, DESIKA; COORAY, ASANTHA. Dusty star-forming galaxies at high redshift. **Physics Reports**, v. 541, n. 2, p. 45–161, August 2014.

CHAPMAN, S. C.; BLAIN, A. W.; IVISON, R. J.; SMAIL, IAN R. A median redshift of 2.4 for galaxies bright at submillimetre wavelengths. **Nature**, v. 422, n. 6933, p. 695–698, April 2003.

CHAPMAN, S. C.; BLAIN, A. W.; SMAIL, IAN; IVISON, R. J. A Redshift Survey of the Submillimeter Galaxy Population. **Astrophysical Journal**, v. 622, n. 2, p. 772–796, April 2005.

CHEN, CHIAN-CHOU; SMAIL, IAN; SWINBANK, A. M.; SIMPSON, J. M.; MA, CHENG-JIUN; ALEXANDER, D. M.; BIGGS, A. D.; BRANDT, W. N.; CHAPMAN, S. C.; COPPIN, K. E. K.; DANIELSON, A. L. R.; DANNERBAUER, H.; EDGE, A. C.; GREVE, T. R.; IVISON, R. J.; KARIM, A.; MENTEN, KARL M.; SCHINNERER, E.; WALTER, F.; WARDLOW, J. L.; WEIß, A.; VAN DER WERF, P. P. An ALMA Survey of Submillimeter Galaxies in the Extended Chandra Deep Field South: Near-infrared Morphologies and Stellar Sizes. **Astrophysical Journal**, v. 799, n. 2, p. 194, February 2015.

CHOMIUK, LAURA; POVICH, MATTHEW S. Toward a Unification of Star Formation Rate Determinations in the Milky Way and Other Galaxies. , v. 142, n. 6, p. 197, December 2011.

CHWOLSON, O. Über eine mögliche Form fiktiver Doppelsterne. **Astronomische Nachrichten**, v. 221, p. 329, June 1924.

CLEMENTS, D. L.; RIGBY, E.; MADDOX, S.; DUNNE, L.; MORTIER, A.; PEARSON, C.; AMBLARD, A.; AULD, R.; BAES, M.; BONFIELD, D.; BURGARELLA, D.; BUTTIGLIONE, S.; CAVA, A.; COORAY, A.; DARIUSH, A.; DE ZOTTI, G.; DYE, S.; EALES, S.; FRAYER, D.; FRITZ, J.; GARDNER, JONATHAN P.; GONZALEZ-NUEVO, J.; HERRANZ, D.; IBAR, E.; IVISON, R.; JARVIS, M. J.; LAGACHE, G.; LEEUW, L.; LOPEZ-CANIEGO, M.; NEGRELLO, M.; PASCALE, E.; POHLEN, M.; RODIGHIERO, G.; SAMUI, S.; SERJEANT, S.; SIBTHORPE, B.; SCOTT, D.; SMITH,

D. J. B.; TEMI, P.; THOMPSON, M.; VALTCHANOV, I.; VAN DER WERF, P.; VERMA, A. Herschel-ATLAS: Extragalactic number counts from 250 to 500 microns. **Astronomy and Astrophysics**, v. 518, p. L8, July 2010.

CONLEY, A.; COORAY, A.; VIEIRA, J. D.; GONZÁLEZ SOLARES, E. A.; KIM, S.; AGUIRRE, J. E.; AMBLARD, A.; AULD, R.; BAKER, A. J.; BEELEN, A.; BLAIN, A.; BLUNDELL, R.; BOCK, J.; BRADFORD, C. M.; BRIDGE, C.; BRISBIN, D.; BURGARELLA, D.; CARPENTER, J. M.; CHANIAL, P.; CHAPIN, E.; CHRISTOPHER, N.; CLEMENTS, D. L.; COX, P.; DJORGOVSKI, S. G.; DOWELL, C. D.; EALES, S.; EARLE, L.; ELLSWORTH-BOWERS, T. P.; FARRAH, D.; FRANCESCHINI, A.; FRAYER, D.; FU, H.; GAVAZZI, R.; GLENN, J.; GRIFFIN, M.; GURWELL, M. A.; HALPERN, M.; IBAR, E.; IVISON, R. J.; JARVIS, M.; KAMENETZKY, J.; KRIPS, M.; LEVENSON, L.; LUPU, R.; MAHABAL, A.; MALONEY, P. D.; MARASTON, C.; MARCHETTI, L.; MARSDEN, G.; MATSUHARA, H.; MORTIER, A. M. J.; MURPHY, E.; NAYLOR, B. J.; NERI, R.; NGUYEN, H. T.; OLIVER, S. J.; OMONT, A.; PAGE, M. J.; PAPAGEORGIOU, A.; PEARSON, C. P.; PÉREZ-FOURNON, I.; POHLEN, M.; RANGWALA, N.; RAWLINGS, J. I.; RAYMOND, G.; RIECHERS, D.; RODIGHIERO, G.; ROSEBOOM, I. G.; ROWAN-ROBINSON, M.; SCHULZ, B.; SCOTT, DOUGLAS; SCOTT, K.; SERRA, P.; SEYMOUR, N.; SHUPE, D. L.; SMITH, A. J.; SYMEONIDIS, M.; TUGWELL, K. E.; VACCARI, M.; VALIANTE, E.; VALTCHANOV, I.; VERMA, A.; VIERO, M. P.; VIGROUX, L.; WANG, L.; WIEBE, D.; WRIGHT, G.; XU, C. K.; ZEIMANN, G.; ZEMCOV, M.; ZMUIDZINAS, J. Discovery of a Multiply Lensed Submillimeter Galaxy in Early HerMES Herschel/SPIRE Data. **Astrophysical Journal Letters**, v. 732, n. 2, p. L35, May 2011.

CONSELICE, CHRISTOPHER J.; CHAPMAN, SCOTT C.; WINDHORST, ROGIER A. Evidence for a Major Merger Origin of High-Redshift Submillimeter Galaxies. **Astrophysical Journal Letters**, v. 596, n. 1, p. L5–L8, October 2003.

DADDI, E.; BOURNAUD, F.; WALTER, F.; DANNERBAUER, H.; CARILLI, C. L.; DICKINSON, M.; ELBAZ, D.; MORRISON, G. E.; RIECHERS, D.; ONODERA, M.; SALMI, F.; KRIPS, M.; STERN, D. Very High Gas Fractions and Extended Gas Reservoirs in z = 1.5 Disk Galaxies. , v. 713, n. 1, p. 686–707, April 2010.

DADDI, E.; DICKINSON, M.; CHARY, R.; POPE, A.; MORRISON, G.; ALEXANDER, D. M.; BAUER, F. E.; BRAND T, W. N.; GIAVALISCO, M.; FERGUSON, H.; LEE, K. S.; LEHMER, B. D.; PAPOVICH, C.; RENZINI, A. The Population of BzK-selected ULIRGs at z ~2. **Astrophysical Journal Letters**, v. 631, n. 1, p. L13–L16, September 2005.

DE ZOTTI, G.; RICCI, R.; MESA, D.; SILVA, L.; MAZZOTTA, P.; TOFFOLATTI, L.; GONZÁLEZ-NUEVO, J. Predictions for high-frequency radio surveys of extragalactic sources. **Astronomy and Astrophysics**, v. 431, n. 3, p. 893–903, March 2005.

DOWNES, D.; SOLOMON, P. M. Rotating Nuclear Rings and Extreme Starbursts in Ultraluminous Galaxies. **Astrophysical Journal**, v. 507, n. 2, p. 615–654, November 1998.

DYE, S.; FURLANETTO, C.; DUNNE, L.; EALES, S. A.; NEGRELLO, M.; NAYYERI, H.; WERF, P. P.VAN DER ; SERJEANT, S.; FARRAH, D.; MICHAÅOWSKI, M. J.; BAES, M.; MARCHETTI, L.; COORAY, A.; RIECHERS, D. A.; AMVROSIADIS, A. Modelling high-resolution ALMA observations of strongly lensed highly star-forming galaxies detected by Herschel. **Monthly Notices of the Royal Astronomical Society**, v. 476, p. 4383–4394, June 2018.

DYE, S.; FURLANETTO, C.; SWINBANK, A. M.; VLAHAKIS, C.; NIGHTINGALE, J. W.; DUNNE, L.; EALES, S. A.; SMAIL, IAN; OTEO, I.; HUNTER, T.; NEGRELLO, M.; DANNERBAUER, H.; IVISON, R. J.; GAVAZZI, R.; COORAY, A.; WERF, P. VAN DER. Revealing the complex nature of the strong gravitationally lensed system H-ATLAS J090311.6+003906 using ALMA. **Monthly Notices of the Royal Astronomical Society**, v. 452, n. 3, p. 2258–2268, September 2015.

DYE, S.; NEGRELLO, M.; HOPWOOD, R.; NIGHTINGALE, J. W.; BUSSMANN, R. S.; AMBER, S.; BOURNE, N.; COORAY, A.; DARIUSH, A.; DUNNE, L.; EALES, S. A.; GONZALEZ-NUEVO, J.; IBAR, E.; IVISON, R. J.; MADDOX, S.; VALIANTE, E.; SMITH, M. Herschel-ATLAS: modelling the first strong gravitational lenses. **Monthly Notices of the Royal Astronomical Society**, v. 440, p. 2013–2025, May 2014.

DYE, S.; WARREN, S. J. Decomposition of the Visible and Dark Matter in the Einstein Ring 0047-2808 by Semilinear Inversion. **The Astrophysical Journal**, v. 623, p. 31–41, April 2005.

DYSON, F. W.; EDDINGTON, A. S.; DAVIDSON, C. A Determination of the Deflection of Light by the Sun's Gravitational Field, from Observations Made at the Total Eclipse of May 29, 1919. **Philosophical Transactions of the Royal Society of London Series A**, v. 220, p. 291–333, January 1920.

EALES, S.; DUNNE, L.; CLEMENTS, D.; COORAY, A.; DE ZOTTI, G.; DYE, S.; IVISON, R.; JARVIS, M.; LAGACHE, G.; MADDOX, S.; NEGRELLO, M.; SERJEANT, S.; THOMPSON, M. A.; VAN KAMPEN, E.; AMBLARD, A.; ANDREANI, P.; BAES, M.; BEELEN, A.; BENDO, G. J.; BENFORD, D.; BERTOLDI, F.; BOCK, J.; BONFIELD, D.; BOSELLI, A.; BRIDGE, C.; BUAT, V.; BURGARELLA, D.; CARLBERG, R.; CAVA, A.; CHANIAL, P.; CHARLOT, S.; CHRISTOPHER, N.; COLES, P.;

CORTESE, L.; DARIUSH, A.; DA CUNHA, E.; DALTON, G.; DANESE, L.; DANNERBAUER, H.; DRIVER, S.; DUNLOP, J.; FAN, L.; FARRAH, D.; FRAYER, D.; FRENK, C.; GEACH, J.; GARDNER, J.; GOMEZ, H.; GONZÁLEZ-NUEVO, J.; GONZÁLEZSOLARES, E.; GRIFFIN, M.; HARDCASTLE, M.; HATZIMINAOGLOU, E.; HERRANZ, D.; HUGHES, D.; IBAR, E.; JEONG, WOONG-SEOB; LACEY, C.; LAPI, A.; LAWRENCE, A.; LEE, M.; LEEUW, L.; LISKE, J.; LÓPEZ-CANIEGO, M.; MÜLLER, T.; NANDRA, K.; PANUZZO, P.; PAPAGEORGIOU, A.; PATANCHON, G.; PEACOCK, J.; PEARSON, C.; PHILLIPPS, S.; POHLEN, M.; POPESCU, C.; RAWLINGS, S.; RIGBY, E.; RIGOPOULOU, M.; ROBOTHAM, A.; RODIGHIERO, G.; SANSOM, A.; SCHULZ, B.; SCOTT, D.; SMITH, D. J. B.; SIBTHORPE, B.; SMAIL, I.; STEVENS, J.; SUTHERLAND, W.; TAKEUCHI, T.; TEDDS, J.; TEMI, P.; TUFFS, R.; TRICHAS, M.; VACCARI, M.; VALTCHANOV, I.; VAN DER WERF, P.; VERMA, A.; VIERIA, J.; VLAHAKIS, C.; WHITE, GLENN J. The Herschel ATLAS. **Publications of the Astronomical Society of the Pacific**, v. 122, n. 891, p. 499, May 2010a.

EALES, S.; DUNNE, L.; CLEMENTS, D.; COORAY, A.; DE ZOTTI, G.; DYE, S.; IVISON, R.; JARVIS, M.; LAGACHE, G.; MADDOX, S.; NEGRELLO, M.; SERJEANT, S.; THOMPSON, M. A.; VAN KAMPEN, E.; AMBLARD, A.; ANDREANI, P.; BAES, M.; BEELEN, A.; BENDO, G. J.; BENFORD, D.; BERTOLDI, F.; BOCK, J.; BONFIELD, D.; BOSELLI, A.; BRIDGE, C.; BUAT, V.; BURGARELLA, D.; CARLBERG, R.; CAVA, A.; CHANIAL, P.; CHARLOT, S.; CHRISTOPHER, N.; COLES, P.; CORTESE, L.; DARIUSH, A.; DA CUNHA, E.; DALTON, G.; DANESE, L.; DANNERBAUER, H.; DRIVER, S.; DUNLOP, J.; FAN, L.; FARRAH, D.; FRAYER, D.; FRENK, C.; GEACH, J.; GARDNER, J.; GOMEZ, H.; GONZÁLEZ-NUEVO, J.; GONZÁLEZSOLARES, E.; GRIFFIN, M.; HARDCASTLE, M.; HATZIMINAOGLOU, E.; HERRANZ, D.; HUGHES, D.; IBAR, E.; JEONG, WOONG-SEOB; LACEY, C.; LAPI, A.; LAWRENCE, A.; LEE, M.; LEEUW, L.; LISKE, J.; LÓPEZ-CANIEGO, M.; MÜLLER, T.; NANDRA, K.; PANUZZO, P.; PAPAGEORGIOU, A.; PATANCHON, G.; PEACOCK, J.; PEARSON, C.; PHILLIPPS, S.; POHLEN, M.; POPESCU, C.; RAWLINGS, S.; RIGBY, E.; RIGOPOULOU, M.; ROBOTHAM, A.; RODIGHIERO, G.; SANSOM, A.; SCHULZ, B.; SCOTT, D.; SMITH, D. J. B.; SIBTHORPE, B.; SMAIL, I.; STEVENS, J.; SUTHERLAND, W.; TAKEUCHI, T.; TEDDS, J.; TEMI, P.; TUFFS, R.; TRICHAS, M.; VACCARI, M.; VALTCHANOV, I.; VAN DER WERF, P.; VERMA, A.; VIERIA, J.; VLAHAKIS, C.; WHITE, GLENN J. The Herschel ATLAS. **Publications of the Astronomical Society of the Pacific**, v. 122, n. 891, p. 499, May 2010b.

EINSTEIN, A. Über den Einfluß der Schwerkraft auf die Ausbreitung des Lichtes. **Annalen der Physik**, v. 340, p. 898–908, 1911.

EINSTEIN, A. Die Grundlage der allgemeinen Relativitätstheorie. **Annalen der Physik**, v. 354, p. 769–822, 1916.

EINSTEIN, ALBERT. Lens-Like Action of a Star by the Deviation of Light in the Gravitational Field. **Science**, v. 84, p. 506–507, December 1936.

EKE, V. R.; BAUGH, CARLTON M.; COLE, SHAUN; FRENK, CARLOS S.; NORBERG, PEDER; PEACOCK, JOHN A.; BALDRY, IVAN K.; BLAND-HAWTHORN, JOSS; BRIDGES, TERRY; CANNON, RUSSELL; COLLESS, MATTHEW; COLLINS, CHRIS; COUCH, WARRICK; DALTON, GAVIN; PROPRIS, ROBERTODE ; DRIVER, SIMON P.; EFSTATHIOU, GEORGE; ELLIS, RICHARD S.; GLAZEBROOK, KARL; JACKSON, CAROLE; LAHAV, OFER; LEWIS, IAN; LUMSDEN, STUART; MADDOX, STEVE; MADGWICK, DARREN; PETERSON, BRUCE A.; SUTHERLAND, WILL; TAYLOR, KEITH. Galaxy groups in the 2dfgrs: the group-finding algorithm and the 2pigg catalogue. **Monthly Notices of the Royal Astronomical Society**, v. 348, p. 866, March 2004.

EL-ZANT, AMR; SHLOSMAN, ISAAC; HOFFMAN, YEHUDA. Dark Halos: The Flattening of the Density Cusp by Dynamical Friction. **The Astrophysical Journal**, v. 560, p. 636, October 2001.

ELBAZ, D.; DICKINSON, M.; HWANG, H. S.; DíAZ-SANTOS, T.; MAGDIS, G.; MAGNELLI, B.; LE BORGNE, D.; GALLIANO, F.; PANNELLA, M.; CHANIAL, P.; ARMUS, L.; CHARMANDARIS, V.; DADDI, E.; AUSSEL, H.; POPESSO, P.; KARTALTEPE, J.; ALTIERI, B.; VALTCHANOV, I.; COIA, D.; DANNERBAUER, H.; DASYRA, K.; LEITON, R.; MAZZARELLA, J.; ALEXANDER, D. M.; BUAT, V.; BURGARELLA, D.; CHARY, R. R.; GILLI, R.; IVISON, R. J.; JUNEAU, S.; LE FLOC'H, E.; LUTZ, D.; MORRISON, G. E.; MULLANEY, J. R.; MURPHY, E.; POPE, A.; SCOTT, D.; BRODWIN, M.; CALZETTI, D.; CESARSKY, C.; CHARLOT, S.; DOLE, H.; EISENHARDT, P.; FERGUSON, H. C.; FÖRSTER SCHREIBER, N.; FRAYER, D.; GIAVALISCO, M.; HUYNH, M.; KOEKEMOER, A. M.; PAPOVICH, C.; REDDY, N.; SURACE, C.; TEPLITZ, H.; YUN, M. S.; WILSON, G. GOODS-Herschel: an infrared main sequence for star-forming galaxies. , v. 533, p. A119, September 2011.

ELÍASDÓTTIR, ÁRDÍS; LIMOUSIN, MARCEAU; RICHARD, JOHAN; HJORTH, JENS; KNEIB, JEAN-PAUL; NATARAJAN, PRIYA; PEDERSEN, KRISTIAN; JULLO, ERIC; PARAFICZ, DANUTA. Where is the matter in the Merging Cluster Abell 2218? **arXiv:0710.5636** [**astro-ph**], October 2007. arXiv: 0710.5636.

ENGEL, H.; TACCONI, L. J.; DAVIES, R. I.; NERI, R.; SMAIL, I.; CHAPMAN, S. C.; GENZEL, R.; COX, P.; GREVE, T. R.; IVISON, R. J.; BLAIN, A.; BERTOLDI, F.; OMONT, A. Most Submillimeter Galaxies are Major Mergers. **Astrophysical Journal**, v. 724, n. 1, p. 233–243, November 2010.

FU, HAI; COORAY, ASANTHA; FERUGLIO, C.; IVISON, R. J.; RIECHERS, D. A.; GURWELL, M.; BUSSMANN, R. S.; HARRIS, A. I.; ALTIERI, B.; AUSSEL, H.; BAKER, A. J.; BOCK, J.; BOYLAN-KOLCHIN, M.; BRIDGE, C.; CALANOG, J. A.; CASEY, C. M.; CAVA, A.; CHAPMAN, S. C.; CLEMENTS, D. L.; CONLEY, A.; COX, P.; FARRAH, D.; FRAYER, D.; HOPWOOD, R.; JIA, J.; MAGDIS, G.; MARSDEN, G.; MARTíNEZ-NAVAJAS, P.; NEGRELLO, M.; NERI, R.; OLIVER, S. J.; OMONT, A.; PAGE, M. J.; PÉREZ-FOURNON, I.; SCHULZ, B.; SCOTT, D.; SMITH, A.; VACCARI, M.; VALTCHANOV, I.; VIEIRA, J. D.; VIERO, M.; WANG, L.; WARDLOW, J. L.; ZEMCOV, M. The rapid assembly of an elliptical galaxy of 400 billion solar masses at a redshift of 2.3. **Nature**, v. 498, n. 7454, p. 338–341, June 2013.

FU, HAI; JULLO, E.; COORAY, A.; BUSSMANN, R. S.; IVISON, R. J.; PÉREZ-FOURNON, I.; DJORGOVSKI, S. G.; SCOVILLE, N.; YAN, L.; RIECHERS, D. A.; AGUIRRE, J.; AULD, R.; BAES, M.; BAKER, A. J.; BRADFORD, M.; CAVA, A.; CLEMENTS, D. L.; DANNERBAUER, H.; DARIUSH, A.; DE ZOTTI, G.; DOLE, H.; DUNNE, L.; DYE, S.; EALES, S.; FRAYER, D.; GAVAZZI, R.; GURWELL, M.; HARRIS, A. I.; HERRANZ, D.; HOPWOOD, R.; HOYOS, C.; IBAR, E.; JARVIS, M. J.; KIM, S.; LEEUW, L.; LUPU, R.; MADDOX, S.; MARTíNEZ-NAVAJAS, P.; MICHAłOWSKI, M. J.; NEGRELLO, M.; OMONT, A.; ROSENMAN, M.; SCOTT, D.; SERJEANT, S.; SMAIL, I.; SWINBANK, A. M.; VALIANTE, E.; VERMA, A.; VIEIRA, J.; WARDLOW, J. L.; VAN DER WERF, P. A Comprehensive View of a Strongly Lensed Planck-Associated Submillimeter Galaxy. **Astrophysical Journal**, v. 753, n. 2, p. 134, July 2012.

FURLANETTO, CRISTINA. Arcos gravitacionais em aglomerados de galáxias: detecção, caracterização e modelamento. p. 161, 2012.

GEACH, J.; SMAIL, I.; LAGOS, C.; MORAN, S.; MACARTHUR, L.; EDGE, A. The evolution of the molecular gas fraction of star-forming galaxies. In: Galaxy Formation, p. 43, July 2011.

GEORGE, R. D.; IVISON, R. J.; HOPWOOD, R.; RIECHERS, D. A.; BUSSMANN, R. S.; COX, P.; DYE, S.; KRIPS, M.; NEGRELLO, M.; NERI, R.; SERJEANT, S.; VALTCHANOV, I.; BAES, M.; BOURNE, N.; CLEMENTS, D. L.; DE ZOTTI, G.; DUNNE, L.; EALES, S. A.; IBAR, E.; MADDOX, S.; SMITH, M. W. L.; VALIANTE, E.; VAN DER WERF, P. Far-infrared spectroscopy of a lensed starburst: a blind redshift from {herschel}. **Monthly Notices of the Royal Astronomical Society**, v. 436, p. L99–L103, November 2013.

GNEDIN, OLEG Y.; KRAVTSOV, ANDREY V.; KLYPIN, ANATOLY A.; NAGAI, DAISUKE. Response of Dark Matter Halos to Condensation of Baryons: Cosmological

Simulations and Improved Adiabatic Contraction Model. **The Astrophysical Journal**, v. 616, n. 1, p. 16, November 2004.

GRIFFIN, M. J.; ABERGEL, A.; ABREU, A.; ADE, P. A. R.; ANDRÉ, P.; AUGUERES, J. L.; BABBEDGE, T.; BAE, Y.; BAILLIE, T.; BALUTEAU, J. P.; BARLOW, M. J.; BENDO, G.; BENIELLI, D.; BOCK, J. J.; BONHOMME, P.; BRISBIN, D.; BROCKLEY-BLATT, C.; CALDWELL, M.; CARA, C.; CASTRO-RODRIGUEZ, N.; CERULLI, R.; CHANIAL, P.; CHEN, S.; CLARK, E.; CLEMENTS, D. L.; CLERC, L.; COKER, J.; COMMUNAL, D.; CONVERSI, L.; COX, P.; CRUMB, D.; CUNNINGHAM, C.; DALY, F.; DAVIS, G. R.; DE ANTONI, P.; DELDERFIELD, J.; DEVIN, N.; DI GIORGIO, A.; DIDSCHUNS, I.; DOHLEN, K.; DONATI, M.; DOWELL, A.; DOWELL, C. D.; DUBAND, L.; DUMAYE, L.; EMERY, R. J.; FERLET, M.; FERRAND, D.; FONTIGNIE, J.; FOX, M.; FRANCESCHINI, A.; FRERKING, M.; FULTON, T.; GARCIA, J.; GASTAUD, R.; GEAR, W. K.; GLENN, J.; GOIZEL, A.; GRIFFIN, D. K.; GRUNDY, T.; GUEST, S.; GUILLEMET, L.; HARGRAVE, P. C.; HARWIT, M.; HASTINGS, P.; HATZIMINAOGLOU, E.; HERMAN, M.; HINDE, B.; HRISTOV, V.; HUANG, M.; IMHOF, P.; ISAAK, K. J.; ISRAELSSON, U.; IVISON, R. J.; JENNINGS, D.; KIERNAN, B.; KING, K. J.; LANGE, A. E.; LATTER, W.; LAURENT, G.; LAURENT, P.; LEEKS, S. J.; LELLOUCH, E.; LEVENSON, L.; LI, B.; LI, J.; LILIENTHAL, J.; LIM, T.; LIU, S. J.; LU, N.; MADDEN, S.; MAINETTI, G.; MARLIANI, P.; MCKAY, D.; MERCIER, K.; MOLINARI, S.; MORRIS, H.; MOSELEY, H.; MULDER, J.; MUR, M.; NAYLOR, D. A.; NGUYEN, H.; O'HALLORAN, B.; OLIVER, S.; OLOFSSON, G.; OLOFSSON, H. G.; ORFEI, R.; PAGE, M. J.; PAIN, I.; PANUZZO, P.; PAPAGEORGIOU, A.; PARKS, G.; PARR-BURMAN, P.; PEARCE, A.; PEARSON, C.; PÉREZ-FOURNON, I.; PINSARD, F.; PISANO, G.; PODOSEK, J.; POHLEN, M.; POLEHAMPTON, E. T.; POULIQUEN, D.; RIGOPOULOU, D.; RIZZO, D.; ROSEBOOM, I. G.; ROUSSEL, H.; ROWAN-ROBINSON, M.; ROWND, B.; SARACENO, P.; SAUVAGE, M.; SAVAGE, R.; SAVINI, G.; SAWYER, E.; SCHARMBERG, C.; SCHMITT, D.; SCHNEIDER, N.; SCHULZ, B.; SCHWARTZ, A.; SHAFER, R.; SHUPE, D. L.; SIBTHORPE, B.; SIDHER, S.; SMITH, A.; SMITH, A. J.; SMITH, D.; SPENCER, L.; STOBIE, B.; SUDIWALA, R.; SUKHATME, K.; SURACE, C.; STEVENS, J. A.; SWINYARD, B. M.; TRICHAS, M.; TOURETTE, T.; TRIOU, H.; TSENG, S.; TUCKER, C.; TURNER, A.; VACCARI, M.; VALTCHANOV, I.; VIGROUX, L.; VIRIQUE, E.; VOELLMER, G.; WALKER, H.; WARD, R.; WASKETT, T.; WEILERT, M.; WESSON, R.; WHITE, G. J.; WHITEHOUSE, N.; WILSON, C. D.; WINTER, B.; WOODCRAFT, A. L.; WRIGHT, G. S.; XU, C. K.; ZAVAGNO, A.; ZEMCOV, M.; ZHANG, L.; ZONCA, E. The Herschel-SPIRE instrument and its in-flight performance. **Astronomy and Astrophysics**, v. 518, p. L3, July 2010.

GRUPPIONI, C.; POZZI, F.; RODIGHIERO, G.; DELVECCHIO, I.; BERTA, S.;

POZZETTI, L.; ZAMORANI, G.; ANDREANI, P.; CIMATTI, A.; ILBERT, O.; LE FLOC'H, E.; LUTZ, D.; MAGNELLI, B.; MARCHETTI, L.; MONACO, P.; NORDON, R.; OLIVER, S.; POPESSO, P.; RIGUCCINI, L.; ROSEBOOM, I.; ROSARIO, D. J.; SARGENT, M.; VACCARI, M.; ALTIERI, B.; AUSSEL, H.; BONGIOVANNI, A.; CEPA, J.; DADDI, E.; DOMíNGUEZ-SÁNCHEZ, H.; ELBAZ, D.; FÖRSTER SCHREIBER, N.; GENZEL, R.; IRIBARREM, A.; MAGLIOCCHETTI, M.; MAIOLINO, R.; POGLITSCH, A.; PÉREZ GARCíA, A.; SANCHEZ-PORTAL, M.; STURM, E.; TACCONI, L.; VALTCHANOV, I.; AMBLARD, A.; ARUMUGAM, V.; BETHERMIN, M.; BOCK, J.; BOSELLI, A.; BUAT, V.; BURGARELLA, D.; CASTRO-RODRíGUEZ, N.; CAVA, A.; CHANIAL, P.; CLEMENTS, D. L.; CONLEY, A.; COORAY, A.; DOWELL, C. D.; DWEK, E.; EALES, S.; FRANCESCHINI, A.; GLENN, J.; GRIFFIN, M.; HATZIMINAOGLOU, E.; IBAR, E.; ISAAK, K.; IVISON, R. J.; LAGACHE, G.; LEVENSON, L.; LU, N.; MADDEN, S.; MAFFEI, B.; MAINETTI, G.; NGUYEN, H. T.; O'HALLORAN, B.; PAGE, M. J.; PANUZZO, P.; PAPAGEORGIOU, A.; PEARSON, C. P.; PÉREZ-FOURNON, I.; POHLEN, M.; RIGOPOULOU, D.; ROWAN-ROBINSON, M.; SCHULZ, B.; SCOTT, D.; SEYMOUR, N.; SHUPE, D. L.; SMITH, A. J.; STEVENS, J. A.; SYMEONIDIS, M.; TRICHAS, M.; TUGWELL, K. E.; VIGROUX, L.; WANG, L.; WRIGHT, G.; XU, C. K.; ZEMCOV, M.; BARDELLI, S.; CAROLLO, M.; CONTINI, T.; LE FÉVRE, O.; LILLY, S.; MAINIERI, V.; RENZINI, A.; SCODEGGIO, M.; ZUCCA, E. The Herschel PEP/HerMES luminosity function - I. Probing the evolution of PACS selected Galaxies to z â 4. **Monthly Notices of the Royal Astronomical Society**, v. 432, n. 1, p. 23–52, June 2013.

HAINLINE, LAURA JEANNINE. **Multi-wavelength properties of submillimeter-selected galaxies**. January 2008. Tese de Doutoramento – California Institute of Technology.

HAMMER, F.; LE FEVRE, O.; JONES, J.; RIGAUT, F.; SOUCAIL, G. Probable additional gravitational images related to the CL 2244-02 arc and B, V, R photometry of the cluster core. **Astronomy and Astrophysics**, v. 208, p. L7–L10, January 1989.

HAMMER, F.; RIGAUT, F. Giant luminous arcs from lensing - Determination of the mass distribution inside distant cluster cores. **Astronomy and Astrophysics**, v. 226, p. 45–56, December 1989.

HEZAVEH, YASHAR D.; HOLDER, GILBERT P. Effects of Strong Gravitational Lensing on Millimeter-wave Galaxy Number Counts. **Astrophysical Journal**, v. 734, n. 1, p. 52, June 2011.

HUGHES, DAVID H.; SERJEANT, STEPHEN; DUNLOP, JAMES; ROWAN-ROBINSON, MICHAEL; BLAIN, ANDREW; MANN, ROBERT G.; IVISON, ROB; PEACOCK, JOHN; EFSTATHIOU, ANDREAS; GEAR, WALTER; OLIVER, SEB; LAWRENCE,

ANDY; LONGAIR, MALCOLM; GOLDSCHMIDT, PIPPA; JENNESS, TIM. High-redshift star formation in the Hubble Deep Field revealed by a submillimetre-wavelength survey. **Nature**, v. 394, n. 6690, p. 241–247, July 1998.

IVISON, R. J.; SMAIL, IAN; AMBLARD, A.; ARUMUGAM, V.; DE BREUCK, C.; EMONTS, B. H. C.; FEAIN, I.; GREVE, T. R.; HAAS, M.; IBAR, E.; JARVIS, M. J.; KOVÁCS, A.; LEHNERT, M. D.; NESVADBA, N. P. H.; RÖTTGERING, H. J. A.; SEYMOUR, N.; WYLEZALEK, D. Gas-rich mergers and feedback are ubiquitous amongst starbursting radio galaxies, as revealed by the VLA, IRAM PdBI and Herschel. **Monthly Notices of the Royal Astronomical Society**, v. 425, n. 2, p. 1320–1331, September 2012.

JULLO, E.; KNEIB, J. P.; LIMOUSIN, M.; ELíASDÓTTIR, Á.; MARSHALL, P. J.; VERDUGO, T. A Bayesian approach to strong lensing modelling of galaxy clusters. **New Journal of Physics**, v. 9, n. 12, p. 447, December 2007.

KNEIB, J. P.; MELLIER, Y.; FORT, B.; MATHEZ, G. The Distribution of Dark Matter in Distant Cluster Lenses - Modelling A:370. **Astronomy and Astrophysics**, v. 273, p. 367, June 1993.

KORMANN, R.; SCHNEIDER, P.; BARTELMANN, M. Isothermal elliptical gravitational lens models. **Astronomy and Astrophysics**, v. 284, p. 285–299, April 1994.

KURTZ, MICHAEL J.; MINK, DOUGLAS J. RVSAO 2.0: Digital Redshifts and Radial Velocities. **Publications of the Astronomical Society of the Pacific**, v. 110, n. 750, p. 934–977, August 1998.

LAPORTE, CHERVIN F. P.; WHITE, SIMON D. M. The redistribution of matter in the cores of galaxy clusters. **Monthly Notices of the Royal Astronomical Society**, v. 451, n. 2, p. 1177, August 2015.

LE FLOC'H, EMERIC; PAPOVICH, CASEY; DOLE, HERVÉ; BELL, ERIC F.; LAGACHE, GUILAINE; RIEKE, GEORGE H.; EGAMI, EIICHI; PÉREZ-GONZÁLEZ, PABLO G.; ALONSO-HERRERO, ALMUDENA; RIEKE, MARCIA J.; BLAYLOCK, MYRA; ENGELBRACHT, CHARLES W.; GORDON, KARL D.; HINES, DEAN C.; MISSELT, KARL A.; MORRISON, JANE E.; MOULD, JEREMY. Infrared Luminosity Functions from the Chandra Deep Field-South: The Spitzer View on the History of Dusty Star Formation at 0 <~z <~1. **Astrophysical Journal**, v. 632, n. 1, p. 169–190, October 2005.

LILLY, S. J.; LE FEVRE, O.; HAMMER, F.; CRAMPTON, DAVID. The Canada-France Redshift Survey: The Luminosity Density and Star Formation History of the Universe to Z approximately 1. **Astrophysical Journal Letters**, v. 460, p. L1, March 1996.

LIMA NETO, GASTÃO. Notas de Aula Astronomia ExtragalÃ¡ctica, 2020.

LOGAN, C. H. A.; FOTOPOULOU, S. Unsupervised star, galaxy, QSO classification. Application of HDBSCAN. **Astronomy and Astrophysics**, v. 633, p. A154, January 2020.

MA, JINGZHE; GONZALEZ, ANTHONY. H.; SPILKER, J. S.; STRAND ET, M.; ASHBY, M. L. N.; ARAVENA, M.; BÉTHERMIN, M.; BOTHWELL, M. S.; DE BREUCK, C.; BRODWIN, M.; CHAPMAN, S. C.; FASSNACHT, C. D.; GREVE, T. R.; GULLBERG, B.; HEZAVEH, Y.; MALKAN, M.; MARRONE, D. P.; SALIWANCHIK, B. R.; VIEIRA, J. D.; WEISS, A.; WELIKALA, N. Stellar Masses and Star Formation Rates of Lensed, Dusty, Star-forming Galaxies from the SPT Survey. **Astrophysical Journal**, v. 812, n. 1, p. 88, October 2015.

MADAU, PIERO; DICKINSON, MARK. Cosmic Star-Formation History. **Annual Review of Astronomy and Astrophysics**, v. 52, p. 415–486, August 2014.

MARTIZZI, DAVIDE; TEYSSIER, ROMAIN; MOORE, BEN. Cusp-core transformations induced by AGN feedback in the progenitors of cluster galaxies. **Monthly Notices of the Royal Astronomical Society**, v. 432, n. 3, p. 1947, July 2013.

MENEGHETTI, MASSIMO. Introduction to Gravitational Lensing. p. 103, 2016.

MESSIAS, HUGO; DYE, SIMON; NAGAR, NEIL; ORELLANA, GUSTAVO; BUSSMANN, R. SHANE; CALANOG, JAE; DANNERBAUER, HELMUT; FU, HAI; IBAR, EDO; INOHARA, ANDREW; IVISON, R. J.; NEGRELLO, MATTIA; RIECHERS, DOMINIK A.; SHEEN, YUN-KYEONG; AGUIRRE, JAMES E.; AMBER, SIMON; BIRKINSHAW, MARK; BOURNE, NATHAN; BRADFORD, CHARLES M.; CLEMENTS, DAVE L.; COORAY, ASANTHA; DE ZOTTI, GIANFRANCO; DEMARCO, RICARDO; DUNNE, LORETTA; EALES, STEPHEN; FLEUREN, SIMONE; KAMENETZKY, JULIA; LUPU, ROXANA E.; MADDOX, STEVE J.; MARRONE, DANIEL P.; MICHAŁOWSKI, MICHAŁ J.; MURPHY, ERIC J.; NGUYEN, HIEN T.; OMONT, ALAIN; ROWLANDS, KATE; SMITH, DAN; SMITH, MATT; VALIANTE, ELISABETTA; VIEIRA, JOAQUIN D. Herschel-ATLAS and ALMA. HATLAS J142935.3-002836, a lensed major merger at redshift 1.027. **Astronomy and Astrophysics**, v. 568, p. A92, August 2014.

MICHAŁOWSKI, M.; HJORTH, J.; WATSON, D. Cosmic evolution of submillimeter galaxies and their contribution to stellar mass assembly. **Astronomy and Astrophysics**, v. 514, p. A67, May 2010.

NAVARRO, J. The Structure of Cold Dark Matter Halos. **New Light on Galaxy Evolution**, v. 171, p. 255, 1996.

NAVARRO, JULIO F.; EKE, VINCENT R.; FRENK, CARLOS S. The cores of dwarf galaxy haloes. **Monthly Notices of the Royal Astronomical Society**, v. 283, p. L72, December 1996.

NAVARRO, JULIO F.; FRENK, CARLOS S.; WHITE, SIMON D. M. A Universal Density Profile from Hierarchical Clustering. **The Astrophysical Journal**, v. 490, n. 2, p. 493, December 1997.

NAYYERI, H.; KEELE, M.; COORAY, A.; RIECHERS, D. A.; IVISON, R. J.; HARRIS, A. I.; FRAYER, D. T.; BAKER, A. J.; CHAPMAN, S. C.; EALES, S.; FARRAH, D.; FU, H.; MARCHETTI, L.; MARQUES-CHAVES, R.; MARTINEZ-NAVAJAS, P. I.; OLIVER, S. J.; OMONT, A.; PEREZ-FOURNON, I.; SCOTT, D.; VACCARI, M.; VIEIRA, J.; VIERO, M.; WANG, L.; WARDLOW, J. CANDIDATE GRAVITATIONALLY LENSED DUSTY STAR-FORMING GALAXIES IN THEHERSCHELWIDE AREA SURVEYS. **The Astrophysical Journal**, v. 823, n. 1, p. 17, May 2016.

NEGRELLO, M.; AMBER, S.; AMVROSIADIS, A.; CAI, Z. Y.; LAPI, A.; GONZALEZ-NUEVO, J.; DE ZOTTI, G.; FURLANETTO, C.; MADDOX, S. J.; ALLEN, M.; BAKX, T.; BUSSMANN, R. S.; COORAY, A.; COVONE, G.; DANESE, L.; DANNERBAUER, H.; FU, H.; GREENSLADE, J.; GURWELL, M.; HOPWOOD, R.; KOOPMANS, L. V. E.; NAPOLITANO, N.; NAYYERI, H.; OMONT, A.; PETRILLO, C. E.; RIECHERS, D. A.; SERJEANT, S.; TORTORA, C.; VALIANTE, E.; VERDOES KLEIJN, G.; VERNARDOS, G.; WARDLOW, J. L.; BAES, M.; BAKER, A. J.; BOURNE, N.; CLEMENTS, D.; CRAWFORD, S. M.; DYE, S.; DUNNE, L.; EALES, S.; IVISON, R. J.; MARCHETTI, L.; MICHAŁOWSKI, M. J.; SMITH, M. W. L.; VACCARI, M.; VAN DER WERF, P. The Herschel-ATLAS: a sample of 500 μm-selected lensed galaxies over 600 deg^2. **Monthly Notices of the Royal Astronomical Society**, v. 465, n. 3, p. 3558–3580, March 2017.

NEGRELLO, M.; PERROTTA, F.; GONZÁLEZ-NUEVO, J.; SILVA, L.; DE ZOTTI, G.; GRANATO, G. L.; BACCIGALUPI, C.; DANESE, L. Astrophysical and cosmological information from large-scale submillimetre surveys of extragalactic sources. **Monthly Notices of the Royal Astronomical Society**, v. 377, n. 4, p. 1557–1568, June 2007.

NEGRELLO, MATTIA. High resolution Near-Infrared imaging of the first sub-mm selected gravitational lens candidates in the Herschel ATLAS. **HST Proposal**, September 2010.

NEGRELLO, MATTIA; HOPWOOD, R.; DE ZOTTI, G.; COORAY, A.; VERMA, A.; BOCK, J.; FRAYER, D. T.; GURWELL, M. A.; OMONT, A.; NERI, R.; DANNERBAUER, H.; LEEUW, L. L.; BARTON, E.; COOKE, J.; KIM, S.; CUNHA, E.DA ; RODIGHIERO, G.; COX, P.; BONFIELD, D. G.; JARVIS, M. J.; SERJEANT, S.; IVISON, R. J.; DYE, S.; ARETXAGA, I.; HUGHES, D. H.; IBAR, E.; BERTOLDI, F.; VALTCHANOV, I.; EALES, S.; DUNNE, L.; DRIVER, S. P.; AULD,

R.; BUTTIGLIONE, S.; CAVA, A.; GRADY, C. A.; CLEMENTS, D. L.; DARIUSH, A.; FRITZ, J.; HILL, D.; HORNBECK, J. B.; KELVIN, L.; LAGACHE, G.; LOPEZ-CANIEGO, M.; GONZALEZ-NUEVO, J.; MADDOX, S.; PASCALE, E.; POHLEN, M.; RIGBY, E. E.; ROBOTHAM, A.; SIMPSON, C.; SMITH, D. J. B.; TEMI, P.; THOMPSON, M. A.; WOODGATE, B. E.; YORK, D. G.; AGUIRRE, J. E.; BEELEN, A.; BLAIN, A.; BAKER, A. J.; BIRKINSHAW, M.; BLUNDELL, R.; BRADFORD, C. M.; BURGARELLA, D.; DANESE, L.; DUNLOP, J. S.; FLEUREN, S.; GLENN, J.; HARRIS, A. I.; KAMENETZKY, J.; LUPU, R. E.; MADDALENA, R. J.; MADORE, B. F.; MALONEY, P. R.; MATSUHARA, H.; MICHAÅOWSKI, M. J.; MURPHY, E. J.; NAYLOR, B. J.; NGUYEN, H.; POPESCU, C.; RAWLINGS, S.; RIGOPOULOU, D.; SCOTT, D.; SCOTT, K. S.; SEIBERT, M.; SMAIL, I.; TUFFS, R. J.; VIEIRA, J. D.; WERF, P. P.VAN DER ; ZMUIDZINAS, J. The Detection of a Population of Submillimeter-Bright, Strongly Lensed Galaxies. **Science**, v. 330, p. 800, November 2010.

NEWMAN, ANDREW B.; ELLIS, RICHARD S.; TREU, TOMMASO. Luminous and Dark Matter Profiles from Galaxies to Clusters: Bridging the Gap with Group-scale Lenses. **The Astrophysical Journal**, v. 814, n. 1, p. 26, November 2015.

NEWMAN, JEFFREY A.; COOPER, MICHAEL C.; DAVIS, MARC; FABER, S. M.; COIL, ALISON L.; GUHATHAKURTA, PURAGRA; KOO, DAVID C.; PHILLIPS, ANDREW C.; CONROY, CHARLIE; DUTTON, AARON A.; FINKBEINER, DOUGLAS P.; GERKE, BRIAN F.; ROSARIO, DAVID J.; WEINER, BENJAMIN J.; WILLMER, C. N. A.; YAN, RENBIN; HARKER, JUSTIN J.; KASSIN, SUSAN A.; KONIDARIS, N. P.; LAI, KAMSON; MADGWICK, DARREN S.; NOESKE, K. G.; WIRTH, GREGORY D.; CONNOLLY, A. J.; KAISER, N.; KIRBY, EVAN N.; LEMAUX, BRIAN C.; LIN, LIHWAI; LOTZ, JENNIFER M.; LUPPINO, G. A.; MARINONI, C.; MATTHEWS, DANIEL J.; METEVIER, ANNE; SCHIAVON, RICARDO P. THE DEEP2 GALAXY REDSHIFT SURVEY: DESIGN, OBSERVATIONS, DATA REDUCTION, AND REDSHIFTS. **The Astrophysical Journal Supplement Series**, v. 208, n. 1, p. 5, August 2013.

NIPOTI, C.; TREU, T.; CIOTTI, L.; STIAVELLI, M. Galactic cannibalism and cold dark matter density profiles. **Monthly Notices of the Royal Astronomical Society**, v. 355, p. 1119, December 2004.

OLIVER, S. J.; BOCK, J.; ALTIERI, B.; AMBLARD, A.; ARUMUGAM, V.; AUSSEL, H.; BABBEDGE, T.; BEELEN, A.; BÉTHERMIN, M.; BLAIN, A.; BOSELLI, A.; BRIDGE, C.; BRISBIN, D.; BUAT, V.; BURGARELLA, D.; CASTRO-RODRíGUEZ, N.; CAVA, A.; CHANIAL, P.; CIRASUOLO, M.; CLEMENTS, D. L.; CONLEY, A.; CONVERSI, L.;

COORAY, A.; DOWELL, C. D.; DUBOIS, E. N.; DWEK, E.; DYE, S.; EALES, S.; ELBAZ, D.; FARRAH, D.; FELTRE, A.; FERRERO, P.; FIOLET, N.; FOX, M.; FRANCESCHINI, A.; GEAR, W.; GIOVANNOLI, E.; GLENN, J.; GONG, Y.; GONZÁLEZ SOLARES, E. A.; GRIFFIN, M.; HALPERN, M.; HARWIT, M.; HATZIMINAOGLOU, E.; HEINIS, S.; HURLEY, P.; HWANG, H. S.; HYDE, A.; IBAR, E.; ILBERT, O.; ISAAK, K.; IVISON, R. J.; LAGACHE, G.; LE FLOC'H, E.; LEVENSON, L.; FARO, B. LO; LU, N.; MADDEN, S.; MAFFEI, B.; MAGDIS, G.; MAINETTI, G.; MARCHETTI, L.; MARSDEN, G.; MARSHALL, J.; MORTIER, A. M. J.; NGUYEN, H. T.; O'HALLORAN, B.; OMONT, A.; PAGE, M. J.; PANUZZO, P.; PAPAGEORGIOU, A.; PATEL, H.; PEARSON, C. P.; PÉREZ-FOURNON, I.; POHLEN, M.; RAWLINGS, J. I.; RAYMOND, G.; RIGOPOULOU, D.; RIGUCCINI, L.; RIZZO, D.; RODIGHIERO, G.; ROSEBOOM, I. G.; ROWAN-ROBINSON, M.; SÁNCHEZ PORTAL, M.; SCHULZ, B.; SCOTT, DOUGLAS; SEYMOUR, N.; SHUPE, D. L.; SMITH, A. J.; STEVENS, J. A.; SYMEONIDIS, M.; TRICHAS, M.; TUGWELL, K. E.; VACCARI, M.; VALTCHANOV, I.; VIEIRA, J. D.; VIERO, M.; VIGROUX, L.; WANG, L.; WARD, R.; WARDLOW, J.; WRIGHT, G.; XU, C. K.; ZEMCOV, M. The Herschel Multi-tiered Extragalactic Survey: HerMES. **Monthly Notices of the Royal Astronomical Society**, v. 424, n. 3, p. 1614–1635, August 2012.

OTEO, I.; IVISON, R. J.; DUNNE, L.; SMAIL, I.; SWINBANK, A. M.; ZHANG, Z. Y.; LEWIS, A.; MADDOX, S.; RIECHERS, D.; SERJEANT, S.; VAN DER WERF, P.; BIGGS, A. D.; BREMER, M.; CIGAN, P.; CLEMENTS, D. L.; COORAY, A.; DANNERBAUER, H.; EALES, S.; IBAR, E.; MESSIAS, H.; MICHAŁOWSKI, M. J.; PÉREZ-FOURNON, I.; VAN KAMPEN, E. Witnessing the Birth of the Red Sequence: ALMA High-resolution Imaging of [C II] and Dust in Two Interacting Ultra-red Starbursts at z = 4.425. **Astrophysical Journal**, v. 827, n. 1, p. 34, August 2016.

PENNELL, ALISON; RUNNOE, JESSIE C.; BROTHERTON, M. S. Updating quasar bolometric luminosity corrections - III. [O III] bolometric corrections. **Monthly Notices of the Royal Astronomical Society**, v. 468, n. 2, p. 1433–1441, June 2017.

PERROTTA, F.; BACCIGALUPI, C.; BARTELMANN, M.; DE ZOTTI, G.; GRANATO, G. L. Gravitational lensing of extended high-redshift sources by dark matter haloes. **Monthly Notices of the Royal Astronomical Society**, v. 329, n. 2, p. 445–455, January 2002.

PERROTTA, F.; MAGLIOCCHETTI, M.; BACCIGALUPI, C.; BARTELMANN, M.; DE ZOTTI, G.; GRANATO, G. L.; SILVA, L.; DANESE, L. Predictions for statistical properties of forming spheroidal galaxies. **Monthly Notices of the Royal Astronomical Society**, v. 338, n. 3, p. 623–636, January 2003.

PLANCK COLLABORATION, ; ADE, P. A. R.; AGHANIM, N.; ARMITAGE-CAPLAN, C.; ARNAUD, M.; ASHDOWN, M.; ATRIO-BARAND ELA, F.; AUMONT, J.; BACCI-GALUPI, C.; BANDAY, A. J.; BARREIRO, R. B.; BARTLETT, J. G.; BATTANER, E.; BENABED, K.; BENOîT, A.; BENOIT-LÉVY, A.; BERNARD, J. P.; BERSANELLI, M.; BIELEWICZ, P.; BOBIN, J.; BOCK, J. J.; BONALDI, A.; BOND, J. R.; BORRILL, J.; BOUCHET, F. R.; BRIDGES, M.; BUCHER, M.; BURIGANA, C.; BUTLER, R. C.; CALABRESE, E.; CAPPELLINI, B.; CARDOSO, J. F.; CATALANO, A.; CHALLINOR, A.; CHAMBALLU, A.; CHARY, R. R.; CHEN, X.; CHIANG, H. C.; CHIANG, L. Y.; CHRISTENSEN, P. R.; CHURCH, S.; CLEMENTS, D. L.; COLOMBI, S.; COLOMBO, L. P. L.; COUCHOT, F.; COULAIS, A.; CRILL, B. P.; CURTO, A.; CUTTAIA, F.; DANESE, L.; DAVIES, R. D.; DAVIS, R. J.; DE BERNARDIS, P.; DE ROSA, A.; DE ZOTTI, G.; DELABROUILLE, J.; DELOUIS, J. M.; DÉSERT, F. X.; DICKINSON, C.; DIEGO, J. M.; DOLAG, K.; DOLE, H.; DONZELLI, S.; DORÉ, O.; DOUSPIS, M.; DUNKLEY, J.; DUPAC, X.; EFSTATHIOU, G.; ELSNER, F.; ENßLIN, T. A.; ERIKSEN, H. K.; FINELLI, F.; FORNI, O.; FRAILIS, M.; FRAISSE, A. A.; FRANCESCHI, E.; GAIER, T. C.; GALEOTTA, S.; GALLI, S.; GANGA, K.; GIARD, M.; GIARDINO, G.; GIRAUD-HÉRAUD, Y.; GJERLøW, E.; GONZÁLEZ-NUEVO, J.; GÓRSKI, K. M.; GRATTON, S.; GREGORIO, A.; GRUPPUSO, A.; GUDMUNDSSON, J. E.; HAISSINSKI, J.; HAMANN, J.; HANSEN, F. K.; HANSON, D.; HARRISON, D.; HENROT-VERSILLÉ, S.; HERNÁNDEZ-MONTEAGUDO, C.; HERRANZ, D.; HILDEBRAND T, S. R.; HIVON, E.; HOBSON, M.; HOLMES, W. A.; HORNSTRUP, A.; HOU, Z.; HOVEST, W.; HUFFENBERGER, K. M.; JAFFE, A. H.; JAFFE, T. R.; JEWELL, J.; JONES, W. C.; JUVELA, M.; KEIHÄNEN, E.; KESKITALO, R.; KISNER, T. S.; KNEISSL, R.; KNOCHE, J.; KNOX, L.; KUNZ, M.; KURKI-SUONIO, H.; LAGACHE, G.; LÄHTEENMÄKI, A.; LAMARRE, J. M.; LASENBY, A.; LATTANZI, M.; LAUREIJS, R. J.; LAWRENCE, C. R.; LEACH, S.; LEAHY, J. P.; LEONARDI, R.; LEÓN-TAVARES, J.; LESGOURGUES, J.; LEWIS, A.; LIGUORI, M.; LILJE, P. B.; LINDEN-VøRNLE, M.; LÓPEZ-CANIEGO, M.; LUBIN, P. M.; MACíAS-PÉREZ, J. F.; MAFFEI, B.; MAINO, D.; MAND OLESI, N.; MARIS, M.; MARSHALL, D. J.; MARTIN, P. G.; MARTíNEZ-GONZÁLEZ, E.; MASI, S.; MASSARDI, M.; MATARRESE, S.; MATTHAI, F.; MAZZOTTA, P.; MEINHOLD, P. R.; MELCHIORRI, A.; MELIN, J. B.; MENDES, L.; MENEGONI, E.; MENNELLA, A.; MIGLIACCIO, M.; MILLEA, M.; MITRA, S.; MIVILLE-DESCHÊNES, M. A.; MONETI, A.; MONTIER, L.; MORGANTE, G.; MORTLOCK, D.; MOSS, A.; MUNSHI, D.; MURPHY, J. A.; NASELSKY, P.; NATI, F.; NATOLI, P.; NETTERFIELD, C. B.; NøRGAARD-NIELSEN, H. U.; NOVIELLO, F.; NOVIKOV, D.; NOVIKOV, I.; O'DWYER, I. J.; OSBORNE, S.; OXBORROW, C. A.; PACI, F.; PAGANO, L.; PAJOT, F.; PALADINI, R.; PAOLETTI, D.; PARTRIDGE, B.; PASIAN, F.; PATANCHON, G.; PEARSON, D.; PEARSON, T. J.; PEIRIS, H. V.; PERDEREAU, O.; PEROTTO, L.; PERROTTA, F.; PETTORINO, V.; PIACENTINI,

F.; PIAT, M.; PIERPAOLI, E.; PIETROBON, D.; PLASZCZYNSKI, S.; PLATANIA, P.; POINTECOUTEAU, E.; POLENTA, G.; PONTHIEU, N.; POPA, L.; POUTANEN, T.; PRATT, G. W.; PRÉZEAU, G.; PRUNET, S.; PUGET, J. L.; RACHEN, J. P.; REACH, W. T.; REBOLO, R.; REINECKE, M.; REMAZEILLES, M.; RENAULT, C.; RICCIARDI, S.; RILLER, T.; RISTORCELLI, I.; ROCHA, G.; ROSSET, C.; ROUDIER, G.; ROWAN-ROBINSON, M.; RUBIÑO-MARTíN, J. A.; RUSHOLME, B.; SANDRI, M.; SANTOS, D.; SAVELAINEN, M.; SAVINI, G.; SCOTT, D.; SEIFFERT, M. D.; SHELLARD, E. P. S.; SPENCER, L. D.; STARCK, J. L.; STOLYAROV, V.; STOMPOR, R.; SUDIWALA, R.; SUNYAEV, R.; SUREAU, F.; SUTTON, D.; SUUR-USKI, A. S.; SYGNET, J. F.; TAUBER, J. A.; TAVAGNACCO, D.; TERENZI, L.; TOFFOLATTI, L.; TOMASI, M.; TRISTRAM, M.; TUCCI, M.; TUOVINEN, J.; TÜRLER, M.; UMANA, G.; VALENZIANO, L.; VALIVIITA, J.; VAN TENT, B.; VIELVA, P.; VILLA, F.; VITTORIO, N.; WADE, L. A.; WANDELT, B. D.; WEHUS, I. K.; WHITE, M.; WHITE, S. D. M.; WILKINSON, A.; YVON, D.; ZACCHEI, A.; ZONCA, A. Planck 2013 results. XVI. Cosmological parameters. **Astronomy and Astrophysics**, v. 571, p. A16, November 2014.

PONTZEN, ANDREW; GOVERNATO, FABIO. How supernova feedback turns dark matter cusps into cores. **Monthly Notices of the Royal Astronomical Society**, v. 421, n. 4, p. 3464, April 2012.

ROWLANDS, K.; DUNNE, L.; DYE, S.; ARAGÓN-SALAMANCA, A.; MADDOX, S.; DA CUNHA, E.; SMITH, D. J. B.; BOURNE, N.; EALES, S.; GOMEZ, H. L.; SMAIL, I.; ALPASLAN, M.; CLARK, C. J. R.; DRIVER, S.; IBAR, E.; IVISON, R. J.; ROBOTHAM, A.; SMITH, M. W. L.; VALIANTE, E. Herschel-ATLAS: properties of dusty massive galaxies at low and high redshifts. **Monthly Notices of the Royal Astronomical Society**, v. 441, n. 2, p. 1017–1039, June 2014.

RYBAK, M.; MCKEAN, J. P.; VEGETTI, S.; ANDREANI, P.; WHITE, S. D. M. ALMA imaging of SDP.81 - I. A pixelated reconstruction of the far-infrared continuum emission. **Monthly Notices of the Royal Astronomical Society**, v. 451, p. L40–L44, July 2015.

SAKAMOTO, K.; SCOVILLE, N. Z.; YUN, M. S.; CROSAS, M.; GENZEL, R.; TACCONI, L. J. Counterrotating Nuclear Disks in ARP 220. **Astrophysical Journal**, v. 514, n. 1, p. 68–76, March 1999.

SAND, DAVID J.; TREU, TOMMASO; ELLIS, RICHARD S.; SMITH, GRAHAM P.; KNEIB, JEAN-PAUL. Separating Baryons and Dark Matter in Cluster Cores: A Full Two-dimensional Lensing and Dynamic Analysis of Abell 383 and MS 2137â23. **The Astrophysical Journal**, v. 674, n. 2, p. 711, February 2008.

SANDERS, D. B.; MIRABEL, I. F. Luminous Infrared Galaxies. , v. 34, p. 749, January 1996.

SCHALLER, MATTHIEU; FRENK, CARLOS S.; BOWER, RICHARD G.; THEUNS, TOM; TRAYFORD, JAMES; CRAIN, ROBERT A.; FURLONG, MICHELLE; SCHAYE, JOOP; DALLA VECCHIA, CLAUDIO; MCCARTHY, I. G. The effect of baryons on the inner density profiles of rich clusters. **Monthly Notices of the Royal Astronomical Society**, v. 452, n. 1, p. 343–355, September 2015.

SCHIMINOVICH, D.; ILBERT, O.; ARNOUTS, S.; MILLIARD, B.; TRESSE, L.; LE FÈVRE, O.; TREYER, M.; WYDER, T. K.; BUDAVÁRI, T.; ZUCCA, E.; ZAMORANI, G.; MARTIN, D. C.; ADAMI, C.; ARNABOLDI, M.; BARDELLI, S.; BARLOW, T.; BIANCHI, L.; BOLZONELLA, M.; BOTTINI, D.; BYUN, Y. I.; CAPPI, A.; CONTINI, T.; CHARLOT, S.; DONAS, J.; FORSTER, K.; FOUCAUD, S.; FRANZETTI, P.; FRIEDMAN, P. G.; GARILLI, B.; GAVIGNAUD, I.; GUZZO, L.; HECKMAN, T. M.; HOOPES, C.; IOVINO, A.; JELINSKY, P.; LE BRUN, V.; LEE, Y. W.; MACCAGNI, D.; MADORE, B. F.; MALINA, R.; MARANO, B.; MARINONI, C.; MCCRACKEN, H. J.; MAZURE, A.; MENEUX, B.; MORRISSEY, P.; NEFF, S.; PALTANI, S.; PELLÒ, R.; PICAT, J. P.; POLLO, A.; POZZETTI, L.; RADOVICH, M.; RICH, R. M.; SCARAMELLA, R.; SCODEGGIO, M.; SEIBERT, M.; SIEGMUND, O.; SMALL, T.; SZALAY, A. S.; VETTOLANI, G.; WELSH, B.; XU, C. K.; ZANICHELLI, A. The GALEX-VVDS Measurement of the Evolution of the Far-Ultraviolet Luminosity Density and the Cosmic Star Formation Rate. **Astrophysical Journal Letters**, v. 619, n. 1, p. L47–L50, January 2005.

SERJEANT, STEPHEN; HARRISON, DIANA. The local submillimetre luminosity functions and predictions from Spitzer to Herschel. **Monthly Notices of the Royal Astronomical Society**, v. 356, n. 1, p. 192–204, January 2005.

SIMPSON, J. M.; SMAIL, IAN; SWINBANK, A. M.; IVISON, R. J.; DUNLOP, J. S.; GEACH, J. E.; ALMAINI, O.; ARUMUGAM, V.; BREMER, M. N.; CHEN, CHIAN-CHOU; CONSELICE, C.; COPPIN, K. E. K.; FARRAH, D.; IBAR, E.; HARTLEY, W. G.; MA, C. J.; MICHAŁOWSKI, M. J.; SCOTT, D.; SPAANS, M.; THOMSON, A. P.; VAN DER WERF, P. P. The SCUBA-2 Cosmology Legacy Survey: Multi-wavelength Properties of ALMA-identified Submillimeter Galaxies in UKIDSS UDS. **Astrophysical Journal**, v. 839, n. 1, p. 58, April 2017.

SIMPSON, J. M.; SWINBANK, A. M.; SMAIL, IAN; ALEXAND ER, D. M.; BRANDT, W. N.; BERTOLDI, F.; DE BREUCK, C.; CHAPMAN, S. C.; COPPIN, K. E. K.; DA CUNHA, E.; DANIELSON, A. L. R.; DANNERBAUER, H.; GREVE, T. R.; HODGE, J. A.; IVISON, R. J.; KARIM, A.; KNUDSEN, K. K.; POGGIANTI, B. M.; SCHINNERER, E.; THOMSON, A. P.; WALTER, F.; WARDLOW, J. L.; WEIß, A.; VAN DER

WERF, P. P. An ALMA Survey of Submillimeter Galaxies in the Extended Chandra Deep Field South: The Redshift Distribution and Evolution of Submillimeter Galaxies. **Astrophysical Journal**, v. 788, n. 2, p. 125, June 2014.

SMAIL, IAN; IVISON, R. J.; BLAIN, A. W. A Deep Sub-millimeter Survey of Lensing Clusters: A New Window on Galaxy Formation and Evolution. **Astrophysical Journal Letters**, v. 490, n. 1, p. L5–L8, November 1997.

SOUCAIL, G.; FORT, B.; MELLIER, Y.; PICAT, J. P. A blue ring-like structure, in the center of the A 370 cluster of galaxies. **Astronomy and Astrophysics**, v. 172, p. L14–L16, January 1987.

STRATEVA, I.; IVEZIĆ, Ž.; KNAPP, G. R.; NARAYANAN, V. K.; STRAUSS, M. A.; GUNN, J. E.; LUPTON, R. H.; SCHLEGEL, D.; BAHCALL, N. A.; BRINKMANN, J.; BRUNNER, R. J.; BUDAVÁRI, T.; CSABAI, I.; CASTANDER, F. J.; DOI, M.; FUKUGITA, M.; GYŐRY, Z.; HAMABE, M.; HENNESSY, G.; ICHIKAWA, T.; KUNSZT, P. Z.; LAMB, D. Q.; MCKAY, T. A.; OKAMURA, S.; RACUSIN, J.; SEKIGUCHI, M.; SCHNEIDER, D. P.; SHIMASAKU, K.; YORK, D. Color Separation of Galaxy Types in the Sloan Digital Sky Survey Imaging Data. , v. 122, p. 1861–1874, October 2001.

SUYU, S. H.; MARSHALL, P. J.; AUGER, M. W.; HILBERT, S.; BLANDFORD, R. D.; KOOPMANS, L. V. E.; FASSNACHT, C. D.; TREU, T. Dissecting the Gravitational lens B1608+656. II. Precision Measurements of the Hubble Constant, Spatial Curvature, and the Dark Energy Equation of State. **The Astrophysical Journal**, v. 711, p. 201–221, March 2010.

SWINBANK, A. M.; SMAIL, IAN; CHAPMAN, S. C.; BORYS, C.; ALEXANDER, D. M.; BLAIN, A. W.; CONSELICE, C. J.; HAINLINE, L. J.; IVISON, R. J. A Hubble Space Telescope NICMOS and ACS morphological study of z ~2 submillimetre galaxies. **Monthly Notices of the Royal Astronomical Society**, v. 405, n. 1, p. 234–244, June 2010.

SYMEONIDIS, M.; VACCARI, M.; BERTA, S.; PAGE, M. J.; LUTZ, D.; ARUMUGAM, V.; AUSSEL, H.; BOCK, J.; BOSELLI, A.; BUAT, V.; CAPAK, P. L.; CLEMENTS, D. L.; CONLEY, A.; CONVERSI, L.; COORAY, A.; DOWELL, C. D.; FARRAH, D.; FRANCESCHINI, A.; GIOVANNOLI, E.; GLENN, J.; GRIFFIN, M.; HATZIMINAOGLOU, E.; HWANG, H. S.; IBAR, E.; ILBERT, O.; IVISON, R. J.; LE FLOC'H, E.; LILLY, S.; KARTALTEPE, J. S.; MAGNELLI, B.; MAGDIS, G.; MARCHETTI, L.; NGUYEN, H. T.; NORDON, R.; O'HALLORAN, B.; OLIVER, S. J.; OMONT, A.; PAPAGEORGIOU, A.; PATEL, H.; PEARSON, C. P.; PÉREZ-FOURNON, I.; POHLEN, M.; POPESSO, P.; POZZI, F.; RIGOPOULOU, D.; RIGUCCINI, L.; ROSARIO, D.; ROSEBOOM, I. G.; ROWAN-ROBINSON, M.; SALVATO, M.; SCHULZ, B.; SCOTT,

DOUGLAS; SEYMOUR, N.; SHUPE, D. L.; SMITH, A. J.; VALTCHANOV, I.; WANG, L.; XU, C. K.; ZEMCOV, M.; WUYTS, S. The Herschel census of infrared SEDs through cosmic time. **Monthly Notices of the Royal Astronomical Society**, v. 431, n. 3, p. 2317–2340, May 2013.

TACCONI, L. J.; GENZEL, R.; NERI, R.; COX, P.; COOPER, M. C.; SHAPIRO, K.; BOLATTO, A.; BOUCHÉ, N.; BOURNAUD, F.; BURKERT, A.; COMBES, F.; COMERFORD, J.; DAVIS, M.; SCHREIBER, N. M. FÖRSTER; GARCIA-BURILLO, S.; GRACIA-CARPIO, J.; LUTZ, D.; NAAB, T.; OMONT, A.; SHAPLEY, A.; STERNBERG, A.; WEINER, B. High molecular gas fractions in normal massive star-forming galaxies in the young Universe. , v. 463, n. 7282, p. 781–784, February 2010.

TACCONI, L. J.; NERI, R.; CHAPMAN, S. C.; GENZEL, R.; SMAIL, I.; IVISON, R. J.; BERTOLDI, F.; BLAIN, A.; COX, P.; GREVE, T.; OMONT, A. High-Resolution Millimeter Imaging of Submillimeter Galaxies. **Astrophysical Journal**, v. 640, n. 1, p. 228–240, March 2006.

TONINI, C.; LAPI, A.; SALUCCI, P. Angular Momentum Transfer in Dark Matter Halos: Erasing the Cusp. **The Astrophysical Journal**, v. 649, p. 591, October 2006.

TREMONTI, C. A.; HECKMAN, T. M.; KAUFFMANN, G.; BRINCHMANN, J.; CHARLOT, S.; WHITE, S. D. M.; SEIBERT, M.; PENG, E. W.; SCHLEGEL, D. J.; UOMOTO, A.; FUKUGITA, M.; BRINKMANN, J. The origin of the mass-metallicity relation: Insights from 53,000 star-forming galaxies in the sloan digital sky survey. **Astrophysical Journal**, v. 613, p. 898–913, October 2004.

TREU, TOMMASO; KOOPMANS, LÃON V. E. The Internal Structure and Formation of Early-Type Galaxies: The Gravitational Lens System MG 2016+112 at z = 1.004*. **The Astrophysical Journal**, v. 575, n. 1, p. 87, August 2002.

VERDUGO, T.; DIEGO, J. A.DE ; LIMOUSIN, MARCEAU. MS 2053.7-0449: Confirmation of a Bimodal Mass Distribution from Strong Gravitational Lensing. **The Astrophysical Journal**, v. 664, p. 702–712, August 2007.

VERDUGO, T.; MOTTA, V.; MUÃOZ, R. P.; LIMOUSIN, M.; CABANAC, R.; RICHARD, J. Gravitational lensing and dynamics in SL2s J02140-0535: probing the mass out to large radius. **Astronomy & Astrophysics**, v. 527, p. A124, March 2011.

VIEIRA, J. D.; CRAWFORD, T. M.; SWITZER, E. R.; ADE, P. A. R.; AIRD, K. A.; ASHBY, M. L. N.; BENSON, B. A.; BLEEM, L. E.; BRODWIN, M.; CARLSTROM, J. E.; CHANG, C. L.; CHO, H. M.; CRITES, A. T.; DE HAAN, T.; DOBBS, M. A.; EVERETT, W.; GEORGE, E. M.; GLADDERS, M.; HALL, N. R.; HALVERSON, N. W.; HIGH, F. W.; HOLDER, G. P.; HOLZAPFEL, W. L.; HRUBES, J. D.; JOY, M.; KEISLER, R.;

KNOX, L.; LEE, A. T.; LEITCH, E. M.; LUEKER, M.; MARRONE, D. P.; MCINTYRE, V.; MCMAHON, J. J.; MEHL, J.; MEYER, S. S.; MOHR, J. J.; MONTROY, T. E.; PADIN, S.; PLAGGE, T.; PRYKE, C.; REICHARDT, C. L.; RUHL, J. E.; SCHAFFER, K. K.; SHAW, L.; SHIROKOFF, E.; SPIELER, H. G.; STALDER, B.; STANISZEWSKI, Z.; STARK, A. A.; VANDERLINDE, K.; WALSH, W.; WILLIAMSON, R.; YANG, Y.; ZAHN, O.; ZENTENO, A. Extragalactic Millimeter-wave Sources in South Pole Telescope Survey Data: Source Counts, Catalog, and Statistics for an 87 Square-degree Field. **Astrophysical Journal**, v. 719, n. 1, p. 763–783, August 2010.

VIEIRA, J. D.; MARRONE, D. P.; CHAPMAN, S. C.; DE BREUCK, C.; HEZAVEH, Y. D.; WEIβ, A.; AGUIRRE, J. E.; AIRD, K. A.; ARAVENA, M.; ASHBY, M. L. N.; BAYLISS, M.; BENSON, B. A.; BIGGS, A. D.; BLEEM, L. E.; BOCK, J. J.; BOTHWELL, M.; BRADFORD, C. M.; BRODWIN, M.; CARLSTROM, J. E.; CHANG, C. L.; CRAWFORD, T. M.; CRITES, A. T.; DE HAAN, T.; DOBBS, M. A.; FOMALONT, E. B.; FASSNACHT, C. D.; GEORGE, E. M.; GLADDERS, M. D.; GONZALEZ, A. H.; GREVE, T. R.; GULLBERG, B.; HALVERSON, N. W.; HIGH, F. W.; HOLDER, G. P.; HOLZAPFEL, W. L.; HOOVER, S.; HRUBES, J. D.; HUNTER, T. R.; KEISLER, R.; LEE, A. T.; LEITCH, E. M.; LUEKER, M.; LUONG-VAN, D.; MALKAN, M.; MCINTYRE, V.; MCMAHON, J. J.; MEHL, J.; MENTEN, K. M.; MEYER, S. S.; MOCANU, L. M.; MURPHY, E. J.; NATOLI, T.; PADIN, S.; PLAGGE, T.; REICHARDT, C. L.; REST, A.; RUEL, J.; RUHL, J. E.; SHARON, K.; SCHAFFER, K. K.; SHAW, L.; SHIROKOFF, E.; SPILKER, J. S.; STALDER, B.; STANISZEWSKI, Z.; STARK, A. A.; STORY, K.; VAND ERLINDE, K.; WELIKALA, N.; WILLIAMSON, R. Dusty starburst galaxies in the early Universe as revealed by gravitational lensing. **Nature**, v. 495, n. 7441, p. 344–347, March 2013.

WALSH, D.; CARSWELL, R. F.; WEYMANN, R. J. 0957 + 561 A, B: twin quasistellar objects or gravitational lens? **Nature**, v. 279, n. 5712, p. 381–384, May 1979a. Number: 5712 Publisher: Nature Publishing Group.

WALSH, D.; WILLS, B. J.; WILLS, D. Spectroscopy of QSO candidates from the Jodrell Bank 966 MHz survey. **Monthly Notices of the Royal Astronomical Society**, v. 189, p. 667–670, December 1979b.

WARDLOW, JULIE L.; COORAY, ASANTHA; DE BERNARDIS, FRANCESCO; AMBLARD, A.; ARUMUGAM, V.; AUSSEL, H.; BAKER, A. J.; BÉTHERMIN, M.; BLUNDELL, R.; BOCK, J.; BOSELLI, A.; BRIDGE, C.; BUAT, V.; BURGARELLA, D.; BUSSMANN, R. S.; CABRERA-LAVERS, A.; CALANOG, J.; CARPENTER, J. M.; CASEY, C. M.; CASTRO-RODRíGUEZ, N.; CAVA, A.; CHANIAL, P.; CHAPIN, E.; CHAPMAN, S. C.; CLEMENTS, D. L.; CONLEY, A.; COX, P.; DOWELL, C. D.; DYE, S.; EALES, S.; FARRAH, D.; FERRERO, P.; FRANCESCHINI, A.; FRAYER, D. T.;

FRAZER, C.; FU, HAI; GAVAZZI, R.; GLENN, J.; GONZÁLEZ SOLARES, E. A.; GRIFFIN, M.; GURWELL, M. A.; HARRIS, A. I.; HATZIMINAOGLOU, E.; HOPWOOD, R.; HYDE, A.; IBAR, E.; IVISON, R. J.; KIM, S.; LAGACHE, G.; LEVENSON, L.; MARCHETTI, L.; MARSDEN, G.; MARTINEZ-NAVAJAS, P.; NEGRELLO, M.; NERI, R.; NGUYEN, H. T.; O'HALLORAN, B.; OLIVER, S. J.; OMONT, A.; PAGE, M. J.; PANUZZO, P.; PAPAGEORGIOU, A.; PEARSON, C. P.; PÉREZ-FOURNON, I.; POHLEN, M.; RIECHERS, D.; RIGOPOULOU, D.; ROSEBOOM, I. G.; ROWAN-ROBINSON, M.; SCHULZ, B.; SCOTT, D.; SCOVILLE, N.; SEYMOUR, N.; SHUPE, D. L.; SMITH, A. J.; STREBLYANSKA, A.; STROM, A.; SYMEONIDIS, M.; TRICHAS, M.; VACCARI, M.; VIEIRA, J. D.; VIERO, M.; WANG, L.; XU, C. K.; YAN, L.; ZEMCOV, M. HerMES: Candidate Gravitationally Lensed Galaxies and Lensing Statistics at Submillimeter Wavelengths. **Astrophysical Journal**, v. 762, n. 1, p. 59, January 2013.

WARREN, S. J.; DYE, S. Semilinear Gravitational Lens Inversion. **The Astrophysical Journal**, v. 590, n. 2, p. 673–682, June 2003.

WUCKNITZ, O.; BIGGS, A. D.; BROWNE, I. W. A. Models for the lens and source of B0218+357: a LENSCLEAN approach to determine H0. **Monthly Notices of the Royal Astronomical Society**, v. 349, p. 14–30, March 2004.

ZWICKY, F. Nebulae as Gravitational Lenses. **Physical Review**, v. 51, p. 290–290, February 1937.